

# New Mexico GEOLOGY

Fall 2018  
Volume 40, Number 2



# New Mexico GEOLOGY

Fall, 2018  
Volume 40, Number 2

The Late Pennsylvanian (Missourian) index  
fusulinid *Eowaeringella* in the Manzanita Mountains  
of central New Mexico

*Bruce D. Allen and Spencer G. Lucas . . . . . 35–44*

Sorting clasts across laminated maar dunes, Kilbourne and  
Hunts Holes, New Mexico: comparisons to sorting across  
aeolian and fluvial bedforms

*Dave W. Love, Allan Gutjahr, and Andreas Lazari . . . . 45–60*

New Mexico Geological Society spring meeting abstracts . . 61–85



Cover

Kilbourne Hole is in the Quaternary Potrillo volcanic field located southwest of Las Cruces, New Mexico. Activity in the volcanic field began at least 900,000 years ago in the West Potrillo Mountains with the most recent activity centered at Aden Crater about 20,000 years ago. Kilbourne Hole is the second youngest volcano in the field. Recent  $^{40}\text{Ar}/^{39}\text{Ar}$  dating suggests an age of about 45,000 years old. Kilbourne Hole is a world-renowned example of a maar volcano, a type of volcano that forms when ascending magma interacts with groundwater leading to highly explosive eruptions composed of ash, lapilli, bombs, and country rocks. Cross-bedded surge deposits, like those featured in the cover image, are common and well exposed along the inner crater rim. A granulometric analysis of deposits associated with Kilbourne Hole maar is presented in the paper beginning on page 45 of this issue. In addition to the world-class volcanic geology, Kilbourne Hole is also widely known for the abundance of peridotite mantle xenoliths, as well as crustal xenoliths, that were incorporated into the ascending magma and now litter the crater rim. In addition to attracting geologists, the National Aeronautics and Space Administration (NASA) has previously used the otherworldly landscape for training astronauts. Much of the volcanic field including Kilbourne Hole, along with regions in the Organ Mountains, Doña Ana Mountains, Robledo Mountains, and Sierra de las Uvas were designated as the Organ Mountains–Desert Peaks National Monument on May 21st, 2014. *Photograph and caption courtesy of Matt Zimmerer.*

A publication of the  
New Mexico Bureau of Geology and  
Mineral Resources,  
a Division of the New Mexico Institute of  
Mining and Technology

Science and Service  
ISSN 0196-948X

New Mexico Bureau of Geology and Mineral Resources  
*Director and State Geologist*  
**Dr. Nelia W. Dunbar**

Geologic Editor: Bruce Allen  
Manager Publications Program/Layout: Brigitte Felix  
Managing Editor: Gina D'Ambrosio

Cartography & Graphics: Bruce Allen, Leo Gabaldon

#### EDITORIAL BOARD

Dan Koning, *NMBGMR*  
Barry S. Kues, *UNM*  
Jennifer Lindline, *NMHU*  
Gary S. Morgan, *NMMNHS*

New Mexico Institute of Mining and Technology  
*President*

**Dr. Stephen G. Wells**

#### BOARD OF REGENTS

*Ex-Officio*

**Susana Martinez**

*Governor of New Mexico*

**Dr. Barbara Damron**

*Secretary of Higher Education*

*Appointed*

**Deborah Peacock**

*President, 2017–2022, Corrales*

**Jerry A. Armijo**

*Secretary/Treasurer, 2015–2020, Socorro*

**David Gonzales**

*2015–2020, Farmington*

**Donald Monette**

*2015–2018, Socorro*

**Emily Silva, student member**

*2017–2018, Farmington*

*New Mexico Geology* is an online publication available as a free PDF download from the New Mexico Bureau of Geology and Mineral Resources website. Subscribe to receive e-mail notices when each issue is available at: [geoinfo.nmt.edu/publications/subscribe](mailto:geoinfo.nmt.edu/publications/subscribe).

*Editorial Matter:* Articles submitted for publication should follow the guidelines at: [geoinfo.nmt.edu/publications/periodicals/nmg/NMG\\_guidelines.html](mailto:geoinfo.nmt.edu/publications/periodicals/nmg/NMG_guidelines.html). Address inquiries to Bruce Allen, Geologic Editor, New Mexico Bureau of Geology and Mineral Resources, 801 Leroy Place, Socorro, NM 87801. For telephone inquiries call (575) 835-5177 or use the email address given below.

*Email:* [NMBG-NMGeology@nmt.edu](mailto:NMBG-NMGeology@nmt.edu)

[geoinfo.nmt.edu/publications/periodicals/nmg](http://geoinfo.nmt.edu/publications/periodicals/nmg)



# The Late Pennsylvanian (Missourian) index fusulinid *Eowaeringella* in the Manzanita Mountains of central New Mexico

Bruce D. Allen<sup>1</sup> and Spencer G. Lucas<sup>2</sup>

<sup>1</sup>New Mexico Bureau of Geology and Mineral Resources, New Mexico Institute of Mining and Technology, Socorro, NM 87801; [bruce.allen@nmt.edu](mailto:bruce.allen@nmt.edu)

<sup>2</sup>New Mexico Museum of Natural History, Albuquerque, NM 87104; [spencer.lucas@state.nm.us](mailto:spencer.lucas@state.nm.us)

## Abstract

The boundary between Middle and Upper Pennsylvanian strata in central New Mexico is generally considered to coincide with the contact between the Gray Mesa and the overlying Atrasado formations. This perception was advanced in the Manzano Mountains by D.A. Myers, who reported the early Missourian fusulinid *Eowaeringella* near the top of the Gray Mesa Formation from a single locality in Gotera Canyon at the northern end of the range. The Gotera Canyon locality was re-examined and the *Eowaeringella* horizon recovered, together with additional strata 20 to 25 meters higher in the section that contain early forms of *Triticites*, including *T. cf. pygmaeus*, *T. wellsi*, and *T. cf. planus*. Thus, at Gotera Canyon, the *Eowaeringella* Zone is present 50 meters above the top of the Gray Mesa Formation, near the base of the Tinajas Member of the Atrasado Formation. The overlying *Triticites*-bearing strata appear to be common in the lower part of the Tinajas Member, from as far south as the Gotera Canyon locality northward to the Sandia Mountains.

## Introduction

Strata of the Pennsylvanian System in New Mexico consist of marine and marginal-marine deposits that are widely exposed in mountain ranges along the flanks of the Rio Grande rift (Fig. 1). Deposition of these strata occurred during a period of regional, Late Paleozoic orogenic activity, resulting in a complex succession of lithofacies across New Mexico. Pennsylvanian strata are subdivided in central New Mexico into three formation-rank units. These are the Sandia Formation, which contains a comparatively large proportion of sandstone and shale (generally 100 m thick or less), followed by the Gray Mesa Formation, largely limestone (generally 100 to 300 m thick), and the Atrasado Formation, consisting of alternating intervals of slope-forming clastic deposits and limestone-dominated ledges and cliffs (generally 200 to 300 m thick). The boundary between Middle and Upper Pennsylvanian strata, corresponding with the Desmoinesian-Missourian Stage boundary (ca. 306 Ma), is generally considered to coincide with the top of the Gray Mesa Formation.



Figure 1. Map showing location of the Gotera Canyon section in the Manzanita Mountains. Blue shaded areas indicate the surface extent of Pennsylvanian rocks. Localities mentioned in the text include Barton (B), Cedro Peak (CP) and Kinney Brick Quarry (KBQ). See Figure 4 for a 1:24,000-scale map of the Gotera Canyon locality.

Here, we report on lower Upper Pennsylvanian fusulinid-bearing strata from a locality in the Manzanita Mountains, Gotera Canyon (Fig. 1), where Myers (1969, 1988) reported an early Missourian fusulinid (genus *Eowaeringella*) from the top of the Gray Mesa Formation. The overall lithostratigraphic architecture of the Pennsylvanian sequence in the vicinity of the locality is typical of exposures encountered in mountains and uplifts bordering the Rio Grande from Socorro to

Albuquerque. A measured section through the lower part of the Atrasado Formation is presented, and the common forms of fusulinids recovered from the locality are described and illustrated. These forms include a species of the early Missourian genus *Eowaeringella*, and late-early to middle Missourian *Triticites* from 20–25 meters higher in the section.

## Background

As summarized above, Pennsylvanian rocks are presently assigned to three formations in central New Mexico—the Sandia, Gray Mesa, and Atrasado formations. The Sandia Formation typically rests on Proterozoic basement, and transitional Pennsylvanian–Permian strata above the Atrasado Formation are assigned to the Bursum Formation. Before the early 2000s, the Gray Mesa and Atrasado formations east of the Rio Grande were commonly referred to as the lower and upper members of the Madera Limestone (Read and Wood, 1947). Myers (1973), who had been mapping and conducting fusulinid biostratigraphy in the Manzano Mountains, formally introduced the names Los Moyos Limestone and Wild Cow Formation to replace “lower” and “upper” Madera in the area (before that, Myers had used lower and upper Madera on his maps). Across the Rio Grande to the west, in the Lucero uplift, these lithostratigraphic units had been named the Gray Mesa and Atrasado members of the Madera Limestone by Kelley and Wood (1946). Following the suggestion of Kues (2001), the names proposed by Kelley and Wood in the Lucero uplift are now used to delineate Pennsylvanian formations over a large portion of central New Mexico, replacing lower and upper Madera as well as the nomenclature proposed by Myers for the Manzano Mountains (e.g., Nelson et al., 2013a, b). The Atrasado Formation has subsequently been divided into eight members, which have been described and discussed in detail elsewhere (e.g., Lucas et al., 2009, 2014, 2016). The units of interest to this study are the Bartolo Member at the base of the Atrasado Formation, characterized by a relative abundance of siliciclastic deposits, followed by the Amado Member, largely consisting of limestone beds, and the overlying Tinajas Member, characterized again by a relative abundance of siliciclastics (Fig. 2).

In his monograph on fusulinids from the Manzano Mountains, Myers (1988) assigned a late Desmoinesian age to the upper part of the Gray Mesa Formation (his Los Moyos Limestone), placing it in his assemblage subzone of *Beedeina sulphurensis*. Rare specimens of the fusulinid *Wedekindellina ellipsoides* were reported by Myers (1988, plate 5) from the upper part of the Gray Mesa Formation near Sol se Mete Peak, approximately 10 km to the northeast of Gotera Canyon, suggesting correlation of those deposits with uppermost lower Desmoinesian (Cherokee Group) strata of the Midcontinent (e.g., Wahlman, 2013). In a more recent study of calcareous microfossils from Cedro Peak, about 15 km to the north of Gotera Canyon, Vachard et al. (2013) suggested a late early Desmoinesian age for the youngest age-diagnostic assemblages they examined from the Gray Mesa Formation, although diagnostic fossils from the uppermost part of the formation were not obtained. Thus, available evidence from the Manzanita Mountains suggests that much of the upper part of the Gray Mesa Formation may be early Desmoinesian in age.

Conodont data from the Cerros de Amado, approximately 100 km to the south of the Manzano Mountains, also suggest an early Desmoinesian age for much of the Gray Mesa Formation, and indicate that the Desmoinesian–Missourian boundary there lies within strata of the overlying Atrasado Formation, at the stratigraphic level of the Amado Member (Lucas et al., 2009; Barrick et al., 2013). Therefore, Myers’ (1988) report of the early Missourian fusulinid *Eowaeringella* near the top of the Gray Mesa Formation at Gotera Canyon seemed anomalous, and merited re-evaluation.

## The Gotera Canyon section

The base of Myers’ (1969) section in Gotera Canyon is in strata of the Gray Mesa Formation near the road that runs along the floor of the drainage, and traverses the steep hillslope to the northeast. Bedding is inclined a few degrees to the east-northeast along the traverse. Near the road at the base of the section, in the Gray Mesa Formation, a several-meter thick channel-fill deposit consisting of coarse-grained pebbly sandstone and conglomerate is present. Although comparatively thin sandstone beds are present in the Gray Mesa Formation, the thick channel sand near the base of the Gotera Canyon section is unusual and noteworthy. Above the sandstone, the Gray Mesa Formation contains beds of fossiliferous wackestone, packstone and some carbonate mudstone, with short covered intervals that for the most part probably represent fine-grained siliciclastic deposits. Limestone beds are commonly cherty, which is typical of the Gray Mesa Formation. The steep hillslope levels off somewhat, approximately 75 meters above the road, marking the top of the Gray Mesa Formation and the base of the Atrasado Formation. The graphic section depicted in Figure 2 begins at the top of the Gray Mesa Formation near this change in slope.

The basal unit of the overlying Atrasado Formation (Bartolo Member base) is up to four meters of coarse-grained, arkosic, trough-crossbedded, pebbly sandstone. This laterally discontinuous but widespread sandstone at the base of the Bartolo Member is the Coyote Sandstone Bed (Lucas et al., 2014), a term that dates back to Herrick’s (1900) early discussions of the rocks of the Pennsylvanian System in the vicinity of the Manzanita–Sandia Mountains. At Gotera Canyon, the Coyote Sandstone is overlain by an additional 29 meters of Bartolo Member strata expressed mainly as covered intervals (shale) with a few decimeter- to meter-scale exposures of limestone and a single reddish- and greenish-gray sandstone bed.

The overlying Amado Member forms the first prominent limestone outcrop above the Gray Mesa Formation. At Gotera Canyon, the Amado is approximately 18 meters thick, consisting of meter-scale beds of both cherty and non-cherty bioclastic wackestone to packstone. Also present are meter-scale intervals consisting of thinner beds of wackestone to carbonate mudstone intercalated with thin shale interbeds and partings. The top of the Amado is 1.2 meters of cherty limestone (unit 21 in Fig. 2). Here, the hillslope along the traverse levels off again, forming a bench that is underlain by interbedded limestone and shale. Thin carbonate beds in these strata on the gentler slope above the Amado Member top contain the fusulinid *Eowaeringella*, apparently corresponding to

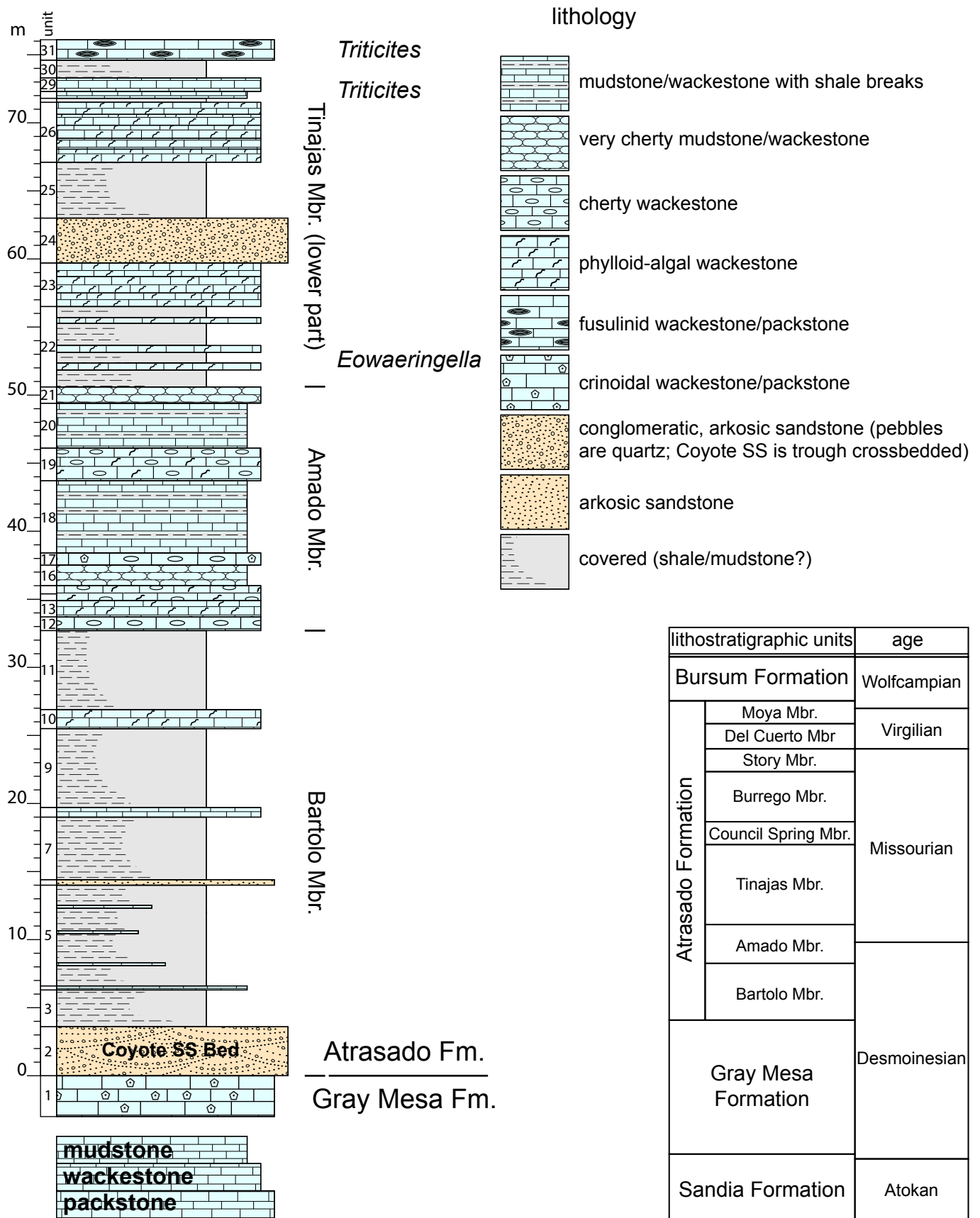


Figure 2. Stratigraphic section of the lower part of the Atrasado Formation at Gotera Canyon. Inset chart summarizes Pennsylvanian lithostratigraphy for central New Mexico, with age estimates for the southern Manzano Mountains (Priest Canyon) provided by Lucas et al. (2016).

Myers' (1988) fusulinid locality f10177 in the "NW1/4 NW1/4 section 20, T. 8 N., R. 6 E."

At Gotera Canyon, the next prominent limestone interval above the Amado Member is 3.2 meters of phylloid-algal wackestone, overlain by 3.3 meters of medium- to coarse-grained pebbly sandstone (unit 24). It could be argued that the top of the Amado Member at Gotera Canyon corresponds with the algal limestone beneath this sandstone. However, the cherty limestone of unit 21 is an equally justifiable Amado top, and that option is presented here (Fig. 2). The important observation, regardless of where the Amado–Tinajas contact is chosen, is that the *Eowaeringella* horizon lies well above the top of the Gray Mesa Formation.

The unit 24 sandstone in the lower part of the Tinajas Member is overlain by a covered interval (4.1 meters; probably mostly shale), followed by another prominent algal wackestone. This unit is overlain by a thin shale unit, 1.5 meters of thinly bedded mudstone to wackestone containing very small *Triticites*, another 1.3 meters of poorly exposed shale, followed by 1.5 meters of fusulinid wackestone to packstone (unit 31). Tinajas Member strata above this unit were not examined. In addition to fusulinids, unit 31 contains an abundance of other invertebrate fossils, including smaller foraminifers, and skeletons and fragments of brachiopods and crinoids. Species of fusulinids recovered from the Gotera Canyon section are described below; illustrated specimens are deposited at the New Mexico Museum of Natural History and Science (NMMNH).

## Paleontology

### Genus *Eowaeringella* Skinner and Wilde *Eowaeringella huecoensis* Stewart Figs. 3.1–4, Table A1

*Eowaeringella huecoensis* Stewart, 1968, Cushman Foundation for Foraminiferal Research, Special Publication 16, p. 16–17, pl. 2, figs. 6, 8–10, table 5.

**Referred specimens**—NMMNH P-55930 (two specimens; figs. 3.1, 3.3), NMMNH P-55931 (fig. 3.2), NMMNH P-55932 (fig. 3.4).

**Description**—The test is elongate-fusiform with convex to nearly straight to concave lateral slopes, rounded to bluntly pointed polar ends, and attains a length of 5.5 to 7.2 mm and a width of 1.4 to 1.8 mm in 6.5 to 8 volutions. The axis of coiling is typically straight, but is curved in some specimens. Early volutions are fusiform and somewhat inflated, expanding evenly, and gradually become more elongate in succeeding whorls. The form ratio for mature individuals ranges from 3.4 to 4.1.

Morphometric data (Table A1) were obtained from four axial and three sagittal sections. The chambers are nearly uniform in height across the central two thirds of the shell. The height of successive whorls averages 58, 54, 78, 96, 123, 165, and 167  $\mu\text{m}$  for the first through the seventh volution. The diameter of the proloculus ranges from 100 to 125  $\mu\text{m}$ , averaging 116  $\mu\text{m}$ . Average form ratios for the first through the seventh volution are 1.9, 2.6, 2.9, 3.2, 3.4, 3.6 and 3.9, respectively. The spirotheca consists of a tectum, a thicker diaphanotheca and an inner tectorium. The wall averages 18, 21, 24, 31, 34, 36

and 41  $\mu\text{m}$  in thickness for the first through the seventh volution. Septa are essentially planar across most of the shell, becoming irregularly folded in the polar extremities. The average septal count for the first through the seventh volution is 11, 16, 18, 20, 21, 24 and 26, respectively. Chomata are discrete mounds with steep to overhanging tunnel sides and more gently inclined poleward sides, and are generally present in all but the final volution. Axial filling is insignificant. The tunnel occupies one half to two thirds the height of the chamber and its path is generally straight, although it appears to wander somewhat in the inner volutions of some specimens. The tunnel angle for the first through the sixth volution averages 15, 20, 26, 29, 34 and 44 degrees, respectively.

**Remarks**—The tight coiling, planar septa becoming folded in the polar extremities, well-developed chomata and the wall structure, in particular, help distinguish *Eowaeringella* from most other genera of fusulinids commonly found in central New Mexico. The relatively large size, elongate shape and large proloculus of the Gotera Canyon forms are consistent with assignment to *E. huecoensis*. Myers (1988) assigned *Eowaeringella* specimens from the Gotera Canyon locality to *E. cf. E. joyitaensis* Stewart, but that species is significantly smaller and has a smaller proloculus than the specimens recovered in this study.

**Occurrence**—Stewart's (1968) type locality for *Eowaeringella huecoensis* is in the Hueco Mountains of El Paso County, Texas. *E. huecoensis* is present at Gotera Canyon in thin-bedded, pale-gray algal wackestone (unit 22 in Fig. 2), a few meters above a prominent cherty limestone assigned here to the top of the Amado Member of the Atrasado Formation. *Eowaeringella* has been found in Pennsylvanian-aged strata in several mountain ranges in New Mexico (Stewart, 1968; Wilde, 2006); it has been reported in the Manzanita Mountains only from the Gotera Canyon locality (Myers, 1988). The presence of this genus indicates correlation with early Missourian strata of the Midcontinent (e.g., Wahlman, 2013).

### Genus *Triticites* Girty *Triticites cf. pygmaeus* Dunbar and Condra Figs. 3.5–8, Table A2

*Triticites cullomensis* var. *pygmaeus* Dunbar and Condra, 1928, Nebraska Geological Survey, Bulletin 2, Series 2, p. 95–96, pl. V, figs. 3, 4.

*Triticites pygmaeus* Dunbar and Skinner, 1937, University of Texas Bulletin 3701, p. 614–616, pl. 48, figs. 13–26.

**Referred specimens**—NMMNH P-55934 (fig. 3.5), NMMNH P-55935 (fig. 3.6), NMMNH P-55936 (fig. 3.7), NMMNH P-55933 (fig. 3.8).

**Description**—A small species of *Triticites* with a fusiform test and rounded to bluntly pointed ends, attaining a length of 2.5 to 3.7 mm and a width of 1.0 to 1.4 mm in five to six volutions. The form ratio ranges from 2.3 to 2.6. The axis of coiling is generally straight; the lateral slopes are typically evenly convex, but are nearly straight to slightly concave in some individuals. The first volution is subspherical, with successive volutions becoming increasingly elongate, typically progressing from elliptical to fusiform in the outer whorls.

Measurements were obtained from seven axial and four sagittal sections (Table A2). The chamber height

varies little across the central portion of the shell, but increases notably toward the polar ends in the outer whorls of mature specimens. The height of successive volutions in the tunnel area averages 54, 65, 102, 138 and 178  $\mu\text{m}$  for the first through the fifth volution, respectively. The diameter of the proloculus ranges from 96 to 140  $\mu\text{m}$ , averaging 120  $\mu\text{m}$ . Average form ratios for the first through the fifth volution are 1.3, 1.8, 2.2, 2.5, and 2.6. The spirotheca is thin, averaging 16, 19, 21, 25, 31, and 35  $\mu\text{m}$  for the first through the sixth volution, and consists of a tectum and keriotheca with alveoli becoming apparent in the outer whorls. Septa are nearly planar across the central part of the shell, becoming irregularly fluted toward the ends. Septal pores are readily apparent. Average septal counts for the first through the fourth volution are 9, 16, 16 and 18. Chomata are well-developed asymmetrical mounds with steep tunnel sides and sloping poleward sides, and are generally present in the penultimate whorl. The tunnel widens through successive volutions, and its path is irregular in some specimens. The tunnel angle for the first through the fifth volution averages 23, 28, 39, 44 and 49 degrees, respectively.

**Remarks**—This small species of *Triticites* is similar to other small, relatively simple Missourian species, such as *T. burgessae* Burma and *T. canyonensis* Wilde. The Gotera Canyon specimens possess a spirotheca that is quite thin, but most other morphometric parameters are quite similar to *T. pygmaeus*. The diameter of the proloculus, in particular, is significantly larger than in comparable species.

**Occurrence**—*Triticites* cf. *pygmaeus* is common in thin, wavy-bedded wackestone, a few meters below the main *Triticites*-bearing horizon at Gotera Canyon, in the lower part of the Tinajas Member of the Atrasado Formation (unit 29 in Fig. 2).

***Triticites wellsii* Needham**  
Figs. 3.9–11, Table A3

*Triticites wellsii* Needham, 1937, New Mexico Bureau of Mines and Mineral Resources, Bulletin 14, p. 37–38, pl. VI, figs. 1–3.

**Referred specimens**—NMMNH P-55940 (fig. 3.9), NMMNH P-55942 (fig. 3.10), NMMNH P-55941 (fig. 3.11).

**Description**—Elongate elliptical tests commonly attain a length of 5 to 5.5 mm and a width of 1.4 to 1.8 mm in six to seven volutions, with a straight to curved axis of coiling and rounded ends. Lateral slopes are typically convex, but may be straight or somewhat concave in specimens with a curved axis. Overall the shell bears a loosely coiled appearance. The form ratio of mature specimens ranges from 2.8 to 3.2.

Measurements were obtained from four axial and three sagittal sections (Table A3). Early volutions are fusiform and somewhat inflated with bluntly pointed ends, becoming progressively more elliptical after the fourth or fifth volution. Averages of the form ratios for the first through seventh volutions are 1.5, 1.8, 2.0, 2.3, 2.6, 2.8 and 2.8, respectively. The proloculus ranges in diameter from 60 to 110  $\mu\text{m}$ , averaging 96  $\mu\text{m}$ . The chambers are uniform in height across much of the shell, with a relative increase in height in the polar extremities of some specimens. The height of successive volutions above the

tunnel averages 42, 53, 78, 118, 174, 229 and 254  $\mu\text{m}$  for the first through the seventh volution. The spirotheca consists of a tectum and keriotheca, with alveoli evident in the outer whorls. Wall thickness averages 13, 17, 23, 28, 38, 46 and 46  $\mu\text{m}$  for the first through the seventh volution. Septa are planar to gently undulating across the central part of the shell and seem rather widely spaced, with average septal counts for the first through the sixth volution of 9, 13, 15, 17, 18 and 19, respectively. Chomata are asymmetrical mounds with comparatively steep faces toward the tunnel and gentler sides toward the poles, and are generally present in all but the last whorl. The tunnel is relatively low, and the tunnel angle for the first through the fifth volution averages 17, 26, 32, 46, and 59 degrees, respectively.

**Remarks**—The elliptical outline of the test, thin walls, minimal septal fluting and modest size distinguish *Triticites wellsii* from most other species of *Triticites* reported from central New Mexico.

**Occurrence**—*Triticites wellsii* is common in unit 31 (Fig. 2) of the Tinajas Member of the Atrasado Formation, about 25 meters above the top of the Amado Member. Topotype specimens of *T. wellsii* collected from Needham's (1937) locality east of Barton in Santa Fe County occupy a similar stratigraphic position, approximately 15 meters above the Amado Member at that locality.

***Triticites* cf. *planus* Thompson and Thomas**  
Figs. 3.12–14, Table A4

*Triticites planus* Thompson and Thomas, 1953, The Geological Survey of Wyoming, Bulletin 46, p. 31–34, pl. 3, figs. 1–19, (?) pl. 4, figs. 1–10.

**Referred specimens**—NMMNH P-55939 (fig. 3.12), NMMNH P-55937 (fig. 3.13), NMMNH P-55938 (fig. 3.14).

**Description**—Tests are elongate fusiform to subcylindrical in shape, with irregular lateral slopes and rounded to blunt ends in mature specimens. Lengths range from 5.7 to 7.5 mm and widths are 1.4 to 2 mm in 6 to 6.5 volutions, resulting in form ratios ranging from 3.9 to 4.8. Volutions are tightly coiled and fusiform, with bluntly pointed ends in the juvenarium, becoming increasingly elongate in successive volutions. After about the fourth volution the axis of coiling tends to become irregular in most specimens and the ends more rounded.

Measurements (Table A4) were obtained from seven axial and three sagittal sections. The average form ratios for the first through the sixth volution are 1.6, 2.2, 2.5, 3.0, 3.5 and 3.9, respectively. The proloculus ranges in diameter from 62 to 116  $\mu\text{m}$  in diameter, averaging 90  $\mu\text{m}$ . The chambers are lowest in the central part of the test and increase in height in the polar areas. The height of successive volutions above the tunnel averages 45, 58, 89, 140, 202 and 242  $\mu\text{m}$  in the first through the sixth volution. The spirotheca consists of a tectum and keriotheca and is relatively thin, averaging 13, 16, 21, 29, 40 and 45  $\mu\text{m}$  for the first through the sixth volution. Septa are nearly planar across the central two thirds of the shell, becoming irregularly folded in the polar extremities. Average septal counts for the first through the fifth volution are 8, 13, 16, 18 and 21. Chomata in the inner few volutions appear to extend to the ends of the shell in some specimens. In later volutions the chomata are small, nearly symmetrical

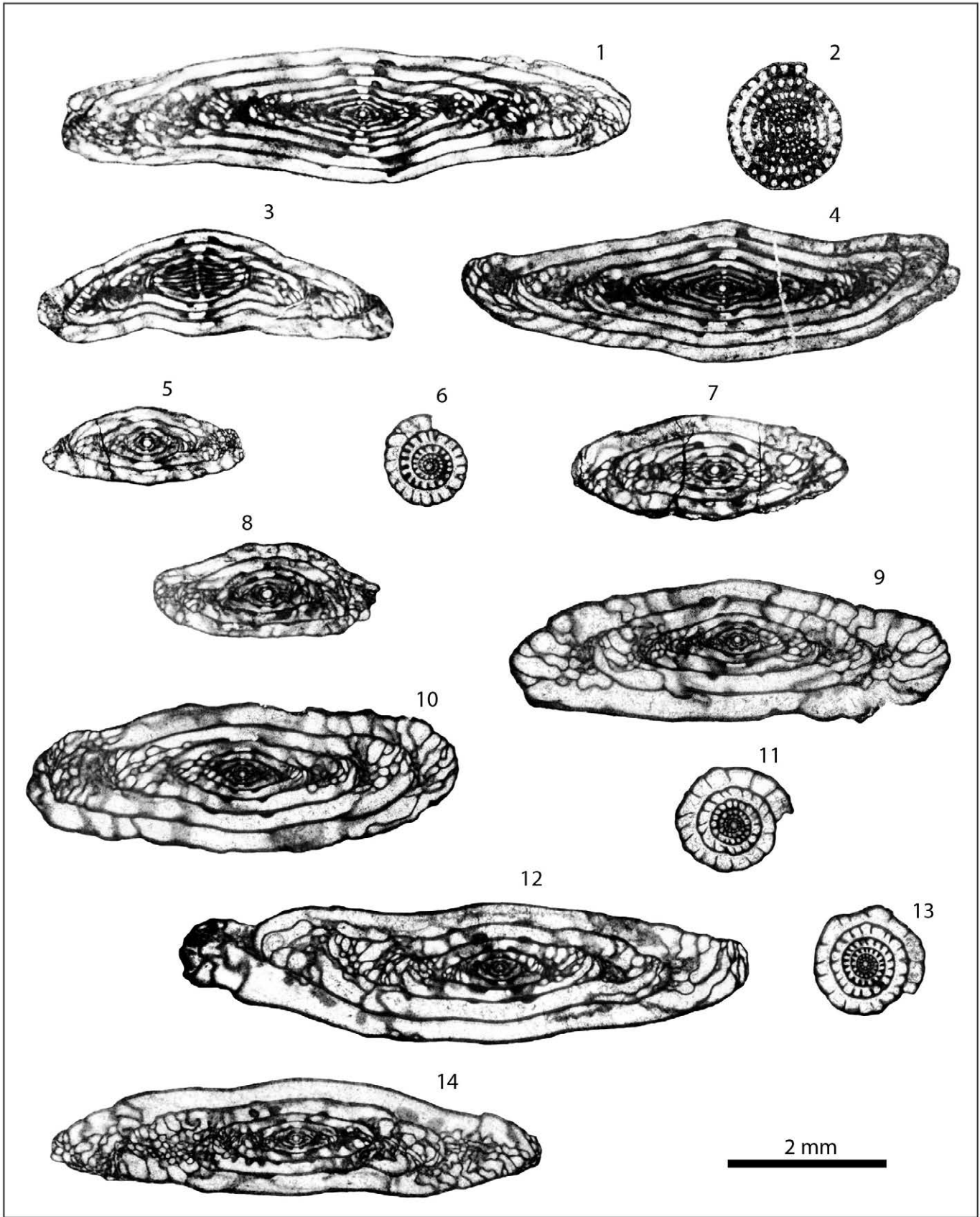


Figure 3. Fusulinids from the lower part of the Tinajas Member at Gotera Canyon in the Manzanita Mountains. All images 15X magnification. 1-4. *Eowaeringella huecoensis* Stewart. 1, 4 (NMMNH P-55930a, NMMNH P-55932), axial sections. 2 (NMMNH P-55931), sagittal section. 3 (NMMNH P-55930b), tangential section of an adolescent specimen with a curved coiling axis. 5-8. *Triticites* cf. *pygmaeus* Dunbar and Condra. 5, 7-8

(NMMNH P-55934, NMMNH P-55936, NMMNH P-55933), axial sections. 6 (NMMNH P-55935), sagittal section. 9-11. *Triticites wellsii* Needham. 9, 10 (NMMNH P-55940, NMMNH P-55942), axial sections. 11 (NMMNH P55941), sagittal section. 12-14. *Triticites* cf. *planus* Thompson and Thomas. 12, 14 (NMMNH P-55939, NMMNH P-55938), axial sections. 13 (NMMNH P55937), sagittal section.

mounds. The tunnel widens from about 25 degrees in the first volution to 65 degrees in the sixth.

**Remarks**—A number of slender, subcylindrical, relatively simple forms of *Triticites* have been reported from central New Mexico (e.g., *T. ohioensis* Thompson) that are similar to the Gotera Canyon specimens discussed here. The comparatively modest septal fluting together with other characteristics of the Gotera Canyon specimens (e.g., lower form ratios relative to *T. ohioensis*) suggest assignment to *T. planus*. The presence of such forms indicates correlation with Missourian (Kansas City Group) strata of the Midcontinent (Thompson and Thomas, 1953).

**Occurrence**—*Triticites* cf. *planus* is common in the Gotera Canyon section in bedded bioclastic wackestone to packstone in the lower part of the Tinajas Member of the Atrasado Formation (unit 31 in Fig. 2). It is associated with *Triticites wellsii* Needham, together with a small, less common species (?*T. nebraskensis* Thompson) that is not discussed here because inadequate oriented sections were obtained. *Triticites planus* has been reported from the Manzanita Mountains near the Kinney Brick Quarry, 10 km north of the Gotera Canyon section, also in the lower part of the Tinajas Member (Lucas et al., 2011).

## Discussion

The Pennsylvanian section has recently been described in detail at Priest Canyon at the southern end of the Manzano Mountains and at Cedro Peak in the Manzanita Mountains at the northern end of the range (Lucas et al., 2014, 2016; Fig. 1). The overall architecture of strata assigned to the Pennsylvanian System appears to be similar across the mountain block, and the lithostratigraphic terminology in current use for the Pennsylvanian System in central New Mexico is clearly applicable at the Gotera Canyon locality, at least for the part of the section that was examined. In particular, the base of the Atrasado Formation is readily distinguished from the underlying Gray Mesa Formation by the presence of approximately 30 meters of slope-forming clastic deposits of the Bartolo Member. Although Myers (1988) reported that the *Eowaeringella* horizon at Gotera Canyon is at the top of the Gray Mesa Formation, and depicted it as such on his graphic section for the locality (Myers, 1969), his geologic map (see Fig. 4) places the top of the Gray Mesa Formation well below the *Eowaeringella*-bearing horizon, in close agreement with the obvious lithologic change from limestone to sandstone marking the top of the formation at this locality.

Stewart (1968) described several species of *Eowaeringella*

from 19 localities in the U.S., including 9 localities in New Mexico. As discussed by Stewart (1968), the fusulinid genus *Eowaeringella* is an important Pennsylvanian index fossil, occupying a narrow stratigraphic interval between the Middle Pennsylvanian fusulinid Zone of *Beedeina* below and the Upper Pennsylvanian Zone of *Triticites* above. Thus, following the demise of the Desmoinesian *Beedeina* fauna, *Eowaeringella* was the first biostratigraphically diagnostic fusulinid to appear, and its presence in strata is considered diagnostic of an early Missourian age.

The stratigraphic position of *Eowaeringella* in the Tinajas Member at Gotera Canyon suggests a Desmoinesian age assignment for some portion of the 50 meters of Atrasado strata underlying the Tinajas. We are unaware of any diagnostic fusulinid data from the lower two members of the Atrasado Formation in the Manzanita Mountains; Lucas et al. (2016) reported a species of *Plectofusulina* from the upper part of the Amado Member at Priest Canyon in the southern Manzano Mountains, which may indicate an early Missourian age. Myers (1969) noted the presence of an unidentified species of the Desmoinesian genus *Fusulina* (= *Beedeina*) approximately 15 meters below what is considered here to be the top of the Gray Mesa Formation at the Gotera Canyon locality. Thus, taking the available data at face value suggests that the Desmoinesian–Missourian boundary lies somewhere within ~65 meters of section extending from 15 meters below the top of the Gray Mesa Formation upward through 50 meters of Atrasado strata comprising the Bartolo and Amado members. As

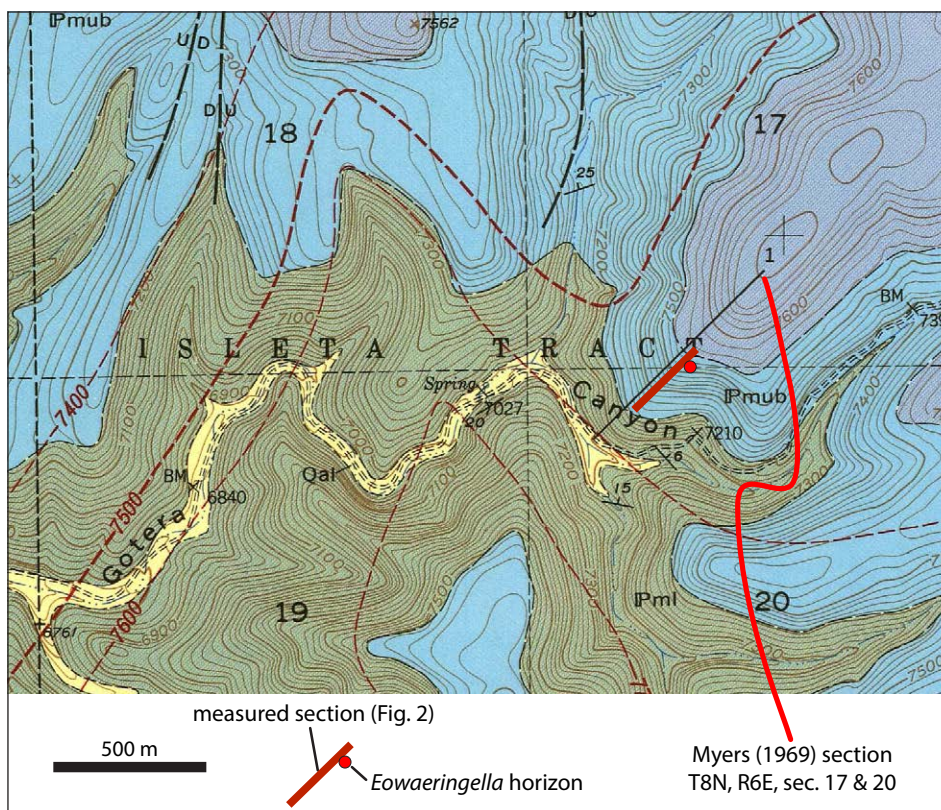


Figure 4. Geologic map of the Gotera Canyon locality (from Myers, 1969; red dashed lines are structure contours), annotated to show the Figure 2 measured-section traverse and *Eowaeringella* locality. Green map unit (IPml – lower Madera Limestone) and blue/purple unit (IPmu – upper Madera Limestone) correspond to the Gray Mesa and Atrasado formations.

noted above, conodont biostratigraphy from the Cerros de Amado east of Socorro (Barrick et al., 2013) suggests that the Desmoinesian-Missourian boundary there lies within the Amado Member.

The limestone beds containing abundant fusulinids 25 meters above the *Eowaeringella* horizon are important for two reasons. First, the forms of *Triticites* that are present indicate an early to middle Missourian age for these strata. Second, similar conditions that led to significant accumulations of *Triticites* in the lower part of the Tinajas Member at Gotera Canyon appear to have occurred over a large area encompassing the Manzanita Mountains northward to the Sandia Mountains. Indeed, examination of dozens of outcrops of the Amado–Tinajas interval in this area has shown that limestone beds containing an abundance of early forms of *Triticites* are usually present in the lower part of the Tinajas Member, a short distance above the prominent Amado Member of the Atrasado Formation. This fusulinid marker horizon in the lower part of the Tinajas Member was an important factor in determining the age of strata comprising the Kinney Brick Quarry Lagerstätte in the Manzanita Mountains, which is located approximately 10 km north of the Gotera Canyon locality. For many years, it was thought that strata exposed at the Kinney Brick Quarry were Virgilian in age (see articles in Zidek, 1992). Recognition that the quarry is in close stratigraphic proximity to the lower

Tinajas Member *Triticites* horizon helped to establish a Missourian age for the strata comprising that important fossil locality, an age assignment confirmed by conodont biostratigraphy (Lucas et al., 2011).

## Conclusions

Lower Missourian fusulinids (*Eowaeringella*) present at the northern end of the Manzano Mountains in Gotera Canyon are readily assignable to strata of the Atrasado Formation, 50 meters above the top of the Gray Mesa Formation, and not at the top of the Gray Mesa as previously reported. Early forms of *Triticites* are present in abundance 75 meters above the base of the Atrasado Formation at Gotera Canyon. This distinctive fusulinid horizon appears to be widespread across the Manzanita–Sandia Mountains, where it consistently occupies a similar stratigraphic position within the lower part of the Missourian Tinajas Member of the Atrasado Formation.

## Acknowledgments

Assistance gaining access to Gotera Canyon by personnel with the Public Services Department, Isleta Pueblo, is gratefully acknowledged. We thank Merlynd Nestell, Daniel Vachard and Gregory Wahlman for their constructive reviews, and Shari Kelley for editorial supervision.

## References

- Barrick, J.E., Lucas, S.G., and Krainer, K., 2013, Conodonts of the Atrasado Formation (uppermost Middle to Upper Pennsylvanian), Cerros de Amado region, central New Mexico, U.S.A.: New Mexico Museum of Natural History and Science, Bulletin 59, p. 239–252.
- Herrick, C.L., 1900, The geology of the White Sands of New Mexico: *Journal of Geology*, v. 8, p. 112–128.
- Kelley, V.C., and Wood, G.H., Jr., 1946, Lucero uplift, Valencia, Socorro, and Bernalillo counties, New Mexico: U.S. Geological Survey, Oil and Gas Investigations Preliminary Map 47, scale 1:63,360.
- Kues, B.S., 2001, The Pennsylvanian System in New Mexico—overview with suggestions for revision of stratigraphic nomenclature: *New Mexico Geology*, v. 23, p. 103–122.
- Lucas, S.G., Krainer, K., and Barrick, J.E., 2009, Pennsylvanian stratigraphy and conodont biostratigraphy in the Cerros de Amado, Socorro County, New Mexico: *in* Lueth, V., Lucas S.G., Chamberlin, R.M., eds., *Geology of Chupadera Mesa*, New Mexico Geological Society, 60th Annual Field Conference, Guidebook, p. 183–211.
- Lucas, S.G., Allen, B.D., Krainer, K., Barrick, J., Vachard, D., Schneider, J.W., DiMichele, W.A., and Bashforth, A.R., 2011, Precise age and biostratigraphic significance of the Kinney Brick Quarry Lagerstätte, Pennsylvanian of New Mexico, USA: *Stratigraphy*, v. 8, p. 7–27.
- Lucas, S.G., Krainer, K., Allen, B.D., and Vachard, D., 2014, The Pennsylvanian section at Cedro Peak: a reference section in the Manzanita Mountains, central New Mexico: *New Mexico Geology*, v. 36, p. 3–24.
- Lucas, S.G., Krainer, K., and Vachard, D., 2016, The Pennsylvanian section at Priest Canyon, southern Manzano Mountains, New Mexico: *in* Frey, B.A., Karlstrom, K.E., Lucas, S.G., William, S., Ziegler, K., McLemore, V., and Ulmer-Scholle, D.S., eds., *The Geology of the Belen Area*, New Mexico Geological Society, 67th Annual Field Conference, Guidebook, p. 275–301.
- Myers, D.A., 1969, Geologic map of the Escabosa quadrangle, Bernalillo County, New Mexico: U.S. Geological Survey, Geologic Quadrangle Map GQ-795, scale 1:24,000.
- Myers, D.A., 1973, The Upper Paleozoic Madera Group in the Manzano Mountains, New Mexico: U.S. Geological Survey, Bulletin 1372-F, 13 p.
- Myers, D.A., 1988, Stratigraphic distribution of fusulinid foraminifera from the Manzano Mountains, New Mexico: U.S. Geological Survey, Professional Paper 1446, 65 p.
- Nelson, W.J., Lucas, S.G. and Krainer, K., 2013[a], The Atrasado and Bar B formations (Middle-Upper Pennsylvanian) in central and southern New Mexico: *New Mexico Museum of Natural History and Science, Bulletin 59*, p. 123–142.
- Nelson, W. J., Lucas, S. G., Krainer, K. and Elrick, S., 2013[b], The Gray Mesa Formation (Middle Pennsylvanian) in New Mexico: *New Mexico Museum of Natural History and Science, Bulletin 59*, p. 101–122.
- Read, C.B. and Wood, G.H., Jr., 1947, Distribution and correlation of Pennsylvanian rocks in Late Paleozoic sedimentary basins of northern New Mexico: *Journal of Geology*, v. 55, p. 220–236.
- Stewart, W.J., 1968, The stratigraphic and phylogenetic significance of the fusulinid genus *Eowaeringella*, with several new species: Cushman Foundation for Foraminiferal Research, Special Publication no. 10, 29 p.
- Thompson, M.L. and Thomas, H.D., 1953, Systematic paleontology of fusulinids from the Casper Formation: *The Geological Survey of Wyoming, Bulletin 46, Part II*, p. 15–56.
- Vachard, D., Krainer, K., and Lucas, S.G., 2013, Pennsylvanian (Late Carboniferous) calcareous microfossils from Cedro Peak (New Mexico, USA): Part 2. Smaller foraminifers and fusulinids: *Annales de Paléontologie*, v. 99, p. 1–42.
- Wahlman, G.P., 2013, Pennsylvanian to Lower Permian (Desmoinesian-Wolfcampian) fusulinid biostratigraphy of Midcontinent North America: *Stratigraphy*, v. 10, p. 73–104.
- Wilde, G.L., 2006, Pennsylvanian-Permian fusulinaceans of the Big Hatchet Mountains, New Mexico: *New Mexico Museum of Natural History and Science, Bulletin 38*, 331 p.
- Zidek, J., ed., 1992, *Geology and paleontology of the Kinney Brick Quarry, Late Pennsylvanian, central New Mexico*: New Mexico Bureau of Mines and Mineral Resources, Bulletin 138, 242 p.

## Appendices

Table A1. Measurements of *Eowaeringella huecoensis* Stewart. Specimens A, E, and C are illustrated in text Figs. 3.1, 3.2, and 3.4, respectively.

Half length (mm)								
Specimen	Volution							
	1	2	3	4	5	6	7	8
A	0.159	0.324	0.612	0.968	1.520	2.129	2.915	3.800
B	0.316	0.651	1.089	1.607	2.064	2.812	—	—
C	0.162	0.305	0.532	0.837	1.209	1.816	2.628	3.305
D	0.162	0.319	0.497	0.814	1.270	1.790	2.664	—

Radius vector (mm)									
Spec.	Volution								
	0	1	2	3	4	5	6	7	8
A	0.058	0.105	0.157	0.222	0.305	0.414	0.556	0.703	0.883
B	0.063	0.135	0.190	0.284	0.390	0.531	0.747	—	—
C	0.063	0.099	0.155	0.224	0.320	0.433	0.583	0.762	0.958
D	0.050	0.074	0.115	0.184	0.271	0.383	0.508	0.652	—
E	0.060	0.153	0.217	0.303	0.398	0.508	0.680	0.867	—
F	0.058	0.131	0.189	0.276	0.382	0.535	0.721	0.898	—
G	0.055	0.117	0.193	0.279	0.375	0.503	0.633	0.808	0.988

Thickness of spirotheca (µm)								
Specimen	Volution							
	1	2	3	4	5	6	7	8
A	16	26	20	37	36	40	30	30
B	18	18	26	24	40	39	—	—
C	13	18	24	29	25	28	35	39
D	14	17	19	28	30	33	40	—
E	25	24	28	44	34	43	50	—
F	26	21	28	32	38	39	51	—
G	16	21	27	25	32	32	40	31

Tunnel angle (deg.)							
Specimen	Volution						
	1	2	3	4	5	6	7
A	17	21	23	28	25	38	44
B	14	23	33	33	43	—	—
C	15	18	20	23	30	44	39
D	13	19	26	31	36	49	—

Septal count								
Specimen	Volution							
	1	2	3	4	5	6	7	8
E	13	17	19	22	24	30	28	—
F	12	15	19	19	21	22	27	—
G	9	15	16	18	18	21	23	24

Table A2. Measurements of *Triticites* cf. *pygmaeus* Dunbar and Condra. Specimens A, I, B, and E are illustrated in text Figs. 3.5, 3.6, 3.7, and 3.8, respectively.

Half length (mm)						
Specimen	Volution					
	1	2	3	4	5	6
A	0.167	0.332	0.616	0.987	1.312	—
B	0.146	0.322	0.704	1.289	1.817	—
C	0.156	0.351	0.556	1.012	1.537	—
D	0.138	0.253	0.440	0.828	1.485	—
E	0.154	0.322	0.648	1.061	1.440	—
F	0.102	0.205	0.382	0.684	1.147	1.815
G	0.126	0.279	0.467	0.711	1.066	1.583

Radius vector (mm)							
Specimen	Volution						
	0	1	2	3	4	5	6
A	0.053	0.088	0.152	0.242	0.360	0.539	—
B	0.061	0.103	0.156	0.256	0.406	0.657	—
C	0.062	0.142	0.216	0.313	0.485	0.674	—
D	0.059	0.119	0.165	0.236	0.359	0.513	—
E	0.070	0.112	0.166	0.258	0.394	0.563	—
F	0.048	0.103	0.145	0.219	0.317	0.459	0.662
G	0.050	0.085	0.132	0.198	0.302	0.440	0.608
H	0.070	0.137	0.237	0.362	0.533	—	—
I	0.065	0.131	0.215	0.378	0.553	—	—
J	0.063	0.107	0.180	0.317	0.446	0.644	—
K	0.055	0.118	0.193	—	—	—	—

Thickness of spirotheca (µm)						
Specimen	Volution					
	1	2	3	4	5	6
A	12	15	18	30	37	—
B	21	23	30	40	38	—
C	25	27	28	32	42	—
D	17	17	19	20	29	—
E	16	20	22	27	34	—
F	15	15	14	14	15	38
G	11	11	13	15	22	33
H	11	19	19	25	—	—
I	17	20	25	32	—	—
J	12	17	23	19	34	—
K	16	23	—	—	—	—

Tunnel angle (deg.)					
Specimen	Volution				
	1	2	3	4	5
A	24	30	36	41	—
B	28	39	52	42	—
C	28	29	46	—	—
D	21	28	33	46	—
E	22	29	45	36	—
F	13	10	31	52	55
G	25	30	27	44	42

Septal count					
Specimen	Volution				
	1	2	3	4	5
H	10	18	14	16	—
I	9	16	17	21	—
J	8	16	18	18	19
K	9	14	—	—	—

Table A3. Measurements of *Triticites wellsii* Needham. Specimens D, B, and G are illustrated in text Figs. 3.9, 3.10, and 3.11, respectively.

Half length (mm)							
Specimen	Volution						
	1	2	3	4	5	6	7
A	0.084	0.186	0.380	0.741	1.277	1.80	2.633
B	0.143	0.310	0.510	0.890	1.484	2.18	2.725
C	0.141	0.262	0.394	0.635	0.938	1.68	2.186
D	0.086	0.177	0.397	0.650	1.109	1.74	2.676

Radius vector (mm)								
Spec.	Volution							
	0	1	2	3	4	5	6	7
A	0.055	0.085	0.131	0.201	0.304	0.439	0.643	0.877
B	0.053	0.080	0.136	0.219	0.344	0.528	0.754	0.998
C	0.052	0.071	0.133	0.210	0.294	0.413	0.586	0.788
D	0.053	0.081	0.132	0.199	0.310	0.464	0.705	1.039
E	0.036	0.106	0.149	0.218	0.332	0.491	0.767	—
F	0.030	0.091	0.141	0.229	0.376	0.623	0.880	—
G	0.055	0.109	0.169	0.258	0.398	0.615	—	—

Thickness of spirotheca (µm)							
Specimen	Volution						
	1	2	3	4	5	6	7
A	13	20	29	29	35	42	40
B	13	18	27	36	51	44	46
C	9	18	22	22	38	46	46
D	8	18	23	27	33	46	51
E	15	12	13	21	27	44	—
F	18	21	25	34	45	55	—
G	16	15	20	24	41	—	—

Tunnel angle (deg.)						
Specimen	Volution					
	1	2	3	4	5	6
A	14	21	33	45	59	55
B	14	31	39	52	54	—
C	21	24	28	42	64	—
D	17	29	26	43	57	—

Septal count						
Specimen	Volution					
	1	2	3	4	5	6
E	8	12	14	18	20	19
F	8	12	15	16	17	19
G	10	14	16	18	16	—

Table A4. Measurements of *Triticites cf. planus* Thompson and Thomas. Specimens D, H, and A are illustrated in text Figs. 3.12, 3.13, and 3.14, respectively.

Half length (mm)						
Specimen	Volution					
	1	2	3	4	5	6
A	0.134	0.302	0.540	1.056	1.898	3.094
B	0.103	0.230	0.427	0.933	1.744	3.021
C	0.200	0.459	1.006	1.791	3.129	—
D	0.212	0.386	0.646	1.340	2.183	3.139
E	0.121	0.316	0.651	1.176	2.029	3.497
F	0.147	0.332	0.566	1.108	1.840	2.881
G	0.108	0.214	0.393	0.760	1.517	3.046

Radius vector (mm)							
Specimen	Volution						
	0	1	2	3	4	5	6
A	0.047	0.080	0.139	0.225	0.330	0.508	0.768
B	0.036	0.062	0.105	0.171	0.294	0.447	0.684
C	0.053	0.111	0.187	0.304	0.509	0.818	—
D	0.058	0.103	0.168	0.282	0.444	0.700	0.962
E	0.055	0.083	0.141	0.221	0.382	0.589	0.845
F	0.037	0.094	0.160	0.240	0.381	0.588	0.903
G	0.031	0.084	0.125	0.209	0.328	0.486	0.673
H	0.040	0.088	0.139	0.234	0.365	0.533	0.710
I	0.048	0.102	0.167	0.254	0.397	0.602	—
J	0.045	0.092	0.146	0.232	0.346	0.529	—

Thickness of spirotheca (µm)						
Specimen	Volution					
	1	2	3	4	5	6
A	11	19	17	25	44	48
B	9	14	18	24	34	46
C	18	21	22	42	54	—
D	11	14	31	34	41	47
E	12	17	28	33	48	44
F	15	17	17	22	34	40
G	12	12	22	30	31	43
H	16	19	21	28	40	45
I	15	17	22	31	40	—
J	10	14	18	24	36	—

Tunnel angle (deg.)					
Specimen	Volution				
	1	2	3	4	5
A	20	33	45	56	69
B	28	26	34	48	50
C	23	37	54	50	—
D	27	32	40	51	64
E	31	39	54	75	—
F	26	35	44	65	—
G	11	20	31	45	69

Septal count						
Specimen	Volution					
	1	2	3	4	5	6
H	8	14	15	19	19	17
I	8	11	15	18	22	—
J	8	14	17	18	22	—

# Sorting clasts across laminated maar dunes, Kilbourne and Hunts Holes, New Mexico: comparisons to sorting across aeolian and fluvial bedforms

Dave W. Love<sup>1</sup>, Allan Gutjahr<sup>2</sup>, and Andreas Lazari<sup>3</sup>

<sup>1</sup>New Mexico Bureau of Geology and Mineral Resources, New Mexico Institute of Mining and Technology, Socorro, NM 87801, david.love@nmt.edu, <sup>2</sup>New Mexico Institute of Mining and Technology, Socorro, NM 87801 (deceased),

<sup>3</sup>Valdosta State University, Valdosta, Georgia, 31698

## Abstract

Unlike aeolian and fluvial grain-size distributions that vary longitudinally across bedforms, unimodal and multimodal grain-size distributions from individual laminae and thin beds across pyroclastic climbing dunes in exposures at Kilbourne and Hunts Hole maars remain similar, regardless of location on the dunes. By analogy with aeolian and fluvial deposits, distributions in the climbing-dune facies of these maar deposits are interpreted to be dominantly a fine-grained (0.15–0.35 mm) saltation mode, with removal of finer particles in suspension and incorporation of lesser creep fractions coarser than the saltation mode. In some laminae, coarser grains up to 10 mm in diameter are present. Like aeolian and some fluvial dune deposits, the saltation distributions may be described by the four parameters of hyperbolic distributions: slopes of asymptotes on fine and coarse sides of the distributions ( $\phi$  and  $\gamma$ ), abscissa of the vertex where the two limiting lines of the hyperbola cross ( $\mu$ ), and peakedness or the shape of the distribution near the mode ( $\delta$ ). Sampled saltation distributions from dunes at Kilbourne and Hunts Hole maars have gentler asymptotic slopes, compared to aeolian and fluvial deposits, and have slightly smaller average  $\mu$  and  $\delta$ . Removal of particles in suspension above individual laminae in the dunes appears to result in two kinds of logarithmic decreases in mass amounts on the fine side of the grain-size distribution curves. One type of decrease is very similar to steep decreases seen in aeolian and fluvial ripples and dunes, perhaps related to flow separation and suspension near the crests of the dunes. The other type is more gradual in laminae that have an order of magnitude more ash incorporated in the thin beds. If the saltation fraction is deposited by aeolian processes, impact threshold velocities at these two maars appear to be on the order of only 0.12 to 4 m/sec. Unlike experimental aeolian saltation fractions, which decrease in modal size and amount downwind in waning wind conditions, the pyroclastic saltation populations remain constant over a distance of at least 0.4 km at Kilbourne Hole, and the saltation populations at Hunts Hole are similar. Coarser-grained creep populations in the surge deposits appear to be more complex than their aeolian counterparts, and in some samples contain maximum grain sizes that are up to nine times coarser than the modal saltation values. The fractions coarser than the saltation mode exhibit a range of decreases in mass amounts and some samples appear to exhibit separate coarse modes similar to distributions seen in some aeolian granule megaripples and fluvial gravelly megaripples. In these pyroclastic surge deposits, coarse grains may have been added by fallout and entrained in thin beds mixed with saltating grains. However, if the coarse grains are mixed with a saltation population and emplaced as thin, dense, granular shear layers, the mechanisms responsible for deposition of discrete, continuous layers across large bedforms are unclear, perhaps analogous in some respects to granular shear layers in fluvial gravelly megaripples.

## Introduction

Phreatomagmatic processes forming various facies in tuffs along maar rims are interpreted to involve pyroclastic surges and dilute pyroclastic density currents generated under a variety of conditions, ranging from high-velocity, hot, dry, ash-laden pyroclastic density currents, to relatively cool, wet, mud-laden winds (Moore, 1967; Fisher, 1970; Waters and Fisher, 1971; Lorenz, 1973; Walker, 1983; Sheridan and Wohletz, 1983; Cas and Wright, 1987; Cole, 1991; Valentine and Fisher, 2000; White and Houghton, 2000; Houghton et al. 2000; Branney and Kokelaar, 2002; Gencalioglu-Kuscu et al., 2007; White and Ross, 2011; Sulpizio et al., 2014; Valentine et al., 2015; Breard and Lube, 2017), to even cooler, wetter pyroclastic density currents wherein steam condensed to water within the moving cloud and along the ground (e.g., Sheridan and Wohletz, 1983; Gencalioglu-Kuscu et al., 2007). Although volcanic eruptions have occurred subaqueously and through shallow groundwater (White and Houghton, 2000; Gencalioglu-Kuscu et al., 2007; White and Ross, 2011; Valentine et al., 2015), the co-eruption of quantities of sediment-laden water along with the pyroclastic surges and flows remains less investigated, even though many bedform descriptions were originally taken from fluvial sedimentology. Variables including temperature, density and concentrations of particles and dust within the ash clouds and a host of other properties make interpretations and models complex. The transport medium makes a big difference in the ways clasts are transported and sorted because rock clasts are more than 2000 times denser than air, whereas the same grains are only 1.8–2.6 times denser than water. In addition, the viscosities of the media are orders of magnitude different (Bagnold, 1979; c.f., Douillet et al., 2014). Thus, wind-driven ballistic impacts in air dislodge and move larger grains downwind as creep, but impacts in water do not. Other more massive and reverse-graded facies are likely generated as debris flows with interstitial fluids being either air or water. Mechanisms of transport and deposition of clasts in many types of pyroclastic deposits continue to be topics of investigation and discussion (Branney and Kokelaar, 2002; White and Ross, 2011; Andrews and Manga, 2012; Sulpizio et al., 2014; Douillet et al., 2014; Valentine et al., 2015; Breard and Lube, 2017). Recently, several researchers have begun wind-tunnel experiments that incorporate volcanic clasts and fine-grained “dust,” coarser-grained clasts on the wind-tunnel bed, and variable bed-slope angles (Andrews and Manga, 2011, 2012; Doronzo and Dellino, 2011; Douillet et al., 2014; Breard and Lube, 2017).

The thin laminae and their grain-size distributions across pyroclastic dunes generate questions and interpretations concerning the processes that resulted in their formation and preservation. Many discussions describe and interpret the generation of bedforms and some types of laminae during passage of pyroclastic surges and dilute pyroclastic flows. Interpretations have included settling of particles from suspension (Dellino et al., 2008), by individual eddies at the base of pyroclastic surges (Andrews and Manga, 2012), high-frequency fluctuations in velocities along the ground surface (Sulpizio et al., 2014), passage of “plug flows” and “traction carpets,” (Sohn 1997; Sohn and Chough, 1989; Douillet et al., 2015) and processes of “fluidization” (Wilson, 1980, 1984; Roche et al., 2004; Gravina et al., 2004; Girolami et al., 2015). Of particular interest is the transport, deposition, and formation of facies and bedforms at the base of pyroclastic surges and currents.

Some researchers approach the problem using principles of fluid dynamics and the physics of particle interactions within currents (Burgisser and Bergantz, 2002; Dellino et al., 2008; Andrews and Manga, 2012; Sulpizio et al., 2014). The basal layer where deposition takes place has been considered in terms of particle concentrations, particle-particle interactions, and rates of shearing within the layer (summarized in Sulpizio et al., 2014; basal granular-fluid flow of Breard and Lube, 2017). In contrast, a simpler set of approaches to gain an understanding of transport and sedimentation by wind, water, and debris flows, based on the basic physics of the ways the masses of individual particles are supported by either fluids or other particles, was offered by Bagnold (1941, 1966, 1968, 1973, 1977, 1979).

Fine particles transported by wind are supported in suspension by turbulent eddies; wind-blown sand grains are supported by episodic contact with the ground surface (saltation), and larger grains are bombarded and moved along the ground surface by impacts of saltating grains (short hops by large grains are called reptation; those that slide and roll are called creep). Grains avalanching down slip faces of dunes also move other grains in a down-gradient direction. Aeolian laminae are generated by at least three processes: the passing of low, wind-driven ripples across larger bedforms or planar surfaces, high-frequency fluctuations of wind speeds along the surface, and avalanching of grains down slip-face slopes of larger dune bedforms (Kok et al., 2012).

Sand grains saltate in water and go into and out of suspension similar to the way they do in turbulent air. Flowing water is more dense and viscous than air, so laminae may be generated by other processes, including planar sheet flow as well as passage of ripples and grain-avalanching off slip faces of ripples or dunes (Allen, 1982; Fourriere et al., 2010). Larger grains in flowing water move more by rolling and dragging along finer-grained beds, without ballistic impacts from other grains, particularly in low-gravel, low-gradient streams. Along gravelly channel bottoms, shear stresses within the bedload move larger clasts upward and they tend to remain at the surface, while smaller clasts move and aggrade beneath them (Bagnold, 1979). In addition, thin layers may be produced by the passage of hyperconcentrated flows or shearing processes within thin gravelly traction-sheets similar to debris flows. Also, along channel-margins,

slower-flowing backwaters and eddies, and under waning flows, finer grains settle from suspension to form climbing ripples and plane beds with continuous laminations. These are very different from the volcanogenic forms discussed herein.

We studied pyroclastic dunes from the rims of Kilbourne and Hunts Holes in southern New Mexico in order to compare grain-size distributions from laminated and thin-bedded maar deposits with previously studied bedforms in wind-tunnel experiments and other aeolian deposits, and from waning flows in rivers. The nature of basal pyroclastic “granular-flow pulses” versus aeolian and fluvial saltation and thin gravelly “debris-flow” sheets leads to questions concerning mechanisms of deposition and the amounts of sediment-laden water generated by phreatomagmatic eruptions at these maars.

Kilbourne and Hunts Holes are 2.7 and 2.4 km-wide, 91 and 76 m deep, late Pleistocene maars located 42 and 47 km southwest of Las Cruces, New Mexico, formed by phreatomagmatic eruptions followed by significant post-eruptive subsidence (Stuart, 1981; Seager, 1987). These are typical maars with low, outward-sloping rims of ejecta cut by collapsed craters below the former ground level as defined by Wood (in Cas and Wright, 1987, p. 376–377) and Vespermann and Schmincke (2000). Kilbourne Hole maar has an age of  $45 \pm 4$  ka (M. Zimmerer, pers. commun., 2017; c.f., Gile, 1987). Hunts Hole remains undated but appears to be similar in age to Kilbourne Hole. The climate is semiarid and depth to groundwater is now approximately 100 m, so little alteration of the ejecta appears to have taken place below the zone of soil development, although commonly the deposits are partially consolidated. Only slight erosion of associated deposits has taken place on the edges of the crater rims. Excellent exposures of bedded and laminated deposits in the maar rims show a progression and repetition of several volcanoclastic facies in 4 to 20 meter vertical sections (Stuart and Brenner, 1979; Wohletz, 1980; Stuart, 1981; Seager, 1987; Bahar, 1991). Bedforms associated with these deposits include massive beds, planar beds, several types of dunes including progressive and regressive forms, and scours (Waters and Fisher, 1971; Stuart, 1981; Sheridan and Wohletz, 1983; Cas and Wright, 1987; Cole, 1991; Douillet et al., 2013). Some of the crossbedded dune deposits are similar to fluvial, pebbly sand crossbeds in subaqueous dunes (Fig. 1). Others are similar to aeolian ripples, dunes, and granule megaripples.

At Kilbourne Hole, Bahar (1991) showed that individual beds within pale, sandy, cross-bedded dune deposits along the maar rim are more than 90 percent reworked fluvial pebbly sand from underlying ancestral Rio Grande deposits, and that darker, coarser beds consist of 25–27 percent juvenile basaltic clasts and 58–71 percent ancestral Rio Grande pebbly sand. The exposed deposits also show many beds with soft-sediment deformation, as well as cratered structures formed by impacts of volcanic bombs that embedded themselves in laminated deposits, indicating water saturation in the deposits shortly after initial deposition. Accretionary lapilli, also characteristic of wet phreatomagmatic deposits, are present at more than one stratigraphic level. The preservation of individual laminae and thin beds within climbing dunes where individual laminae can be traced across parts or all of the



Figure 1. Pyroclastic sand-wave bedforms exposed at Kilbourne Hole maar. A) Exposure of crest, lee, bottomset, stoss, and crest of successive climbing dunes on the southeast side of Kilbourne Hole where samples were taken. Trenching tool for scale. B) Closeup of migrating stoss, crest, and lee bedsets (type b dune of Cole, 1991). Tape measure is extended 30 cm.

bedforms (i.e., types b and c sand waves of Cole, 1991; very different from dunes described by Douillet et al., 2013; Fig. 1) permits sampling and granulometric analysis of discrete depositional units. Granulometric analyses of volcanoclastic deposits in general are important to understand mechanisms of mobilization, transport, and deposition of clastic grains, and secondarily for purposes of classification of these types of deposits (Wohletz, 1980; Sheridan et al., 1987; Bahar, 1991; Wohletz et al., 1995; Gencalioglu-Kuscu et al., 2007). At Kilbourne Hole, sampling was done in low-amplitude climbing dunes (Stuart and Brenner, 1979; type c sand waves of Cole, 1991), in which stoss, lee, and bottomset beds are preserved during aggradation on the south and southwest exposures

1.8 to 2.2 km from the center of the crater and about 4 m above the base of the surge deposits. Following bedding terminology summarized by Reineck and Singh (1980), the smallest-scale depositional units in the dunes consist of laminae and thin beds (Figs. 1, 3).

In this paper we (1) describe Bagnold's (1937) illustrative technique and Barndorff-Nielsen's (1977, 1979) hyperbolic mathematical models to characterize grain-size distributions; (2) present the results of grain-size analyses of individual laminae from climbing dunes along the rims of Kilbourne and Hunts Holes; (3) compare these results with Bagnold's (1941) experimental aeolian deposits created under waning wind conditions and other reported aeolian megaripples, and with deposits in waning-flow

fluvial dunes from the Rio Grande, (4) present hyperbolic models for some of the grain-size distributions and (5) speculate on the processes generating both the laminae and grain-size distributions.

## Methods

We sampled individual layers in dune bedsets that could be traced longitudinally over distances of a few meters because the dunes progressively climb down-gradient; stoss, crests, lee sides, and bottomsets are preserved. One particular bedset at Kilbourne Hole contains a pinkish clay coating that allows it to be traced laterally, so that adjacent bedsets above and below can be identified and sampled accordingly. In the climbing dunes we studied, crests progress down-gradient and increase in height, but due to thickened deposition on the lee slope and bottomsets, the bedsets shallow upward before the sequence tops out in nearly horizontal parallel laminae. Similar sequences of bedforms in the section may be interrupted by scour, with completely preserved bedforms above and below. We used the terminology shown in the Figure 3 field sketch, and sampled individual beds at locations indicated by letters on the sketch. Centimeter-scale samples of stoss, crest, lee, and bottomset beds of fine parallel laminae ranged in mass from 15–50 g. Coarse beds were sampled in masses as much as 1,400 g. We used quarter-phi-size brass sieves to determine the masses of grain sizes from 0.045 to 10 mm.

As an alternative to conventional probabilistic lognormal sedimentological methods, we use the graphical technique presented by Bagnold (1937, 1941) to illustrate grain-size distributions using log grain size–log mass frequency plots (discussed below). This illustrative technique is independent of assumed probabilistic models of distributions and is quasi-independent of sieves used as long as the sieve interval is relatively narrow. The technique also may show problems with aperture diameters in individual sieves if one assumes that the distribution curves should be smooth. In the following log-differential plots, it can be seen that some of the sieves are less than ideal, having mesh holes larger or smaller than labeled, such as the 0.212 mm sieve, producing downward deflections in the curves at 0.212 mm. Also note that the slopes of plots at the fine-grained ends (silt sizes) are likely influenced by the assumed size of the smallest fraction (0.001 mm). The illustrative technique has led to the formulation of hyperbolic probability distributions (Barndorff-Nielsen, 1977, 1979) that may be applied to aeolian and fluvial, and here to pyroclastic maar-rim deposits.

### Bagnold's illustrative technique and resulting models

Bagnold (1937, 1941) developed log-differential diagrams to illustrate grain-size distributions. He pointed out that sieves do not have ideal aperture sizes or uniform intervals between successive sieves. He also pointed out the large range in mass percentages caught on the sieves. In order to account for and normalize effects from non-ideal sieves and size intervals, the mass percentage for each size interval is divided by the difference in the logarithms of the sizes of the largest

and smallest clast (in mm) in the interval. The resulting number is plotted using a logarithmic ordinate, with the logarithmic midpoint of the size interval as abscissa. Such diagrams show small size-grade amounts equitably with larger amounts, and because each interval is quasi-independent of other intervals, the shapes of portions of the curves remain similar even if portions of other sizes are added or subtracted. The illustrative technique is independent of any assumed probability model for the distribution.

Traditional lognormal probability distributions are parabolas on log-differential diagrams, but as Bagnold (1937, 1941; Bagnold and Barndorff-Nielsen, 1980) has shown, size distributions of many aeolian and fluvial deposits are hyperbolic in shape (Fig. 2). Furthermore, Bagnold (1941) indicated that for “regular” aeolian sands, the slopes of the lines on the coarse and fine sides of the distribution curves (asymptotic lines) approach limits of approximately 9 and 2.5 respectively (“regular” sands are those with size-grading curves that illustrate nearly linear slopes descending from a modal value of grain diameter).

Barndorff-Nielsen (1977) developed a family of mathematical equations for hyperbolic distributions using four parameters. Hyperbolic distributions can be generated in both deterministic and random ways, including being the product of infinite mixtures of lognormal distributions. Unlike the four moment descriptors commonly used in sedimentology (mean, standard deviation, skewness, and kurtosis), the four hyperbolic parameters can be used quantitatively in probability expressions to model grain-size distributions.

Barndorff-Nielsen et al. (1982) showed that the four parameters of hyperbolic size distributions varied longitudinally across a small aeolian dune. Love et al. (1987) showed that fluvial grain-size distributions were also location-dependent, and varied as flow waned. In addition, they showed that sorting processes take place on at least two scales, affecting the four hyperbolic parameters in different ways in a down-flow direction.

### Mathematical treatment of log-hyperbolic distributions

As developed by Barndorff-Nielsen (1977) and applied by Love et al. (1987), hyperbolic distributions are generalizations of normal distributions and require four parameters. For appropriate grain-size data, the logarithm of the grain diameter is assumed to have a hyperbolic distribution. By analogy with lognormal distributions, the grain size is thus said to be a log-hyperbolic random variable.

If  $V = \ln d$  (where  $d$  is grain diameter), the probability density function of  $V$  with four parameters is:

$$\ln f(V) = C_0 - ([\delta^2 + (V - \mu^2)]^{1/2} (\varphi + \gamma))/2 + (V - \mu) (\varphi - \gamma)/2 \quad (1)$$

where  $\mu$  is the abscissa of the point where the asymptotes cross,  $\delta$  is a scale parameter influencing the sharpness of curvature of the peak, and  $\varphi$  and  $\gamma$  represent the slopes of the asymptotic lines of the hyperbola.  $C_0$  is the ordinate of the point where the two limbs of the hyperbola cross above the vertex, and is a constant related to an expression involving  $K_1$ , which is a modified Bessel function of the third kind with index  $\nu = 1$ .

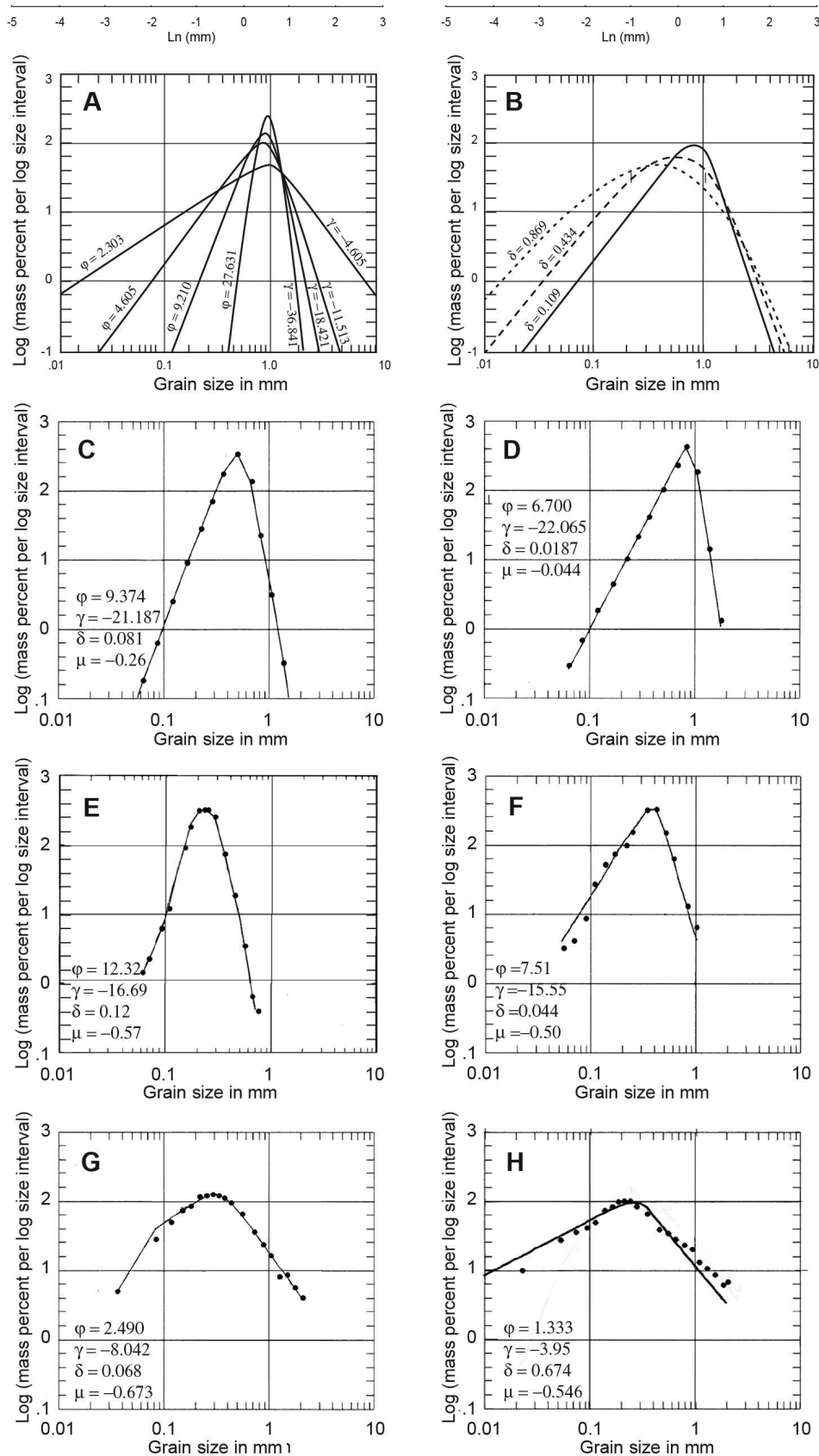


Figure 2. Hyperbolic models of grain-size distributions. A) Effect of slopes of asymptotes ( $\phi$ ,  $\gamma$ ) on shapes of hyperbolic grain-size distributions. Upper abscissa scale is  $\log_{10}$ , lower scale is natural log. B) Effect of parameter  $\delta$  on peakedness of hyperbolic distributions. C, D) Hyperbolic fits (lines) to grain-size data (dots) for aeolian deposits. Data from Bagnold (1941) are “regular” (C, saltation) and “skewed” (D, ultimate creep) modes, showing hyperbolic shapes and slopes of the coarse and fine limbs of the curves. Hyperbolic model parameters ( $\phi$ ,  $\gamma$ ,  $\delta$ , and  $\mu$ ) are  $\log_{10}$  values. E, F) Fluvial examples are an upper foreset of a sandy dune, and a large ripple, both from the Rio Grande (Love et al., 1987). G, H) Pyroclastic-surge examples from bottomset and stoss locations from Kilbourne Hole deposits (v and t respectively in Fig. 3).

According to Barndorff-Nielsen (1977),  $C_o$  can be calculated as follows:

$$C_o = \ln [\omega/\delta\kappa K_1(\delta\kappa)] \quad (2)$$

where

$$\kappa = (\varphi\gamma)^{1/2} \quad (3)$$

$$\omega = \frac{\varphi\gamma}{\varphi + \gamma} \quad (4)$$

If (1) is used to describe the behavior of  $V = \ln d$ , the proportion ( $P_i$ ) of grains with  $d$  between  $d_{1i}$  and  $d_{2i}$  can be calculated by letting  $V_{1i} = \ln d_{1i}$ ,  $V_{2i} = \ln d_{2i}$  and evaluating

$$P_i(\mu, \delta, \varphi, \gamma) = \int_{V_{1i}}^{V_{2i}} f(V; \mu, \delta, \varphi, \gamma) dV \quad (5)$$

If  $\ln d_{1i} - \ln d_{2i}$  is small, then the ratio  $P_i/(\ln d_{1i} - \ln d_{2i})$  approximates the hyperbolic probability density.

The mode, or maximum value for the probability density function is given by

$$V_m = \mu + \delta(\varphi - \gamma)2\varphi\gamma \quad (10)$$

The four parameters are estimated using a maximum likelihood iterative technique

$$MLE = \sum_{i=1}^m r_i \ln P_i(\mu, \delta, \varphi, \gamma) \quad (11)$$

where  $r_i$  is the observed proportion of grains found in the range  $d_{1i}$  to  $d_{2i}$ . We used the Rosenbrock hill-climbing method with constraints (Kuester and Mize, 1973) to approximate the integral for  $P_i$ .

For illustrative purposes, the abscissa on the data graphs presented here use a  $\log_{10}$  rather than a natural log scale and  $\mu$ , the point on the abscissa where the two asymptotes cross, is left in  $\log_{10}$  units rather than mm. Because one of the four parameters used in Barndorff-Nielsen's analysis is designated  $\varphi$ , we use  $\varphi$  for the mathematical parameter and use the spelled-out term "phi-size" to distinguish the commonly used sedimentological units of sieve size. Figures 2A and B illustrate how the slopes of the two asymptotes ( $\varphi$  and  $\gamma$ ) affect the shape of the distribution, and how the scale parameter ( $\delta$ ) affects the sharpness of the peak of the distribution.

Bagnold and Barndorff-Nielsen (1980) show that on log size-linear percent graphs, the hyperbolic distributions can be used to illustrate the properties of skewness and kurtosis commonly used to describe deviations from normal probability distributions.

## Comparisons of grain-size distributions from maar-rim, aeolian, and fluvial deposits

### Kilbourne and Hunts Hole bedforms and distributions

As Figure 3 shows, variability of size distributions is large from similar locations on a dune (such as stoss, crest, lee, or bottomset beds), but size distributions along individual beds are similar, despite location on the form. At most,

lee-location beds tend to have slightly more rounded modal portions (Fig. 3: d, v) due to increased amounts in the 0.3 to 2 mm range relative to the adjacent stoss and bottomset samples. Some beds show unimodal hyperbolic distributions, but exhibit variable coarse and fine slopes. The decreases in masses of grains finer than about 0.2 mm have two types of slopes—steep slopes (Fig. 3: k, l, n, q) and gradual slopes (Fig. 3: a, e, g) (Stuart, 1981). Those with gradual slopes are apparently affected by a large (up to 33 percent) fraction of grains less than about 0.09 mm in diameter. Similarly, the coarse sides of the distributions have more than one type of slope, some steep, some gradual, and some extending subhorizontally with significant coarse fractions between 0.9 and 10 mm in size (Fig. 3: l, m, p). Many of the distributions have hyperbolic shapes in sand sizes, with additions of coarser fractions (Fig. 3: j, k). The coarser fractions may or may not be in separate modes (Fig. 3: k, l, m, p, q). In some cases the distribution on the coarse end is nearly flat over a wide range of sizes, and decreases in a "regular" manner on the fine side of the distribution (Fig. 3: m, p). Samples from similar locations along, above, and below the pink marker bed on the next well-exposed dune away from the crater (a few meters down-gradient) showed nearly identical size distributions. Samples from a smaller, more distal bedform 2.2 km from the center of Kilbourne Hole showed similar unimodal distributions. In particular, the mode and the shape of the fine portions were nearly identical to the distributions observed from samples obtained closer to the center of the maar (e.g., Fig. 3: g, u, w).

At Hunts Hole, samples were taken from fine and coarse bottomset, stoss, crest, and lee positions along beds forming a large climbing dune with a progressively enlarged amplitude of over 3 m, similar to the one illustrated by Stuart (1981, fig. 3). Except for the coarsest fractions, the distributions along the fine-grained bed are similar, very "regular," and match the fine-grained distributions at Kilbourne Hole (Fig. 4). The coarse lee sample (Fig. 4F) shows a separate coarse fraction with a mode of 2.18 mm (mid-point), similar to some of the distributions from Kilbourne Hole samples (e.g., Fig. 3: k, n, o, q).

### Grain-size distributions from wind-tunnel experiments and other aeolian investigations

Although many studies of aeolian transport following Bagnold (1941) have addressed sand saltation and suspension of dust, few have examined the processes of creep or reptation (cf., Rice et al., 1995; Rasmussen et al., 1996; Butterfield, 1999; Zou et al., 2001; Dong et al., 2002; Namikas, 2003, 2006; Yizhaq, 2008; Duran et al., 2011; Kok et al., 2012; Qian et al., 2012; Farrell et al., 2012; Ho et al., 2014; Rasmussen et al., 2015; Valance et al., 2015; Mayaud et al., 2017). A literature search did not reveal other investigations replicating or expanding on Bagnold's (1941) investigations of creep in decreasing winds. Bagnold (1941) constructed a wind tunnel with a sediment trap to collect the creep fraction, and a ceiling that diverged downwind to decrease wind velocity (Fig. 5A). He spread sand with a broad range of sizes on the upper end of the tunnel, ran experiments at several wind velocities, and analyzed the amounts and grain sizes at down-tunnel locations. His experiments show that first, as wind slackens down gradient, the amount of

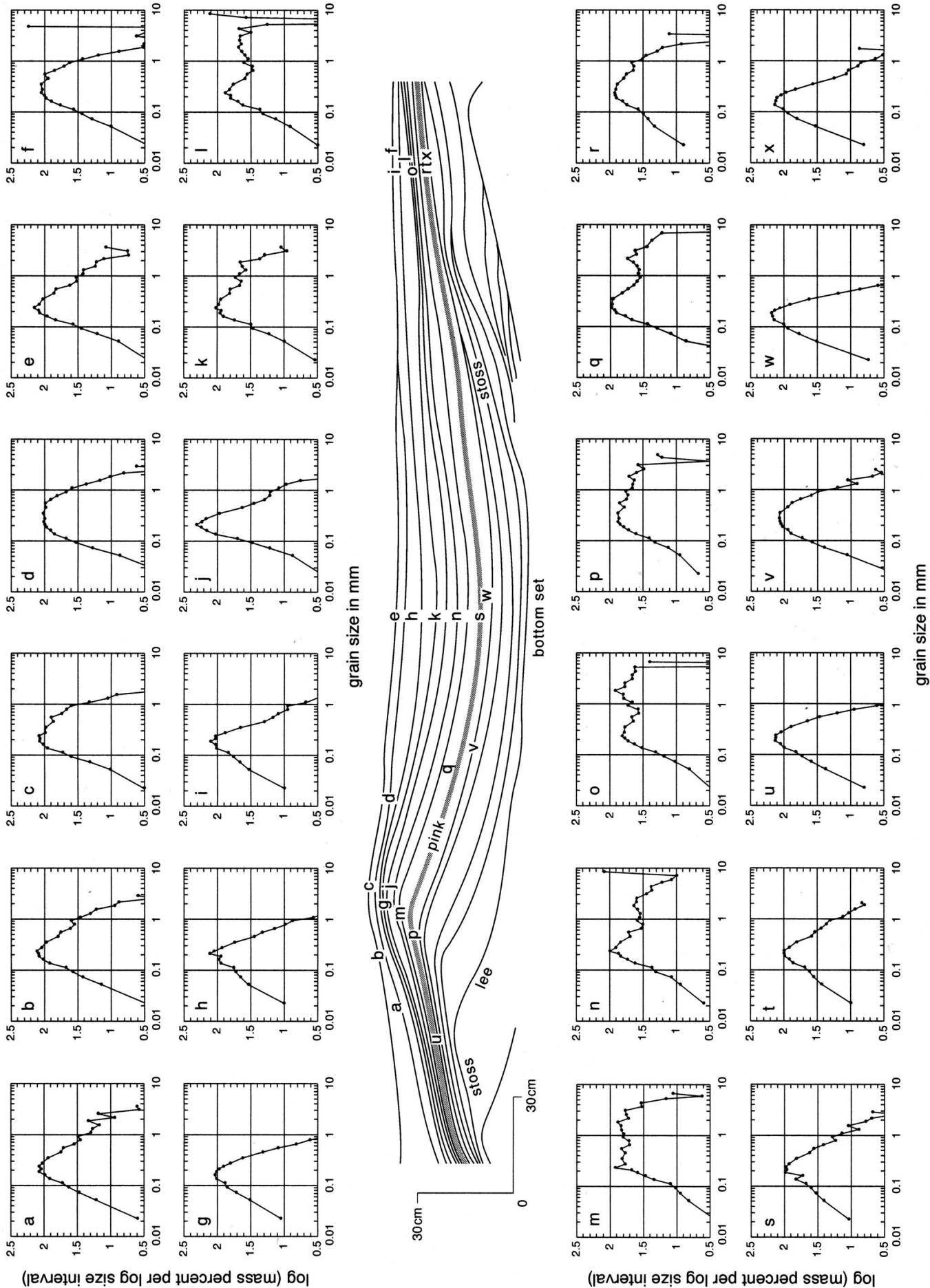


Figure 3. Labeled sketch of climbing-dune bedforms at Kilbourne Hole maar, and grain-size distributions from stoss, crest, lee, and bottomset locations. Sample locations for corresponding data plots are shown on the sketch. The bedforms were sampled on the southeast side of the maar, 1.8 km from the center. "Pink" on sketch refers to distinctive marker bed discussed in text.

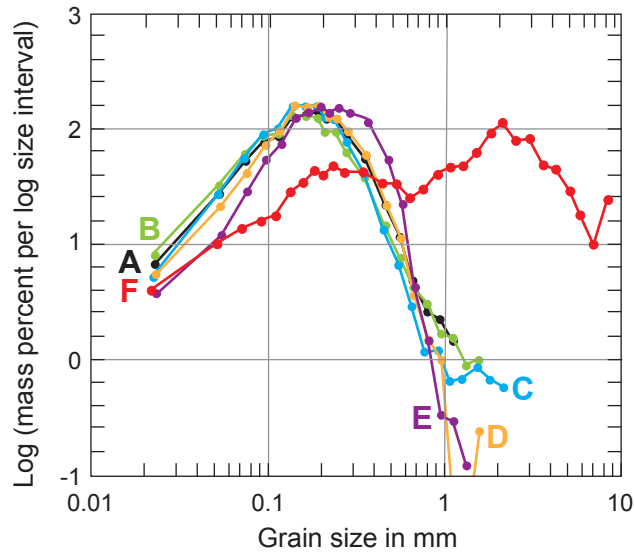


Figure 4. Grain-size distributions from Hunts Hole large climbing dune. A) Fine stoss; B) Fine crest; C) Fine lee; D) Medium-coarse stoss; E) Medium-coarse lee; F) Coarse lee.

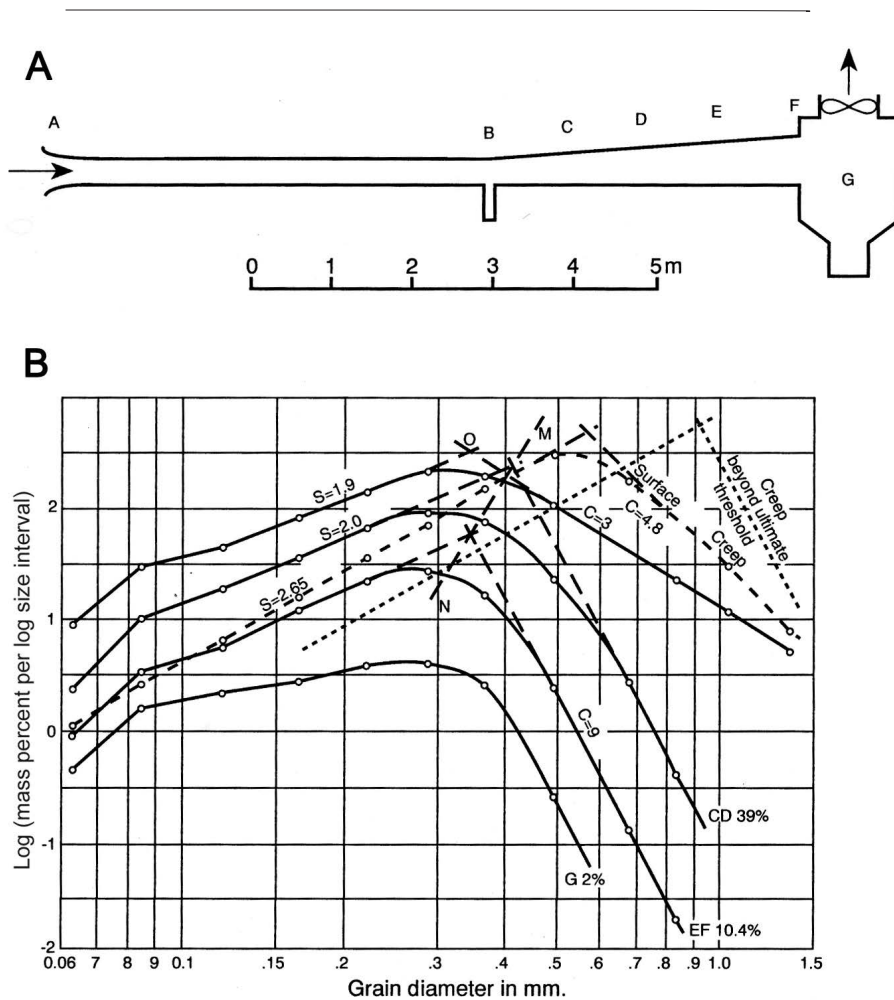


Figure 5. Sketch of Bagnold's wind tunnel and grain-size distributions from different locations after experiments under strong, but decreasing wind conditions (redrawn from Bagnold, 1941). A) Longitudinal section of wind tunnel showing creep trap ("B") and other sample locations along expansion reach of decreasing wind velocity. B) Grain-size distributions under strong wind conditions after only two minutes. Upper solid curve is beginning distribution. Individual curves below are labeled by sample locality in the wind tunnel, and percentage of beginning mass of sand mobilized when sample was taken. Slopes of the asymptotic lines on the fine and coarse sides of the distributions are indicated by "S =" and by "C =". Note that the modal grain size decreases downwind from M to N ("O" is the original sand mixture). The mode of the surface creep (dashed lines, from creep-trap samples) coarsens from 0.55 to about 0.9 mm in hypothetical "ultimate creep" (short dashed lines to right of others).

sand in transit decreases and the peaks of the size distributions get finer in proportion to the decreasing amounts (Fig. 5B). Initially, the wind-sorted bed had peak sizes smaller than that of the original mixture of sand. Later, as the experiment continued, the bed stabilized at coarser sizes, but with the same proportional decrease in size downwind. Second, the slopes of the hyperbolic lines increased to 9 for the coarse-end slope and near 2.5 for the fine-end slope (except for the sediment trap samples at the downwind end of the tunnel). Third, surface creep also resulted in a “regular” distribution, but had different asymptotic slopes (Fig. 2D; Fig. 5B; surface creep and creep beyond ultimate threshold). Thus, the creep distribution affects the size distribution of downwind deposits as the creep load overtakes them, increasing the amount of the coarsest sizes and decreasing the coarse-end slope. Strong winds shift the creep distribution to even coarser sizes and steepen the slope of the coarse end of the distribution.

Williams (1964) ran experiments on sorting of different shapes of sand grains saltating in a wind tunnel that did not expand downwind. The size distributions of grains closest to the floor of the tunnel (within 0.5 cm above the surface) were similar to those of Bagnold’s creep fraction, while those saltating to greater heights were similar to Bagnold’s “regular” saltation fractions. Williams concluded that initial surface size distribution and sphericity as well as the impact shear velocity gradient affected the size proportions in saltating grains.

Anderson (1990) and Anderson and Bunas (1993) investigated and modeled ripple-migration laminations described by Hunter (1977). Coarse grains move less than fine grains when impacted by other sand grains so they tend to concentrate near the crests of the ripples, whereas finer grains move farther and tend to gather in the lower lee faces and troughs of the ripples. This process leads to the generation of nearly planar, fine and coarse laminae as ripples move and climb downwind.

Rice et al. (1995) investigated the effects that three-sizes of saltating “impactor” sand grains had on beds of sand having three different sand sizes. As expected, they demonstrated that smaller sizes of sand on the bed were ejected at larger concentrations and speeds whereas larger grains were ejected at lower speeds and made only short “hops.” They suggested that grains could be sorted by the distances they move, with smaller grains moving farther and more quickly downwind, leaving larger grains behind, while large grains moved more slowly over shorter distances, perhaps forming separate coarse populations.

Namikas (2003, 2006) investigated particle sizes, mass fluxes, and energy partitioning of saltating aeolian sand grains. He concluded that there is a constant kinetic energy level at liftoff for all sand size classes, which therefore reflects an inelastic impact regime between the saltating grains and the loose bed. Following Anderson (1990) and Rice et al. (1995), Namikas suggested that this provides a mechanism for size sorting wherein larger grains “hop” or reptate only short distances close to the bed whereas smaller grains take higher, longer trajectories. This may explain Bagnold’s (1941) and Williams’ (1964) results regarding sizes of “creep” along the floor of the expanding wind tunnel.

A lesser amount of literature describes and models aeolian ripples that are larger and coarser than normal aeolian ripples, known as “ridges,” “aeolian megaripples,” “gravel ripples,” or “granule ripples.” Among others Yizhaq (2008) and Qian et al. (2012) summarized what is known about granule ripples. Yizhaq (2008) presented a model for their generation, whereas Qian et al. (2012) measured wavelengths, heights and grain sizes in granule ripples generated in four areas of the Kumtagh Desert, China. The granule ripples had wavelengths between 0.31 and 26 m with heights between 0.015 and 1 m. The granule ripples had bimodal or trimodal grain-size distributions with fine modes between 0.105 and 0.125 mm and coarse modes at 2 mm. Some of these coarse ripples had a secondary coarse mode between 1 and 1.25 mm. None of the coarsest grains were more than 4 mm in diameter. The distributions shown by Qian et al. (2012) are similar to those that include very coarse fractions shown in Figures 3 and 4, but the bedforms and internal stratigraphy of the granule ripples are dissimilar to the pyroclastic deposits. Yizhaq’s (2008) model generated granule megaripples by concentrating reptating coarse grains (<4 mm) on larger ripples and coalescing ripples into megaripples with coarse crests and finer stoss, lee, and bottomsets.

### Grain-size distributions from waning-flow bedforms of the Rio Grande

Love et al. (1985, 1987) illustrated grain-size distributions from subaqueous sandy ripples and dunes and gravelly megaripples from waning flow in the Rio Grande near Socorro, New Mexico. Many of the sandy distributions are either unimodal (Fig. 2C, D), or bimodal, which could be modeled by mixing two hyperbolic distributions. The dominant hyperbolic distributions are considered to be the saltation fraction, either forming sandy ripples or redeposited as the ripples cascade off slip faces of larger bedforms. Coarser sand and gravel fractions are not hyperbolic and are multimodal (illustrated below). It is possible that due to dispersive stresses of granular flow along the long stoss surfaces of the gravelly megaripples, the coarsest grains are concentrated at the surface of the bedforms and that grains below the surface are less coarse. In the sampled gravelly megaripples the very-fine-sand and silt fraction formed a separate mode even though most of the fine-grained fraction (between 0.06 and 0.2 mm) behaved similarly to the fine fractions of sandy fluvial dunes.

## Discussion

The maar-rim dunes we studied are consistently well-organized forms with multiple fine laminae and thin beds creating the bedforms. They have consistent grain-size distributions, suggesting some uniformity in mechanisms of transport and deposition. The modes of the main sand-sized fractions (0.15–0.35 mm) are rather fine-grained and are similar to both saltating wind-blown sand and fluvial dune crests. The steep and gradual types of linear decreases in amounts of fine fraction (less than about 0.2 mm), described earlier, suggest that fine grains are commonly only partially transported away in suspension, or are incorporated in laminae of dunes in more than one way. The differences in amounts of fine grains (at least an order of magnitude) in the two types is illustrated in Figure 6C (f and o versus n and q). Those distributions

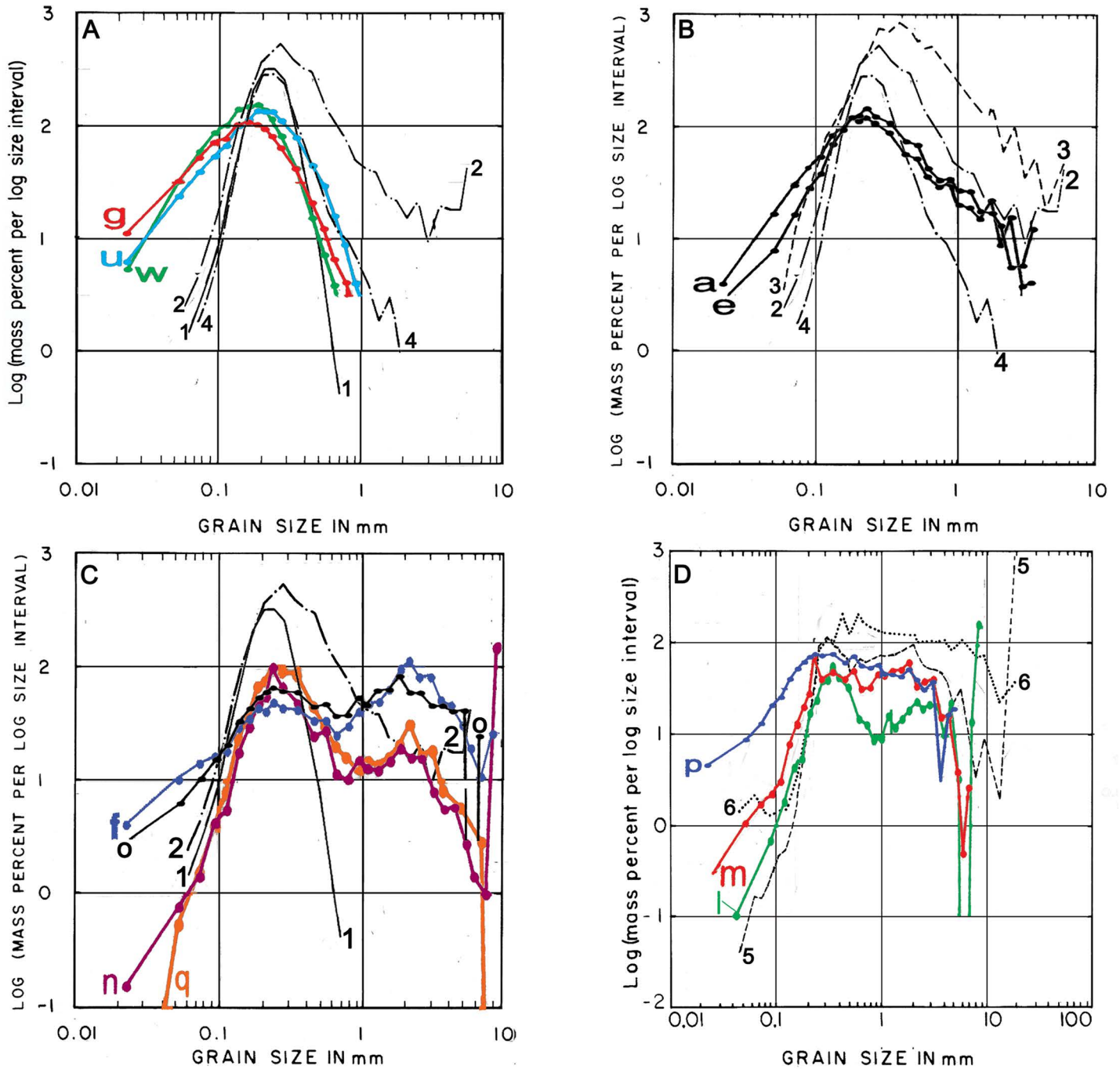


Figure 6. Comparison of grain-size distributions of upper foresets from sandy and pebbly megaripples in the Rio Grande (numbered lines, from Love et al., 1985, 1987), and laminated dune deposits from Kilbourne Hole (lettered lines— see Fig. 3 for sample locations). A) The volcaniclastic dune distributions are slightly finer grained than the fluvial dunes, and the shapes of the peaks are also different. The slope of the coarse-side fractions ( $\gamma$ ) for the volcaniclastic deposits are similar to those for the fluvial sandy dunes. The slope of the fine-grained limbs ( $\phi$ ), however, are different from the fluvial examples. The amounts of fine sand and silt (probably fragmental ash) are nearly an order of magnitude more than in the fluvial examples. B) For the volcaniclastic samples, the modes are finer and the peaks broader than the fluvial examples, coarser grains are within the range of the fluvial examples, and the slopes of the finer fractions are more similar to the fluvial examples than in Fig. 6A. C) These curves were selected as examples of coarser-grained volcaniclastic deposits showing bimodal distributions. Included is a sample from Hunts Hole (curve "F" from Fig. 4). The modes for the saltation fractions are all between 0.2 and 0.3 mm. Coarser fractions (>0.9 mm) for the surge deposits in these examples appear to have a separate mode between 2 and 3.5 mm. D) Examples of coarser-grained deposits from Kilbourne Hole, together with two samples from coarser-grained fluvial megaripples from the Rio Grande (Love et al., 1985). Note that the distributions still have a saltation mode between 0.2 and 0.35 mm, with a flat or slightly peaked distribution from 1 to about 6 mm.

showing relatively large amounts of fine sand and silt (gradual fine-end slopes) are distinctly different from fluvial sandy megaripple deposits. Other distributions show a substantial decrease in sand and silt smaller than the modes, similar to decreases seen in fluvial sandy dune deposits (e.g., Fig. 6C, D).

Two observations may bear upon the question of why there are two types of decreases on the fine end of the hyperbolic distributions. First, low amounts of fines appear to correlate with a well-defined gravel mode that makes up less than half of the whole distribution (e.g., Fig. 6C: n and q). Second, if one considers flow separation and attachment similar to fluvial examples, perhaps both flow separation and movement of a coarser gravel mode could increase suspended load so less ash (particularly in lee and bottomset positions) is deposited down-gradient.

Considering an aeolian analogy for deposition of the pyroclastic deposits, the distributions may be explained as mixtures of saltation and one or more coarse (possibly creep) populations. The data are suggestive, but we certainly cannot prove that these populations are generated in such an analogous manner, or that other mechanisms of sorting are not taking place. The variability of fine and coarse slopes of the saltation populations suggests that the processes of saltation impacts, producing short hops for larger grains and longer flights for smaller grains, are only partially initiated and not as complete as the processes resulting from aeolian and fluvial transport. The amounts of fine grains incorporated in the saltation fraction may also depend on the concentration of dust near the surface during transport.

The small size range of the fine mode (between 0.125 and 0.350 mm) of the putative “saltation” fraction is perhaps surprising, considering the documented turbulence of pyroclastic density currents (Moore, 1967; Thorarinsson, 1967; White and Houghton, 2000). However, the important part of the pyroclastic cloud from a depositional standpoint is near the ground surface, where velocities go to zero and basal shear is set up. From Bagnold’s (1941) and Anderson and Hallet’s (1986) work, at ambient atmospheric conditions of temperature and pressure, the calculated critical-impact shear stress for saltating grains would be on the order of only 0.02 to 0.05 N/m<sup>2</sup>, and the impact threshold velocity would be on the order of 0.12 to 2 m/sec. Douillet et al. (2014) calculated velocities between 1.26 and 3.95 m/sec to drive saltating granules (2–4 mm) of scoria in their wind-tunnel experiments, depending on pressure and temperature of the atmosphere within the pyroclastic currents. Following Walker (1984), both the climbing aggradation of lamina in the bedforms and the rather small dominant size of the saltation fraction suggest wind speeds near the ground may not have been substantial, or that other factors (such as moisture or abundant suspended dust) were modifying the depositional conditions.

In the dunes we sampled, the mechanisms sorting the coarser grains did not produce the uniform distributions exhibited by the finer mode, suggesting that processes sorting coarse grains are not as uniform, continuous, or as long-lasting as those in normal aeolian dunes. Coarse grains may have been added initially by fall out of ejecta, but the grains have been entrained in the transporting medium and deposited with the rest of the grains. Coarse modes are up to nine times larger than fine modes, possibly

suggesting that large saltating grains played a dominant role in movement of the creep contribution to the coarse side of the grain-size distribution.

However, the incorporation of grains as large as 1 cm in diameter raises questions about mechanics of transport and deposition of the grains. First, aeolian creep and reptation of coarse grains requires saltating grains to dislodge and drive them along the surface. The coarsest of the saltation grains are 2–3 mm in diameter and are only a small fraction of the total, while the modes of the saltating population are less than a tenth as large, so how many of these grains must frequently impact the larger grains to drive them along? Second, if the decrease on the coarse end of the saltation fraction is due to lessening reptation of increasingly coarse grains, why is there a separate increase in even coarser grains (in samples with distinct coarse modes, including some with more coarse mode than saltation mode)? Third, are both the saltation and coarser populations produced during the same transport episode, or might they be inherited from separate processes? For example, could the saltation fraction and incorporated amount of fines be generated during part of an episode of pyroclastic flow, while the coarser fraction is generated as a thin debris flow that incorporates the saltation fraction too? Fourth, if the proposed debris-flow mechanism is viable, how does it follow bedform topography rather than concentrate along bottomsets? Is it dry or water-saturated? If possible, tracing individual beds over longer distances may provide evidence for “downwind” sorting.

Yet, similar size distributions from different locations in the climbing-dune facies of the maars at Kilbourne and Hunts Holes argue for similar depositional conditions and mechanisms. These mechanisms must be set up at the base of the pyroclastic cloud without regard for variations in velocities within the clouds, and must be maintained over distances of at least 0.4 km. Such conditions must have been maintained at a nearly constant threshold shear velocity and critical shear stress over distances at least on an order of hundreds of meters, producing nearly identical sorting. Additional wind-tunnel experiments would probably provide stronger evidence for these mechanisms under dry base-surge conditions. The range in amounts of the coarse fraction(s) suggests that the mechanism for transporting and depositing coarse grains does not depend on ballistic-impact drivers.

Considering that many historic phreatomagmatic eruptions also disperse large amounts of water, a water-transported analogy should be considered as an alternative for deposition of the pyroclastic-surge dunes. Clearly the bedforms are different from “normal” subaqueous dunes and ripples. However, some of the grain-size distributions are remarkably similar to distributions from bedforms deposited in the Rio Grande (Fig. 6). The sand fractions of the surge deposits coarser than the modes are similar to fluvial sandy dunes; some have steep decreases in amounts of coarser grains, whereas others have larger, variable amounts of coarser grains (Fig. 6A, B). The coarse sand-granule-small pebble fractions may derive from a separate mode (Fig. 3: l, n, o, q; Fig. 6B, C, D), which is also similar to distributions observed in some fluvial deposits (c.f., Love et al., 1985, 1987). The fact that most of the sand fraction in the surge deposits is derived from reworked ancestral Rio Grande deposits

might indicate that the distribution is partly inherited, but the sorting must still take place under conditions of transport and deposition in the bedforms as they develop, and fine-grained clasts must still be winnowed away in a log-hyperbolic fashion.

Individual laminae or thin beds were deposited on top of the previous layers with minimal reworking of the underlying layer (i.e., coarse clasts, if present, stay within the previously deposited layer). If the dunes with their thin beds were laid down by shallow moving water, the implication would be that the water depth was at least as much as the height of the dunes, but that seems extremely unlikely. One could envision that an individual lamina could be laid down by an individual pulse of shallow, muddy water, hyperconcentrated flow, or a thin, wet debris flow driven laterally by hydromagmatic explosions and/or cloud collapse. One could envision runout zones similar to those at distal positions of alluvial fans where muddy water, hyperconcentrated flows, and debris flows spread into sheet flows producing thin laminated bedsets.

The water could come out of the developing crater as steam-driven pulses with incorporated sand from underlying ancestral Rio Grande deposits, or from condensation of water from clouds of steam moving away from the crater. The former condition would explain the erosion, transportation, and deposition of these sandy deposits, but the latter mechanism would still need to explain how adequate amounts of sand and coarser grains could fall out of clouds, be entrained by a wet fluid, and make consistent bedforms and grain-size distributions over broad areas.

Bagnold (1977) showed that in flowing water, the bedload transport rate decreases as an inverse function of the ratio of flow depth ( $Y$ ) to bedload grain size ( $D$ ),  $Y/D$ , so that where flows spread out and  $Y$  becomes shallow, larger clasts are deposited and the size of transported clasts decreases down gradient as  $Y$  decreases. However, if the coarsest fractions are added from ballistic fallout, large clasts may not decrease solely by mechanisms related to transport in flowing water. If the coarse grains are transported in thin debris flows, they would tend to move toward the free surface and toward the front of the flows (Bagnold, 1977), perhaps increasing the lateral extent of coarse grains. If each blast of hypothetical flowing water wanes at each location and away from the constructional maar rims, why are sandy ripples and fine-grained plane beds, so pervasive in sandy bedforms in waning fluvial-flow regimes (e.g. Allen, 1982; Love et al., 1987), not abundant? Probably because such a mechanism did not happen. If the saltation and larger grain-size fractions are mixed together to form laminae across the dunes, is it possible that thin, wind-driven, wet debris flows only a few particles thick, incorporating larger grains as well as saltation populations, could move across and deposit laminae uniformly on climbing dunes? Wet debris might be able to stick to and not erode previously formed topography better than dry, wind-driven avalanches. After all, muddy debris is a small step beyond mud-encrusted grains (pink layer and accretionary lapilli) known from these deposits.

Bimodal grain-size distributions of pyroclastic deposits have been reported from many other volcanoes, such as Mount St. Helens, Washington (Rowley et al., 1985), Campi Flegrei, Italy (Dellino et al., 2004), Cora Maar, Anatolia (Gencalioglu-Kuscu et al., 2007), Tungurahua,

Ecuador (Eychenne et al., 2012), and Hekla volcano, Iceland (Janebo et al., 2018). None of these bimodal distributions is attributed to more than one mode of transportation and deposition. Instead, most of the distributions are within proximal massive or reverse-graded deposits and attributed to direct settling from pyroclastic density currents.

## Hyperbolic fits to aeolian, fluvial, and pyroclastic dune deposits

Where aeolian and fluvial saltation populations and pyroclastic-surge grain-size distributions appear to be unimodal hyperbolic distributions (Figs. 3, 6A, 6B), hyperbolic curves may be fitted to them (Fig. 2). A wide range in the four model parameters is indicated, particularly in the slopes of the asymptotes and peakedness ( $\phi$ ,  $\gamma$ , and  $\delta$ ). The parameters  $\phi$  and  $\gamma$  for aeolian distributions are consistently larger (steeper slopes) than for the pyroclastic-surge dunes. Fluvial distributions show a wider range in  $\phi$  and  $\gamma$  (particularly  $\gamma$ ) than aeolian distributions, but not as broad as pyroclastic dune distributions. Parameters  $\delta$  and  $\mu$  for aeolian distributions are only slightly larger and smaller, respectively, than for surge distributions (Fig. 2). If more than one population is present, two or more curves may be suggested (Figs. 3, 6). However, because the coarse population is never found by itself without the finer population, we have not determined the nature of the coarse population(s), or the nature of the overlap between the two suggested distributions. Do bimodal distributions reflect mixtures of two continuous, overlapping distributions, as Bagnold (1941) interpreted for bimodal aeolian sands, or are they truncated at either coarse or fine ends due to changes in transport and depositional mechanisms? In waning flow in the Rio Grande, small bedforms overtook larger bedforms to mix grain-size populations, but there is no evidence of small bedforms preserved in the pyroclastic-surge dunes.

An iterative technique to obtain best-fit estimates for two overlapping hyperbolic distributions was not developed here. It is straightforward, however, to mix two hypothetical distributions with specified parameters to construct bimodal distributions (Fig. 7). Such combinations can clearly mimic bimodal distributions from Kilbourne Hole, Hunts Hole, or from other pyroclastic deposits such as those mentioned above. In previous interpretations of “base-surge” grain-size distributions (Wohletz, 1983; Bahar, 1991; Wohletz et al., 1995), as many as five physical processes were invoked to explain inferred mixtures of lognormal populations as combinations of ballistic, rolling, saltation, and suspension populations. However, similar distributions may be reconstructed by combining just two hyperbolic distributions. This illustrates the hazard of interpreting populations based on assumptions about models and the difficulty of interpreting transport mechanisms solely from multiple lognormal fits to granulometric data.

## Conclusions

We compared grain-size distributions from laminae in pyroclastic-surge dunes from maar rims at Kilbourne and Hunts Holes with distributions from aeolian and fluvial deposits, and illustrated the log-differential nature of grain-size distributions of these laminae. We

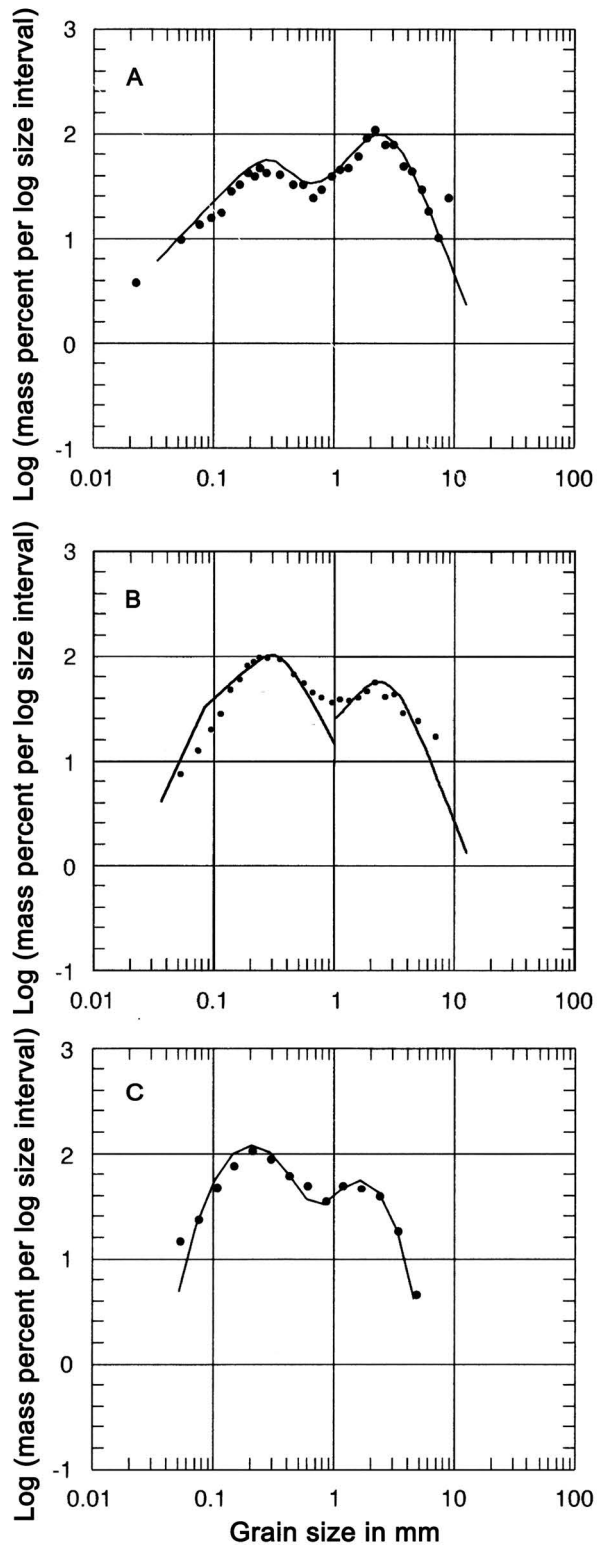


Figure 7. Combined hyperbolic distributions (lines) that mimic bimodal data (points) from base-surge deposits. A) Mixture of two distributions that reproduce a bimodal distribution from Hunts Hole (mix 42 percent  $\phi = 1.228$ ,  $\gamma = -1.718$ ,  $\delta = 0.307$ ,  $\mu = -.548$  with 58 percent of  $\phi = 2.17$ ,  $\gamma = -3.32$ ,  $\delta = 0.569$ ,  $\mu = 0.326$ ). B) Mixture of two distributions that reproduce a bimodal distribution from Kilbourne Hole (mix 66 percent  $\phi = 2.490$ ,  $\gamma = -8.042$ ,  $\delta = 0.068$ ,  $\mu = -0.673$  with 34 percent of  $\phi = 2.17$ ,  $\gamma = -3.32$ ,  $\delta = 0.569$ ,  $\mu = 0.996$ ). C) Mixture of two hyperbolic distributions that reproduce a bimodal distribution from Kilbourne Hole (data from Wohletz (1980) sample 8 A1; half phi-size sieve intervals (mix 29 percent of  $\phi = 6.05$ ,  $\gamma = -19.24$ ,  $\delta = 1.95$ ,  $\mu = -0.674$ , with 61 percent  $\phi = 18.605$ ,  $\gamma = -9.079$ ,  $\delta = 3.620$ , and  $\mu = 0.149$ ).

interpreted these pyroclastic-surge grain-size distributions as having saltation modes that are as fine-grained or finer than modes in aeolian and fluvial dunes. The saltation fractions from surge laminae exhibit log-hyperbolic distributions that are much more spread out (lower slopes  $\phi$  and  $\gamma$  of the fine and coarse sides of the distributions). If moving air is the transport medium, the addition of fines and/or moisture may have affected the nature of ballistic collisions and resulting driving forces on the dominant grains, but the cumulative processes affecting transport and deposition of individual grains still generated hyperbolic saltation populations. Many fine-end limbs of the hyperbolic distributions have an order of magnitude more fine sand and silt (ash) than their aeolian and fluvial counterparts, but others have steeply decreasing amounts of fine sand and silt, similar to their aeolian and fluvial counterparts. These slopes on the fine end of the distribution curves must reflect the amount of removal of fine particles through suspension.

The parts of the distributions coarser than the saltation fraction may be creep components, similar to aeolian granule-megaripple distributions, but most are more similar to fluvial bedload distributions from gravelly megaripples. Some grain-size distributions have more coarse grains and larger clasts than would be driven by ballistic impacts of saltating grains. We suspect that these coarse grains may have moved as thin, granular basal shear flows mixed with an already existing saltation fraction, but the mechanics of moving such flows across preexisting dunes remains undetermined. Because of the similarity of the multi-modal distributions of coarse laminae from pyroclastic dunes and fluvial gravelly megaripples, the possibility that water was included as part of these basal shear flows cannot be ruled out.

The mixtures of hyperbolic saltation populations with coarser populations also raises questions about how they are mixed. The low slope values for the fine sides of the coarse populations do not appear to continue beyond the coarse limit of the saltation population, so are the two populations truncated where they meet or do they overlap at lesser logarithmic amounts?

Aeolian, some fluvial, and some pyroclastic-surge grain-size distributions exhibit hyperbolic shapes that can be modeled using four parameters. The hyperbolic parameters are different for the three kinds of deposits, with the slope of the two asymptotic lines ( $\phi$  and  $\gamma$ ) more gentle for the pyroclastic-surge deposits. Because coarser modes in bimodal distributions do not occur by themselves, we cannot determine hyperbolic fits for them. However, mixtures of two hyperbolic models are able to reproduce bimodal distributions from Kilbourne and Hunts Holes (and other deposits of pyroclastic density currents). We suggest that such bimodal models have a slightly firmer physical basis (from aeolian and fluvial analogies) than previously proposed models using mixtures of several lognormal distributions (Wohletz, 1983; Wohletz et al., 1995).

## Acknowledgments

This project was initiated at the New Mexico Bureau of Mines and Mineral Resources under the direction of Dr. Frank Kottowski. Dr. Gutjahr suggested that we do more work modeling the transport and deposition of the clasts,

but the senior author was reassigned and Dr. Gutjahr became ill and died, so the project was put on a back shelf for years. We thank Bill Seager, Mike McCurry, Dana Bahar, and Ken Wolhertz for advice, field tours, and helpful discussions at Kilbourne and Hunts Holes. Dana Bahar provided some of the samples from Kilbourne Hole and sent her thesis to the senior author. We are grateful to Sylveen Robinson-Cook, Ghavan Mostafavi, Randy Roberts, Carol Rison, Mark Lund, Meredith Worden, Ellen Limburg, and Bob Friesen for help with

the size analyses and reduction of computer data through the years. Bill Haneberg and Alex Rinehart graciously advised on computer manipulation of text and formulae. We are indebted to Bruce Allen for thoroughly reviewing several versions of the manuscript and suggesting many clarifying improvements. We are grateful to Dana Bahar and an anonymous reviewer for critical reviews that made this a much better and more comprehensive article. Becky Titus and Mickey Wooldridge drafted the graphs, and Leo Gabaldon provided additional drafting assistance.

## References

- Allen, J.R.L., 1982, Sedimentary structures, their character and physical basis: Developments in Sedimentology, Part I, 30A and Part II, 30B: Elsevier, Amsterdam, p. A1-593; B1-663.
- Anderson, R.S., 1990, Eolian ripples as examples of self-organization in geomorphological systems: *Earth-Science Reviews*, v. 29, p. 77-96.
- Anderson, R.S. and Bunas, K.L., 1993, Grain size segregation and stratigraphy in aeolian ripples modelled with a cellular automaton: *Nature*, v. 365, p. 740-743.
- Anderson, R.S., and Hallet, B., 1986, Sediment transport by wind: toward a general model: *Geological Society of America Bulletin*, v. 97, p. 523-535.
- Andrews, B.J., and Manga, M., 2011, Effects of topography on pyroclastic density current runout and formation of coignimbrites: *Geology*, v. 39, p. 1099-1102.
- Andrews, B.J., and Manga, M., 2012, Experimental study of turbulence, sedimentation and coignimbrite mass partitioning in dilute pyroclastic density currents: *Journal of Volcanology and Geothermal Research*, v. 225-226, p. 30-44.
- Bagnold, R.A., 1937, The size grading of sand by wind: *Proceedings of the Royal Society of London, Series A.*, v. 163, p. 252-564.
- Bagnold, R.A., 1941, The physics of blown sand and desert dunes: *Mehuen*, London, 265 p.
- Bagnold, R.A., 1966, An approach to the sediment transport problem from general physics: *U.S. Geological Survey Professional Paper 422-I*, 37 p.
- Bagnold, R.A., 1968, Deposition in the process of hydraulic transport: *Sedimentology*, v.10, p. 45-56.
- Bagnold, R.A., 1973, The nature of saltation and of bed-load transport in water: *Proceedings of the Royal Society, Series A*, v. 332, p. 473-504.
- Bagnold, R.A., 1977, Bed-load transport by natural rivers: *Water Resources Research*, v. 13, p. 303-312.
- Bagnold, R.A., 1979, Sediment transport by wind and water: *Nordic Hydrology*, v. 10, p. 309-322.
- Bagnold, R.A., and Barndorff-Nielsen, O., 1980, The pattern of natural size distributions: *Sedimentology*, v. 27, p. 199-207.
- Bahar, D., 1991, Evolution of the base surge deposits at Kilbourne Hole maar, south-central New Mexico [M.S. Thesis]: New Mexico State University, Las Cruces, 116 p.
- Barndorff-Nielsen, O., 1977, Exponentially decreasing distributions for the logarithm of particle size: *Proceedings of the Royal Society of London, Series A.*, v. 353, p. 401-419.
- Barndorff-Nielsen, O., 1979, Models for non-Gaussian variation with applications to turbulence: *Proceedings of the Royal Society of London, Series A.*, v. 368, p. 501-520.
- Barndorff-Nielsen, O., Dalsgaard, K., Halgreen, C., Kuhlman, H., Moller, J.T., and Schou, G., 1982, Variation in particle size distribution over a small dune: *Sedimentology*, v. 29, p. 53-65.
- Branney, M.J., and Kokelaar, P., 2002, Pyroclastic density currents and the sedimentation of ignimbrites: *Geological Society of London, Memoir 27*, 143 p.
- Breard, E.C.P., and Lube, G., 2017, Inside pyroclastic density currents—uncovering the enigmatic flow structure and transport behavior in large-scale experiments: *Earth and Planetary Science Letters*, v. 458, p. 22-36.
- Burgisser, A., and Bergantz, G.W., 2002, Reconciling pyroclastic flow and surge: the multiphase physics of pyroclastic density currents: *Earth and Planetary Science Letters* v. 202, p. 405-418.
- Butterfield, G.R., 1999, Near-bed mass flux profiles in aeolian sand transport: high-resolution measurements in a wind tunnel: *Earth Surface Processes and Landforms*, v. 24, p. 393-412.
- Cas, R.A.F., and Wright, J.V., 1987, *Volcanic successions, modern and ancient*: Allen and Unwin, London, 528 p.
- Cole, P.D., 1991, Migration direction of sand-wave structures in pyroclastic surge deposits: implications for depositional processes: *Geology*, v. 19, p. 1108-1111.
- Dellino, P., Isaia, P.R., and Veneruso, M., 2004, Turbulent boundary layer shear flows as an approximation of base surges at Campi Flegrei (southern Italy): *Journal of Volcanology and Geothermal Research*, v.133, p. 211-228.
- Dellino, P., Mele, D., Sulpizio, R., La Volpe, L., and Braia, G., 2008, A method for the calculation of the impact parameters of dilute pyroclastic density currents based on deposit particle characteristics: *Journal of Geophysical Research*, v. 113, p. B7206-7227.
- Dong, Z., Liu, X., Wang, H., Zhao, A., and Wang, X., 2002, The flux profile of a slowing sand cloud: a wind tunnel investigation: *Geomorphology*, v. 49, p. 219-230.
- Doronzo, D.M., and Dellino, P., 2011, Interaction between pyroclastic density currents and buildings: Numerical simulation and first experiments: *Earth and Planetary Science Letters*, v. 310, p. 286-292.
- Douillet, G.A., Pacheco, D.A., Kueppers, U., Letort, J., Tsang-Hin-Sun, E., Bustillos, J., Hall, M., Ramon, P., and Dingwell, D.B., 2013, Dune bedforms produced by dilute pyroclastic density currents from the August 2006 eruption of Tungurahua volcano, Ecuador: *Bulletin of Volcanology*, v. 75:762, 20 p.
- Douillet, G.A., Rasumssen K.R., Kueppers, U. Lo Castro, D., Merrison, J.P., Iversen, J.J. and Dingwell, 2014, Saltation threshold for pyroclasts at various bed slopes: Wind tunnel measurements: *Journal of Volcanology and Geothermal Research*, v. 278-279, p. 14-24.
- Douillet, G.A., Taisne, B, Tsang-Hin-Sun, E., Muller, S.K., Kueppers, U., and Dingwell, D.B., 2015, Syn-eruptive, soft-sediment deformation of deposits from dilute pyroclastic density current: triggers from granular shear, dynamic pore pressure, ballistic impacts and shock waves: *Solid Earth*, v. 6, p. 553-572.
- Duran, O., Claudin, P., and Andreotti, B., 2011, On aeolian transport: grain-scale interactions, dynamical mechanisms and scaling laws: *Aeolian Research*, v. 3, p. 243-270.
- Eychenne, J., Le Penec, J.L., Troncoso, L., Gouhier, M., and Nedelec, J.M., 2012, Causes and consequences of bimodal grain-size distributions of tephra deposited during the August 2006, Tungurahua eruption (Ecuador): *Bulletin of Volcanology*, v. 74, p. 187-205.
- Farrell, E.J., Sherman, D.J., Ellis, J.T., and Li, B., 2012, Vertical distribution of grain size for wind blown sand: *Aeolian Research*, v. 7, p. 51-61.
- Fisher, R.V., 1970, Base surge bed forms in maar volcanoes: *American Journal Science*, v. 268, pp. 157-180.
- Fourriere, A., Claudin, P., and Andreotti, B., 2010, Bedforms in a turbulent stream: formation of ripples by primary linear instability and of dunes by nonlinear pattern coarsening: *Journal of Fluid Mechanics*, v. 649, p. 287-328.
- Gile, L.H., 1987, A pedogenic chronology for Kilbourne Hole, southern New Mexico-II: time of the explosions and soil events before the explosions: *Journal of the Soil Science Society of America*, v. 51, p. 746-760.

- Gencalioglu-Kuscu, G. Atilla, C., Cas, R.A.F., and Kuscu, I., 2007, Base surge deposits, eruption history, and depositional processes of a wet phreatomagmatic volcano in Central Anatolia (Cora Maar): *Journal of Volcanology and Geothermal Research*, v. 159, p. 198–209.
- Girolami, L., Druitt, T.H., and Roche O., 2015, Towards a quantitative understanding of pyroclastic flows: effects of expansion on the dynamics of laboratory fluidized granular flows: *Journal of Volcanology and Geothermal Research*, v. 296, p. 31–39.
- Gravina, T., Lirera, L., Marzocchella, A., Petrosino, P., and Salatinob, P., 2004, Fluidization and attrition of pyroclastic granular solids: *Journal of Volcanology and Geothermal Research*, v. 147, p. 27–42.
- Ho, T.D., Valance, A., Dupont, P., and El Moctar, A.O., 2014, Aeolian sand transport: length and height distributions of saltation trajectories: *Aeolian Research*, v. 12, p. 65–74.
- Houghton, B.F., Wilson, C.J.N., Smith, R.T., and Gilbert J.S., 2000, Phreatoplinian eruptions: *in* H. Sigurdsson, B. Houghton, S.R. McNutt, H. Rymer, and J. Stix, eds., *Encyclopedia of Volcanoes*: Academic Press, London, p. 513–525.
- Hunter, R.E., 1977, Basic types of stratification in small eolian dunes: *Sedimentology*, v. 24, p. 361–387.
- Janebo, M.H., Houghton, B.F., Thordarson, T., Bonadonna, C., and Carey, R.J., 2018, Total grain-size distribution of four subplinian-Plinian tephra from Hekla volcano, Iceland: implications for sedimentation dynamics and eruption source parameters: *Journal of Volcanology and Geothermal Research*, v. 357, p. 25–38.
- Kok, J.F., Parteli, E.J.R., Michaels, T.I., and Karam, D.B., 2012, The physics of wind-blown sand and dust: *Reports on Progress in Physics*, v. 75, 72 p.
- Kuester, J.L., and Mize, J.H., 1973, Optimization techniques with Fortran: McGraw-Hill, New York, 500 p.
- Lorenz, V., 1973, On the formation of maars: *Bulletin Volcanologique*, v. 37, p. 183–204.
- Love, D.W., Boyle, J.T., Robinson, S., and Hemingway, M., 1985, Location-dependent sediment sorting in gravelly megaripples from the Rio Grande, central New Mexico: *New Mexico Geology*, v. 7, pp. 26–30.
- Love, D.W., Gutjahr, A., and Robinson-Cook, S., 1987, Location-dependent sediment sorting in bedforms under waning flow in the Rio Grande, central New Mexico: *Society for Economic Paleontologists and Mineralogists, Special Publication 39*, p. 37–47.
- Mayaud, J.R., Bailey, R.M., Wiggs, G.F.S., and Weaver, C.M., 2017, Modelling aeolian sand transport using a dynamic mass balancing approach: *Geomorphology*, v. 280, p. 108–121.
- Moore, J.G., 1967, Base surge in recent volcanic eruptions: *Bulletin of Volcanology*, v. 30, p. 337–363.
- Namikas, S.L., 2003, Field measurement and numerical modelling of aeolian mass flux distributions on a sandy beach: *Sedimentology*, v. 50, p. 303–326.
- Namikas, S.L., 2006, A conceptual model of energy partitioning in the collision of saltating grains with an unconsolidated sediment bed: *Journal of Coastal Research*, v. 22, p. 1250–1259.
- Qian, G., Dong, Z., Zhang, Z., Luo, W., and Lu, J., 2012, Granule ripples in the Kumtagh Desert, China: morphology, grain size, and influencing factors: *Sedimentology*, v. 59, p. 1888–1901.
- Rasmussen, K.R., Iversen, J.D., and Rautahemio, P., 1996, Saltation and wind-flow interaction in a variable slope wind tunnel: *Geomorphology*, v. 17, p. 19–28.
- Rasmussen, K.R., Valance, A., and Merrison, J., 2015, Laboratory studies of aeolian sediment transport processes on planetary surfaces: *Geomorphology*, v. 344, p. 74–94.
- Rice, M.A., Willetts, B.B., and McEwan, I.K., 1995, An experimental study of multiple grain-size ejecta produced by collisions of saltation grains with a flat bed: *Sedimentology*, v. 42, p. 695–706.
- Reineck, H.E., and Singh, I.B., 1980, *Depositional sedimentary environments*: Springer-Verlag, New York, 549 p.
- Roche, O., Gilbertson, M.A., Phillips, J.C., and Sparks, R.S.J., 2004, Experimental study of gas-fluidized granular flows with implications for pyroclastic flow emplacement, *Journal of Geophysical Research*, v.109, B10201, 14 p.
- Rowley, P.D., MacLeod, N.S., Kuntz, M.A., and Kaplan, A.M., 1985, Proximal bedded deposits related to pyroclastic flows of May 18, 1980 Mount St. Helens, Washington: *Geological Society of America Bulletin*, v. 96, p. 1373–1383.
- Seager, W.R., 1987, Caldera-like collapse at Kilbourne Hole Maar, New Mexico: *New Mexico Geology*, v. 9, p. 69–73.
- Sheridan, M.F., and Wohletz, K.H., 1983, Hydrovolcanism: basic considerations and review: *Journal of Volcanology and Geothermal Research*, v. 17, p. 1–29.
- Sheridan, M.F., Wohletz, K.H., and Dehn, J., 1987, Discrimination of grain-size subpopulations in pyroclastic deposits: *Geology*, v. 15, p. 367–370.
- Sohn, Y.K., 1997, On traction-carpet sedimentation: *Journal of Sedimentary Research*, v. 67, p. 502–509.
- Sohn, Y.K., and Chough, S.K., 1989, Depositional processes of the Suwolbong Tuff Ring, Cheju Island (Korea): *Sedimentology*, v. 36, p. 837–855.
- Stuart, C.J., 1981, Hunt's Hole maar volcano, Dona Ana County, south-central New Mexico: *El Paso Geological Society Guidebook*, 1981 field conference, p. 64–72.
- Stuart, C.J., and Brenner, M.G., 1979, "Low-regime" base surge dunes—an example from Kilbourne and Hunts Holes, south-central New Mexico [abstract]: *Geological Society of America Abstracts with Programs*, v. 11, p. 525.
- Sulpizio, R., Dellino, P., Doronzo, D.M., and Sarocchi, D., 2014, Pyroclastic density currents: state of the art and perspectives: *Journal of Volcanology and Geothermal Research*, v. 283, p. 36–65.
- Thorarinnsson, S., 1967, Surtsey: The new island in the north Atlantic: Viking, New York, 47 p.
- Valance, A., Rasmussen, K.R., El Moctar, A.O., and Dupont, P., 2015, The physics of aeolian sand transport: *Comptes Rendus Physique, Granular physics*, v. 16, p. 105–117.
- Valentine, G.A., and Fisher, R.V., 2000, Pyroclastic surges and blasts: *in* H. Sigurdsson, B. Houghton, S.R. McNutt, H. Rymer, and J. Stix, eds., *Encyclopedia of Volcanoes*, Academic Press, London, p. 571–580.
- Valentine, G.A., Sottili, G., Palladino, D.M., and Taddeucci, J., 2015, Tephra ring interpretation in light of evolving maar-diatreme concepts: Stracciacappa maar (central Italy): *Journal of Volcanology and Geothermal Research*, v. 308, p. 19–29.
- Vespermann, D., and Schmincke, H.U., 2000, Scoria cones and tuff rings: *in* H. Sigurdsson, B. Houghton, S.R. McNutt, H. Rymer, and J. Stix, eds., *Encyclopedia of Volcanoes*, Academic Press, London, p. 683–694.
- Waters, A.C., and Fisher, R.V., 1971, Base surges and their deposits: Capelinhos and Taal volcanoes: *Journal of Geophysical Research*, v. 76, p. 5596–5614.
- Walker, G.P.L., 1983, Ignimbrite types and ignimbrite problems: *Journal of Volcanology and Geothermal Research*, v. 17, p. 65–88.
- Walker, G.P.L., 1984, Characteristics of dune-bedded pyroclastic surge bedsets: *Journal of Volcanology and Geothermal Research*, v. 20, p. 281–296.
- White, J.D.L., and Houghton, B., 2000, Surtseyan and related phreatomagmatic eruptions: *in* H. Sigurdsson, B. Houghton, S.R. McNutt, H. Rymer, and J. Stix, eds., *Encyclopedia of Volcanoes*, Academic Press, London, p. 495–511.
- White, J.D.L., and Ross, P.S., 2011, Maar-diatreme volcanoes: a review: *Journal of Volcanology and Geothermal Research*, v. 201, p. 1–29.
- Williams, G., 1964, Some aspects of the eolian saltation load: *Sedimentology*, v. 3, p. 257–287.
- Wilson, C.J.N., 1980, The role of fluidization in the emplacement of pyroclastic flows: *Journal of Volcanology and Geothermal Research*, v. 8, p. 231–249.
- Wilson, C.J.N., 1984, The role of fluidization in the emplacement of pyroclastic flow 2: experimental results and their interpretation: *Journal of Volcanology and Geothermal Research*, v. 20, p. 55–78.
- Wohletz, K.H., 1980, Explosive hydro-magmatic volcanism [Ph.D. dissertation]: Arizona State University, Tempe, Arizona, 303 p.
- Wohletz, K.H., 1983, Mechanisms of hydro-volcanic pyroclast formation: grain-size, scanning electron microscopy, and experimental studies: *Journal of Volcanology and Geothermal Research*, v. 17, p. 31–63.
- Wohletz, K.H., Orsi, G., and Vota, S., 1995, Eruptive mechanisms of the Neapolitan Yellow Tuff interpreted from stratigraphic, chemical, and granulometric data: *Journal of Volcanology and Geothermal Research*, v. 67, p. 263–290.

- Yizhaq, H., 2008, Aeolian megaripples: mathematical model and numerical simulations: *Journal of Coastal Research*, v. 24, p. 1369–1378.
- Zou, X.Y., Wang, Z.L., Hao, Q.Z., Z. C.L., Liu, Y.Z., and Dong, G.R., 2001, The distribution of velocity and energy of saltating sand grains in a wind tunnel: *Geomorphology*, v. 36, p. 155–165.

# New Mexico Geological Society spring meeting abstracts

The following are the abstracts from the New Mexico Geological Society annual spring meeting, listed alphabetically, which was held on April 13, 2018 at the Macy Center, New Mexico Tech campus, Socorro. Find a PDF of the program at: [nmgs.nmt.edu/meeting/](http://nmgs.nmt.edu/meeting/)

## SCARP MORPHOLOGY ALONG THE ALAMOGORDO FAULT, SACRAMENTO MOUNTAINS FROM A HIGH-RESOLUTION AERIAL TOPOGRAPHIC SURVEY

Lynn A. Acosta and Reed J. Burgette

New Mexico State University, Geological Sciences MSC 3AB, PO Box 30001, Las Cruces, NM, 88003

The Alamogordo fault bounds the Sacramento Mountains in the south-central portion of New Mexico. The Sacramento Mountains are a fault-block range that extends north and south for 137 km as well as 68 km wide. We investigated a prominent scarp at the mouth of Mule Canyon, ~7.5 km south of the city of Alamogordo, a site that was the subject of earlier paleoseismic reconnaissance. The height of the scarp and its form indicates the magnitude and recency of earthquake slip along this fault in the southern Rio Grande rift. In this study we show the promise of recent advances in high-resolution topographic surveying for characterizing late Quaternary deformation along active faults in the landscape of southern New Mexico.

We have collected two high-resolution topographic datasets from the Mule Canyon site on the Alamogordo fault through field projects conducted by the NMSU Neotectonics course. A terrestrial lidar scan of the site collected in 2013 yielded a dense point cloud and a digital elevation model gridded at 10 cm resolution. This presentation focuses on analysis of the second survey conducted with Structure-from-Motion (SfM) photogrammetry. In the fall of 2017, a survey was conducted using photos collected from a camera on a helium balloon accompanied by GPS surveying to provide ground control points. The aerial images were processed with the ground control information using Agisoft Photoscan SfM software. Products generated include a point cloud with 39 million points, and a DEM and orthophoto gridded at 4 cm and 1 cm resolutions, respectively. These products were output and the ArcMap Geographic Information System (GIS) software will be used to analyze the topographic data and output profiles for numerical models of scarp evolution. Analysis of the scarp using a hillslope diffusion model will be completed in Matlab to assess spatial variations in scarp form and the temporal evolution of the scarp. Comparison with the previous terrestrial lidar data will be used to assess the precision and accuracy of the surveying techniques in this environment. Preliminary analysis of the

SfM DEM shows a ~7 m vertical separation of an alluvial fan surface across the scarp. This evidence of late Quaternary deformation indicates ongoing extension in the southern Rio Grande rift and associated earthquake hazard for southern New Mexico.

## EVIDENCE FOR MULTIPLE MAGMATIC SOURCES OVER TIME ALONG THE SOUTHWESTERN LAURENTIAN MARGIN DURING THE GRENVILLE OROGENY

Anthony M. Alvarez, Munazzam Ali Mahar, Jason W. Ricketts, and Philip C. Goodell

The University of Texas at El Paso, 500 W. University Ave, Geology Bldg Rm 101, El Paso, TX, 79968, [amalvarez3@utep.edu](mailto:amalvarez3@utep.edu)

This poster provides LA-MC-ICP-MS U-Pb geochronology and LA-MC-ICP-MS time-constrained zircon Hf isotope composition on five samples from two stages of the Red Bluff Granitic Suite and two samples from ferroan basalt dikes within the Franklin Mountains of El Paso, Texas. Zircon U-Pb geochronology yielded concordia ages of  $1121.3 \pm 2.9$  Ma and  $1118.4 \pm 5.4$  Ma for the stage-1 syenite and main body of stage-2 granite, respectively. The basaltic dikes yielded a similar weighted mean age of  $1124 \pm 14.1$  Ma. Our new zircon U-Pb ages coupled with the previous geochronological efforts revealed the subtle differences in the timing of emplacement for the different stages. In fact, U-Pb ages are overlapping within the error. This suggests that the earlier less-evolved magmas and subsequent more differentiated magmatic bodies emplaced within a short span of time not more than 3 Ma. We consider the concordant dates that are 10 to 20 Ma older than the weighted mean/concordia age as the antecrystic zircons. The range for antecrystic zircons is from 1130 to 1138 Ma. Xenocrystic inheritance from 1141 to 1260 Ma also occurred. The initial Hf isotope composition of the plutons studied remained mostly positive. The weighted mean  $\epsilon_{\text{Hf}}(t)$  for the stage 1 and 2 varies from +5.3 to 7.2. Two basaltic dike samples revealed the similar but more scattered  $\epsilon_{\text{Hf}}(t)$  values with weighted mean  $\epsilon_{\text{Hf}}(t)$  of  $+6.7 \pm 2.6$  and  $+5.2 \pm 3.3$ . Geochemistry shows characteristics of A-type granites, indicate strong plagioclase fractionation of basaltic magma and are an indication against metasomatism or crustal contamination. Given the absence of older inheritance such as 1.65–1.60 Ga Mazatzal, geochemistry, and radiogenic

Hf isotopic compositions of the Red Bluff granites, a minimal contribution from older Mesoproterozoic crust is suggested. Based on the timing and geochemical composition, we suggest that the magmatism at the Franklin Mountains and Llano Uplift recorded the partial melting of the subcontinental lithospheric mantle at around 1.1 Ga, possibly, during a rifting event within the overall convergence zone of southwestern Laurentian front. Alternatively, partial melting of a recently-placed basaltic underplate is suggested. Temporal, tectonic and isotopic evidence presented here supports distinct ages and sources of SW Laurentia during the Grenville Orogeny for southwest U.S. and northern Mexico. Temporal and Hf isotopes suggest three episodes of magma generation at 1) 1125–1100, 2) 1097–1082, and 3) 1081–1068 Ma.

## TWO METHODS TO DESCRIBE THE VASTNESS OF TIME: A VIRTUAL TOUR OF THE GEOLOGIC HISTORY OF THE EL PASO/JUAREZ REGION AND A 12 MONTH PROPORTIONAL RELATION OF THIS PALEOHISTORY

Anthony M. Alvarez<sup>1</sup>, Eric J. Kappus<sup>2</sup>, and Erik M. Day<sup>1</sup>

<sup>1</sup>The University of Texas at El Paso, 500 W. University Ave, El Paso, TX, 79968, [amalvarez3@utep.edu](mailto:amalvarez3@utep.edu)

<sup>2</sup>Southwest University, 1414 Geronimo Dr., El Paso, TX, 79925

Here we illustrate two methods to describe the vastness of time. Various field and technology-integrated approaches were used to construct videos illustrating the geology of a specific locations for the first group of practicing teachers. The videos were organized into a geo-spatial and chronologically organized virtual tour that collectively shared the billion year geologic story of the El Paso/Juarez region and described systematic tectonic and paleogeographic changes to North America through this time. Non-related flipped-based learning videos were provided for a second group of grant-funded teachers part of the Texas Regional Collaborative; these videos were used for field trips to El Paso's Great Unconformity. Instructional methods were designed to calculate the date local formations proportionally relate to a 12 month calendar with respect to all of Earth time. For example, how approximately five hundred million years of rock record went missing. The aim of both the class and the

grant were three-part: 1) introduce emergent technologies, 2) focus on pedagogical tools and cultural significance, such as problem-based learning, flipped-based learning, constructionism, connectivism, and sense of place, and 3) teach Earth science based content in order for teachers to describe how local landforms are made and change over time. The combination of these concepts and tools will give future teachers the ability to apply new and emerging technologies into their classrooms and the ability to learn and teach geologic concepts such as the vastness of time, in order to integrate these concepts into in their future classrooms.

#### FLAT-SLAB BULLDOZING OF BASAL CONTINENTAL MANTLE LITHOSPHERE: 2D NUMERICAL MODELS AND APPLICATION TO THE LARAMIDE OROGENY

Gary Axen<sup>1</sup>, Jolante van Wijk<sup>1</sup>, and Claire A. Currie<sup>2</sup>

<sup>1</sup>New Mexico Tech, 801 Leroy Place, E&ES Dept., Socorro, NM, 87801, gary.axen@nmt.edu

<sup>2</sup>Dept. of Physics, University of Alberta, Edmonton, Alberta, T6G 2E1, Canada

Flat-slab (horizontal) subduction occurs along ~10% of subduction margins, forms magmatic gaps, causes upper-plate deformation to migrate inland, and is thought to have caused the Laramide Orogeny. We investigate bulldozing of basal continental mantle lithosphere (CML) by the flat Farallon slab, using 2D numerical thermal-mechanical models. We vary CML density and strength to understand controls on the bulldozing process. Flat-slab subduction begins when an oceanic plateau, which makes the slab buoyant, enters the trench. The dense slab ahead of the plateau detaches and continues to sink, and subduction erosion of the continental margin begins. A slab hinge is quickly re-established at the front of the flat slab. The advancing flat slab erodes (bulldozes) the basal ~25–50 km of continental mantle lithosphere (CML), thinning it. Buoyant (depleted) bulldozed CML can accumulate ahead of the slab hinge, in a growing, migrating wedge up to ~200 km thick, that is wider (up to ~700 km) if bulldozed CML is weak, or narrower if CML is strong. We suggest that bulldozed wedges transmit contact stress into the upper plate, driving crustal deformation ahead of the flat slab itself. Dense bulldozed CML, especially if also strong, is entrained with the sinking slab, so would be imaged with it in seismic tomography. It is probable that bulldozed CML also may accumulate along one or both sides of the contact zone between slab and upper plate. Whether buoyant or dense, bulldozed CML fills the asthenospheric wedge, which would end arc-type melting during flat-slab advance. Flat-slab rollback reopens the asthenospheric wedge, renews melting, and leaves a step and/or a thickened keel in the CML at/ahead of the farthest slab extent.

Most modern South American flat slab segments coincide with subducted ocean ridges, have correspondingly narrow contact zones with the upper plate, and are bounded laterally by sagging or torn ocean lithosphere. Recent geodynamic models of subduction under North America suggest that the contact zone between Farallon and North American plates also was narrow, much more so than typically envisioned in older literature. This contact zone probably was bounded in southern Arizona–New Mexico by a slab tear, because arc volcanism farther south continued much closer to the coast. We interpret two geophysical anomalies under the western U.S. as fossil basal CML steps/wedges that define the limit of flat-slab advance. An upper-mantle fast-velocity anomaly below southeast New Mexico and west Texas is probably a keel now “dripping” into the asthenosphere. CML below southwest Colorado thickens northeastward across a step that probably defines the northeast limit of the Laramide flat-slab contact zone. If correct, then Farallon flat-slab contact ended hundreds of kilometers southwest of the Laramide front in Wyoming. Most Laramide-age magmatism was northwest or southeast of the contact zone, but some occurred above it: the Colorado mineral belt probably was above a slab tear and Laramide magmatism in western Arizona and southeastern California probably reflects petit-spot type melting where the slab was flexed concave-up. Modern examples of active flat-slab bulldozing probably exist in South America.

#### CHEMICAL AND MINERAL COMPOSITIONS AND COMPOSITIONAL TRENDS OF TWO PLEISTOCENE PALEOSOLS FROM THE TAOS PLATEAU, NEW MEXICO

April R. Bates

University of New Mexico at Valencia, 280 La Entrada Rd., Belen, NM, 87031, apbates63@unm.edu

The Taos Plateau in northern New Mexico contains multiple basaltic lava flows, some of which preserve underlying paleosols. Here we present the composition of two paleosols from the Servilleta Basalts north of Tres Piedras, New Mexico. Basalt stratigraphy suggests that these paleosols are approximately 4 million years old. The two paleosols are separated by a two-meter-thick lava flow. They contain a large amount of sand and silt-sized quartz, with considerable amounts of finer-grained matrix, mafic minerals, feldspar, and volcanic glass. The observed distinct increase in felsic mineral content in paleosols suggests that there were significant additions from outside the andesitic to basaltic Taos Plateau to the soils during pedogenesis. The presence of unweathered pumice and volcanic glass in the paleosol profiles is indicative of volcanism during pedogenesis, some of which might have been explosive. Many unweathered clasts from the paleosol B horizons

display smectite argillans that suggest relatively arid pedogenic conditions. Argillans are discontinuous and <5 μm thick. Primary mafic minerals make up only about 13% of paleosol B horizon materials; where they exist, however, they are mostly to completely unweathered. Weathering of primary minerals comprises minor clay alteration along grain margins and fractures. Clasts of basalt within paleosol B horizon suggest incorporation of underlying bedrock materials into the soil profile during pedogenesis. Bioturbation is a possible explanatory mechanism. The upwards increase in quartz and upwards decrease in average clast grain size through both paleosol profiles are interpreted here as evidence of accretionary conditions during pedogenesis in a dust-rich environment.

#### UPDATE ON GROUNDWATER IN THE SOUTHERN TAOS VALLEY, NEW MEXICO

Anthony Benson<sup>1</sup>, David C. Jacobs<sup>2</sup>, and Peter Vigil<sup>3</sup>

<sup>1</sup>Retired Geologist, PO Box 2848, Taos, NM, 87571, benson1@newmex.com

<sup>2</sup>GeoGrande Consulting, PO Box 1606, El Prado, NM, 87529

<sup>3</sup>Taos Soil & Water Conservation District, P. O. Box 2787, Ranchos de Taos, NM, 87557

This study, funded by the Taos Soil & Water Conservation District, is a follow up to the findings of the NMBGMR OFR 581, published in 2016 by Johnson, Bauer, and Felix. They reported (1) a decline in water levels between 2011 and 2015 in the southern Taos Valley; (2) a severe water level drop measured in the West Romero Road area; and (3) postulated fault barriers to groundwater recharge. New water level measurements made in 2017 in the West Romero Road area show that the water-level decline bottomed in winter 2014. The time of declining water level is within the 1993–2014 drought, as recorded at the nearby Taos airport, at NRCS SNOTEL stations in the headwaters of the Sangre de Cristo Mountains, and by declining stream flows at the Rio Pueblo de Taos gage. However, the lack of normal precipitation since August 2017 and winter 2018 indicate a resumption of drought conditions. Wells that were drilled as far back as 1975 requiring OSE well permits and being located accurately by GPS in the 2000's had static water levels reported both high and low to recent measurements for various reasons. A water table elevation map, which used well water levels measured in the 2011–2017 period and contoured on a 10-foot contour interval, shows regional variations in both water level and recharge sources. Major recharge sources include Rio Pueblo de Taos, Rio Grande del Rancho, several acéquias, and some arroyos. Seasonal groundwater levels change less than one foot within a half mile of rivers. Seasonal changes near acéquias vary from one foot to over five feet. The West Romero Road area has a high water table

elevation from recent recharge from the Rio Grande del Rancho and the Llano Quemado acéquia, but probably is among the first to lower during a drought. Small groundwater highs underlie many arroyos and probably are derived from occasional local flash floods. Multiple deeper aquifers that vary in extent and permeability can have either short-term fast or longer-term slow recharge. Upwelling warm waters along fault zones and changing pressure gradients add to water-table changes. The four major Los Córdovas faults and their branches locally appear to interrupt the groundwater level. These faults, which are visible in outcrop of alluvium north of Rio Pueblo de Taos, deepen southward under the southern Taos Valley and might be offset by east-west trending Picuris faults. The intersection of the Los Córdovas and Picuris faults, which is suggested by high resolution aeromagnetics, probably has produced fault-compartmentalized blocks that are likely to also have contributed both to water-level changes and to water geochemistry differences within aquifers. Other factors that might be affecting the substantial water table drop in the West Romero Road area include (1) limited downward infiltration from the Llano Quemado acéquia during drought, (2) variable supply of water from major rivers, and (3) excessive field and garden irrigation. Long-term solutions to declining groundwater levels include roof-rainwater harvesting, acéquia improvements and development, and construction of arroyo infiltration dams and ponds.

#### EXTENSION RATES IMPACT ON ENDORHEIC DRAINAGE LONGEVITY AND REGIONAL SEDIMENT DISCHARGE

Michael Berry<sup>1</sup>, Jolante van Wijk<sup>1</sup>, Daniel Cadol<sup>1</sup>, Daniel Garica-Costellanos<sup>2</sup>, and Erica Emry<sup>2</sup>

<sup>1</sup>New Mexico Tech, Socorro, NM, 87801, michael.berry@student.nmt.edu

<sup>2</sup>ICTJA-CSIC, Barcelona, Spain

Tectonic and climate drivers exert co-equal forces on the evolution of tectonic sedimentary basins. The Rio Grande rift and its drainages provide a backdrop for discussing which drivers drive the transition from endorheic or closed drainage basins to exorheic or open, through-going drainage basins, with both climatic and tectonic drivers being proposed by researchers. With a dearth of regional scale extensional landscape modeling studies to draw from, we explore the impact of tectonic extension on endorheic-exorheic transitions and regional sediment and water discharge in both a “dry” and “wet” runoff regimes. We show that holding climate-induced runoff constant, that greater extensional rates correspond to a longer period of sedimentation capture, tectonically induced gradients significantly increase sedimentation long after tectonic activity has terminated, and that developing an endorheic basin is very difficult in high runoff regimes.

#### EFFECTS OF LONG-TERM AND SHORT-TERM CLIMATIC CHANGES SEEN THROUGH THE TRANSITIONAL PROCESS GEOMORPHOLOGY OF A DEGLACIATING STRATOVOLCANO, MOUNT RAINIER, WASHINGTON, USA

Jonathan D. Beyeler<sup>1</sup> and David R. Montgomery<sup>2</sup>

<sup>1</sup>University of Washington / State of NM Environment Department, 1190 S St. Francis Drive, PO Box 5469, Santa Fe, NM, 87502, beyeler@uw.edu

<sup>2</sup>University of Washington, Earth and Space Sciences Department, Johnson Hall Rm-070, Box 351310, 4000 15th Avenue NE, Seattle, WA, 98195

Regionally deglaciating climate coupled with sediment loading of historically stable single-thread glacial rivers on the flanks of Mount Rainier have driven recent extreme fluvial network evolution on sub-decadal timescales. Rapid river channel widening, streambank erosion, braidplain development, and channel-bed aggradation are a transient sediment storage signals that are morphodynamically prograding downstream through major river corridors. Major rivers emanate from steep boulder-clogged meltwater channels beneath retreating glaciers that transition to single- and multi-thread gravel-bedded channels towards Mount Rainier National Park (MRNP) boundaries. Coarse glaciogenic sediment is delivered to high-gradient (>10%) fluvial systems through high-ratio sediment:water flows. Flows intermediately deposit sediment along riparian corridors as channel gradients transitionally decrease from transport to depositional slopes (~5–10%) as rivers approach MRNP boundaries (~1–2%). Historical photo analysis of MRNP river channels suggests a lag in the onset of long-term paraglacial sedimentation processes (post-1880) that has been rapidly accelerated by the effects of modern climate change and the increased frequency of extreme weather (i.e., atmospheric rivers) since ~1990. Current aggradation along downstream reaches of the Carbon River is contrary to historically stable surveys done pre-2009 due to an avulsion (ca. 2009) that relocated the full mainstem to an adjacent lower-elevation late-seral stage conifer forested floodplain (i.e., old growth 200–400+ years old) which initiated incision into the sediment accumulation historically restricted to headwater reaches proximal to glaciogenic sediment sources. Large wood recruitment and accumulation along high gradient reaches exacerbates deposition and transient storage of coarse sediment, observed to force >10 meters of deposition along headwater river corridors. Aggrading channels, despite widening, have diminished flow capacity. Flooding within MRNP during historically frequent river discharges is strongly associated with the downstream progradation of transient in-channel sediment and wood storage. High-magnitude precipitation events have increased in frequency across the western United States, from Washington

to southern California. New Mexico and the desert southwest are particularly sensitive to the effects of changing climate on regional precipitation regimes.

#### SEDIMENT DISPERSAL TRENDS AND TIMING OF BASEMENT-BLOCK UPLIFT DURING THE EARLY PERMIAN PHASE OF THE ANCESTRAL ROCKY MOUNTAINS, NEW MEXICO

Alicia L. Bonar, Brian A. Hampton, Greg H. Mack, and Jeffrey M. Amato  
New Mexico State University, Department of Geological Sciences, P.O. Box 30001, Las Cruces, NM, 88003, albonar@nmsu.edu

U-Pb detrital zircon geochronology and sandstone modal composition trends from the nonmarine, synorogenic Early Permian (Wolfcampian) Abo Formation (and equivalent strata) are presented here in the context of constraining sediment dispersal patterns as well as basement-block uplift and subsequent onlap histories during the final phase of Ancestral Rocky Mountain (ARM) orogenesis in New Mexico.

Bulk U-Pb age trends (n=662) from Early Permian strata reveal a primary peak age of 1689 Ma (Mazatzal–Yavapai province), with secondary peaks at 1247 Ma (Grenville province/De Baca Group) and 1378 Ma (Granite-Rhyolite province/Mesoproterozoic granitoids), and minor occurrences of Paleozoic, Neoproterozoic, and Archean age zircon. However, despite the lithologic homogeneity of these strata throughout New Mexico, U-Pb age spectra from individual samples (N=7) vary considerably. Early Permian strata in north-central and central New Mexico exhibit primary peak ages of 1692–1694 Ma and are locally sourced from the southern Uncompahgre (San Luis uplift). Fine-grained strata that crop out southeast of the Defiance-Zuni uplift in west-central New Mexico have a primary peak age of 1706 Ma and a secondary peak age of 1451 Ma, suggesting a more distal sediment source from the northern Uncompahgre uplift in Colorado. In northeastern New Mexico, strata exhibit a primary peak age of 1376 Ma and a secondary peak age of 1686 Ma and were likely sourced from the Sierra Grande and Uncompahgre uplifts (and Cimarron Arch) with no evidence of detrital contributions from Frontrangia. Strata in southeastern New Mexico exhibit one primary peak age of 1251 Ma reflecting local derivation from the Pederal uplift. In south-central New Mexico, strata have no primary peaks and instead show a wide range of ages from 270–3106 Ma. These strata were likely locally and distally sourced with possible eolian contributions.

Sandstone modal composition trends from Early Permian strata show elevated occurrences of quartz and feldspar grains with minor lithic fragments (Q=53%, F=45%, L=2%) and are interpreted to have been derived from continental-block/basement source areas. Feldspar consist of both

plagioclase and potassium feldspar grains (Qm=49%, P=38%, K=13%). However, northern samples contain both plagioclase and potassium feldspar grains (Qm=47%, P=34%, K=19%) whereas southern samples are marked by a near absence of potassium feldspar (Qm=55%, P=45%, K<1%). North-south trends in feldspar abundance are interpreted to be the result of secondary albitization during diagenesis of the Orogrande basin along the southern shoreline margin of the Hueco Sea.

Provenance data provide a powerful approach for testing uplift history and detrital contributions from basement-block uplifts and allow for an Early Permian sediment dispersal model for the final phase of ARM orogenesis. Data support a model where the Pedernal, Uncompahgre, and Sierra Grande uplifts were the primary detrital contributors during the Early Permian, with the Pedernal acting as a topographic barrier between discrete north-south flowing fluvial systems to the east and west. The Defiance-Zuni and Peñasco uplifts were likely tectonically inactive and overlapped by this time. Provenance trends support the existence of a topographic high (Cimarron Arch) separating drainage networks in northeastern New Mexico from southeastern Colorado.

#### CARBON DIOXIDE AND HELIUM GASES IN NEW MEXICO: DISTRIBUTION AND RELATION TO OTHER GASES IN THE RESERVOIR

Ronald F. Broadhead

New Mexico Bureau of Geology and Mineral Resources, New Mexico Tech, 801 Leroy Place, Socorro, NM, 87801, ron.broadhead@nmt.edu

Carbon dioxide is a common component of natural gases. In most gases CO<sub>2</sub> is less than 1%, with either hydrocarbons or N<sub>2</sub> being the dominant components. In other less common gases, CO<sub>2</sub> is dominant and may constitute more than 99% of the gas. The major CO<sub>2</sub> reservoir in New Mexico is the Bravo Dome field in the northeast part of the state. This giant field with more than 10 TCF original reserves is formed by a combination structural-stratigraphic trap in the Yeso Fm. (Lower Permian) and has produced 3.5 TCF CO<sub>2</sub>. Gases that are mostly CO<sub>2</sub> are also present in the Las Vegas and Raton Basins of north-central New Mexico and under Chupadera Mesa and in the Estancia Basin of central New Mexico and have also been encountered by exploratory wells drilled in west-central New Mexico. The main source of CO<sub>2</sub> appears to have been degassing of Tertiary-age magmas.

Commercial production of helium in New Mexico has been from 8 small oil and gas fields on the Four Corners Platform of northwest New Mexico. Almost 1 BCF He have been produced from reservoirs of Permian, Pennsylvanian, Mississippian and Devonian age. In southeast New Mexico

gases with enhanced He content have been produced from Lower Permian Abo red beds with He content increasing in proximity to northeast trending strike-slip faults. Gases with enhanced He content have been encountered in Lower Permian strata under Chupadera Mesa in central New Mexico and in Pennsylvanian strata in the Tucumcari Basin. Although most He in crustal reservoirs has probably been generated by radioactive decay of uranium in granitic rocks, isotopic analysis of Chupadera Mesa He indicates that a portion of the He was derived from juvenile sources in the mantle.

There is an inverse correlation between He content of gases and CO<sub>2</sub> content and hydrocarbon gas content. Most gases with CO<sub>2</sub> more than 5% have He less than 1%. All gases with CO<sub>2</sub> more than 20% have He less than 1%. He content also decreases with increasing BTU value of the gas, a proxy for hydrocarbon content. All gases with heating values more than 1000 BTU/ft<sup>3</sup> have He substantially less than 1%. He increases with N<sub>2</sub> content, an indication of incomplete charge of reservoirs with either hydrocarbons or with CO<sub>2</sub>. CO<sub>2</sub> and hydrocarbons appear to dilute the He that has migrated into the reservoirs from either granitic basement or via deep-seated faults that penetrate to the mantle.

#### PARAGENESIS OF URANIUM MINERALS IN THE GRANTS MINERAL BELT, NEW MEXICO: APPLIED GEOCHEMISTRY AND THE DEVELOPMENT OF OXIDIZED URANIUM MINERALIZATION

Samantha Caldwell and William X. Chavez  
Minerals Engineering Department,  
New Mexico Institute of Mining and  
Technology, 801 Leroy place, Socorro, NM,  
87801, samantha.caldwell@student.nmt.edu

Deposition of reduced uranium ores in the Grants Mineral Belt was succeeded by locally well-developed oxidation and the generation of secondary or tertiary uranium (vanadium) minerals. Detailed study of these succeeding-generation minerals indicates that oxidation of reduced uranium mineralization was effected by carbonate-, sulfate-bearing meteoric waters that engendered a series of generally hydrated uranyl-carbonate (e.g., andersonite, (Na<sub>2</sub>Ca(UO<sub>2</sub>)(CO<sub>3</sub>)<sub>3</sub>·6H<sub>2</sub>O; Chávez, 1979)) and sulfate (e.g., zippeite-like minerals, Mt. Taylor mine, Chávez, 1988; K<sub>4</sub>(UO<sub>2</sub>)<sub>6</sub>(SO<sub>4</sub>)<sub>3</sub>(OH)<sub>10</sub>·4H<sub>2</sub>O; see also Moench and Schlee, 1967, pp. 57–61) minerals.

Initial X-ray diffraction (XRD) analyses of reduced uranium minerals from organic-rich arkosic sandstones of the Westwater Canyon Member of the Jurassic-age Morrison Formation from the Mt. Taylor mine show that various organic compounds are associated with the strongly-reducing environment characterizing primary uranium minerals and associated V, Se, Mo and Fe. Oxidation of these reduced, organic-rich host

rocks (Squyres, 1980) apparently produced carbonic acid and generated weakly acidic solutions capable of continued oxidation of uranium. Deposition of native selenium (Poison Canyon Mine; Tessendorf, 1979) and weakly-crystallized MoS<sub>2</sub> as “jordisite” (Kao et al., 2001) suggests that the oxidation environment was variable immediately following uranium deposition and that weathering-derived supergene solutions served to modify both reduced and initially-oxidized uranium-vanadium ores. XRD analyses of green oxide coatings and black ores from Section 31 and yellow oxide coatings from the St. Anthony mine show that the ores host andersonite and gypsum, indicating that CO<sub>3</sub><sup>2-</sup>(aq) and SO<sub>4</sub><sup>2-</sup>(aq)-bearing, oxidizing groundwaters were responsible for developing a series of paragenetically-complex carbonate and sulfate minerals that reflect local groundwater compositions and composition changes through time.

Comparison of Grants Mineral Belt uranium mineralogy with the paragenesis of U-V minerals in other regions of the Colorado Plateau suggests that regional oxidation (Adams and Saucier, 1981) was likely responsible for uranium transport and later oxidative replacement of reduced uranium minerals (compare to Arizona Strip breccia pipe-hosted U-(Cu, Ag, Ni, Co) mineralization; e.g., see Van Gosen and Wenrich, 1989; Wenrich, et al., 1992). Latest oxidation is attributed to supergene processes coinciding with the onset of regional uplift and erosion in Laramide times of the southern portion of the Colorado Plateau.

#### A NEW TYRANNOSAURID DINOSAUR FROM THE DE-NA-ZIN MEMBER OF THE KIRTLAND FORMATION (LATE CRETACEOUS, CAMPANIAN), NORTHWESTERN NEW MEXICO

Sebastian G. Dalman<sup>1</sup> and  
Spencer G. Lucas<sup>2</sup>

<sup>1</sup>New Mexico Museum of Natural History and Science / Fort Hays State University, Hays, Kansas, 251 Hendren Ln NE, Albuquerque, NM, 87123, USA, sebastiandalman@yahoo.com

<sup>2</sup>New Mexico Museum of Natural History and Science, 1801 Mountain RD NW, Albuquerque, NM, 87104

We document a new tyrannosaurid dinosaur from the Upper Cretaceous De-na-zin Member of the Kirtland Formation, New Mexico. The new tyrannosaurid is known from an isolated but diagnostic right anterior dentary collected by the 1924 Amherst College paleontological expedition led by Frederic Brewster Loomis. The dentary is differentiated from other tyrannosaurid by the following characters: two closely spaced foramina intermandibularis oralis situated in the vicinity of the weakly declined anterior terminus of the Meckelian groove, medial surface of the lingual bar at the level of the first and second alveoli directly dorsal to the

interdentary symphysis bulges medially and has an ovoid shape, the anterior terminus of the Meckelian groove is weakly declined ventrally, and the posterior surface of the anterior step of the lingual bar is diminutive and situated at the level of the posterior end of the second alveolus/interdental plate. Overall proportions of the dentary fall in line with the “short-snouted” tyrannosaurids, such as *Lytbronax argestes* and *Teratophoneus curriei* from the Campanian of Utah. Additionally, we describe two isolated dentaries and several axial and appendicular skeletal elements, including isolated teeth, of tyrannosaurids from the De-na-zin Member. The occurrence of an additional tyrannosaurid in the southern biome of the Western Interior Basin of North America during the late Campanian adds important new information about the morphologic and taxonomic diversity of Tyrannosauridae and the paleobiogeographic distribution of these iconic predators. Furthermore, the data presented here suggest that the new tyrannosaurid is a descendant of the tyrannosaurids that lived during the Campanian in what is now the San Juan Basin in northwestern New Mexico and not the result of paleobiogeographic isolation by a physical barrier such as a rise or fall of sea level or a mountain range.

#### NEW EVIDENCE FOR PREDATORY BEHAVIOR IN TYRANOSAURID DINOSAURS FROM THE FARMINGTON SANDSTONE MEMBER OF THE KIRTLAND FORMATION (LATE CRETACEOUS, CAMPANIAN), NORTHWESTERN NEW MEXICO

Sebastian G. Dalman<sup>1</sup> and Spencer G. Lucas<sup>2</sup>

<sup>1</sup>New Mexico Museum of Natural History and Science / Fort Hays State University, Hays, Kansas, 251 Hendren Ln NE, Albuquerque, NM, 87123, sebastiandalman@yahoo.com

<sup>2</sup>New Mexico Museum of Natural History and Science, 1801 Mountain RD NW, Albuquerque, NM, 87104

A nearly complete skull of a chasmosaurine ceratopsian dinosaur from the upper Campanian Kirtland Formation (Farmington Sandstone Member) of northwestern New Mexico shows evidence of an attack by a large tyrannosaurid dinosaur. The right maxilla, the right epijugal, the right squamosal, and the left premaxilla exhibit extensive trauma in the form of several bite marks (dentalites). The bite marks on the right maxilla, the right squamosal, and the left premaxilla are full penetrations, whereas those on the epijugal are partial penetrations. Some of the largest bite marks are located on the left premaxilla and are approximately 6 cm long. Furthermore, the orientation of the bite marks indicates the angle of inclination of the head of the tyrannosaurid during

biting. The bite marks on the right side of the skull, especially those on the maxilla, record two events. During one of the events, the tyrannosaurid kept its head at a 70° angle relative to the ceratopsian head and attacked it from the side. The second event shows the tyrannosaurid facing the ceratopsian and biting it along the long axis of the maxilla. The bite marks on the left premaxilla show the position of the tyrannosaurid head at a 70° angle in relation to the ceratopsian head. The bone surface around the largest bite mark on the right maxilla has smooth margins that demonstrate that the ceratopsian survived the attack by the tyrannosaurid. However, the lack of bone remodeling around other identified bite marks suggests that most of the biting likely occurred postmortem or resulted from a dealy attack that killed the ceratopsian. Furthermore, based on the position of the bite marks and their accumulation on both sides of the ceratopsian skull, the tyrannosaurid attacked from the right and the left sides. This specimen adds new documentation of active predation by a tyrannosaurid dinosaur and thus runs contrary to the idea that tyrannosaurids were scavengers.

#### CONTINUING MENTORSHIP OF UNDERREPRESENTED STUDENTS IN GEOPHYSICS THROUGH THE EDUCATIONAL INTERNSHIP IN PHYSICAL SCIENCES (EIPS)

Deandra De Los Santos<sup>1</sup>, Sarah Pon, Frankie Enriquez, Guadalupe Alvarez-Rodriguez, Sophia Terrazas, Jason Ricketts, and John G. Olgin, <sup>1</sup>dde6@miners.utep.edu

The number of underrepresented minorities pursuing STEM fields, specifically in the sciences, has declined in recent times (Lane and Christensen, 2013). In response, the Educational Internship in Physical Sciences (EIPS) provides a mentoring environment where students can actively engage in science projects with professionals in their field to gain valuable experience in an academic setting. Assigned research projects focus on identifying surface hydrology in Mexico and New Mexico and creating laboratories related to their research for introductory physics and planetary astronomy classes. These experiences allow students to develop new skill sets and gain in-depth knowledge in their field. Interns harness and build on what they have learned through the program, and directly apply it in an academic environment in El Paso Community College (EPCC) classes on solar system astronomy. Since the majority of interns are transfer students or alumni of EPCC, they give a unique perspective and dimension of interaction, giving them an opportunity to personally guide and encourage current students to pursue available STEM opportunities. Therefore not only will interns gain valuable lessons in teaching, research, and public speaking, but those engaged at the community college will learn of the multiple possibilities and careers

in the STEM fields. They will also collaborate with past interns on research projects (Enriquez et al, 2017). Their experiences and methodologies are presented here.

#### ALPINE HYDROLOGY OF PHOENIX SPRING AND LAKE FORK OF THE RIO HONDO, TAOS SKI VALLEY, NM

P. Drakos, A. J. Tafoya, J. Lazarus, and J. Riesterer

Glorieta Geoscience, Inc., PO Box 5727, Santa Fe, NM, 87502, drakos@glorietageo.com

The Phoenix Spring complex currently provides the entire municipal water supply for the Village of Taos Ski Valley, NM, and is one of the primary sources of stream flow in the upper reaches of the Lake Fork of the Rio Hondo. Water is also diverted during winter low-flow conditions for snow making by Taos Ski Valley, Inc. A field investigation was initiated in 2016 to develop a conceptual model of the alpine hydrology of the groundwater and surface water systems. This investigation included collection of precipitation samples and discrete intervals of the snowpack for tritium and stable isotope analyses, installation of piezometers and water level monitoring upgradient of the Phoenix Spring complex, sampling of springs, piezometers and Williams Lake for general chemistry, tritium, and stable isotopes, and gaging of stream flows.

Phoenix Spring is situated at an elevation of 10,310 ft in the Lake Fork valley, a north-to-northwest-trending glacial valley draining the Williams Lake cirque and Wheeler Peak. The Lake Fork Valley is underlain by glacial deposits including rock glacier and thick valley bottom till. Recharge occurs both in Williams Lake Cirque and along the Lake Fork Valley, with snowmelt and monsoonal precipitation infiltrating directly into the highly permeable glacial deposits. No surface water flow leaves the cirque; instead groundwater discharges further down the valley through springs and directly to the Lake Fork. Phoenix Spring discharges at a location where the width of glacial deposits narrows between a bedrock constriction formed by Precambrian gneiss and schist. Spring discharge ranges from a low of 200–300 gallons per minute (gpm) or less from December through April to a high of over 1,000 gpm in June and July. The Lake Fork above Phoenix Spring is an intermittent stream that flows during spring runoff in response to discharge from South Fork Lake Fork and East Fork Lake Fork springs. These springs both discharge at a rate up to several cubic feet per second (cfs) during peak spring runoff, but are typically dry by August of each year. The Lake Fork is a gaining stream from its origin at the Phoenix Spring to the confluence with the North Fork. Below this confluence the Rio Hondo is a gaining reach to the USGS gaging station at Valdez.

Preliminary analysis of  $\delta^{18}\text{O}$ - $\delta^2\text{H}$  data indicate a greater contribution to recharge from summer monsoonal precipitation than

has been found in previous studies, although recharge is still dominated by winter precipitation. Tritium data from springs are within the range of tritium concentrations indicative of a modern recharge source. Precipitation data and water levels measured in piezometers in September, 2017 show that shallow groundwater is recharged by monsoonal precipitation events with an approximate two-week lag time. Preliminary study results indicate that winter precipitation is the predominant component of recharge to Phoenix Spring, with a significant component of summer monsoonal precipitation.

#### A LABORATORY SIMULATION OF CU, PB AND FE RELEASE FROM SULFIDE-CONTAINING MINE TAILINGS IN SEAWATER

Rodrigo Frayna Embile, Jr.<sup>1</sup>, Ingar Walder<sup>2</sup>, Christopher Schub<sup>3</sup>, and Jenna Donatelli<sup>1</sup>

<sup>1</sup>NM Institute of Mining and Tech, PO Box 3777, 801 Leroy Place, Socorro, NM, 87801, rodrigojr.embile@student.nmt.edu  
<sup>2</sup>E&ES, New Mexico Tech, 801 Leroy Place, Socorro, NM, 87801

<sup>3</sup>Queen's University, Kingston, Ontario, Canada

Cu, Pb and Fe release from the deposition of sulfide-containing tailings in seawater was investigated using a batch reaction experiment. Tailings from a porphyry Cu-Au and a sediment-hosted Cu deposit were submerged in 1.8 L synthetic seawater. Pore water and overlying seawater samples were collected and analyzed for pH, redox potential and trace metals (Cu, Pb and Fe) concentration. Results from this study show that there is very low Cu (10–40 µg/L), Pb (2–10 µg/L) and Fe (5–50 µg/L) released into solution throughout the course of 87 days. Trace metal concentration was generally very stable (Cu, Fe) or declined (Pb) through time. The release of acid into solution was also very low due to the high buffering capacity of seawater. Long-term trace metal release from tailings in seawater is therefore theorized to be low and is a slow process.

#### THE SHORT NORMAL PALEOMAGNETIC INTERVAL—C29R.1N—IS WITHIN THE PALEOCENE OJO ALAMO SANDSTONE, SAN JUAN BASIN, NEW MEXICO

James E. Fassett

USGS retired, Independent Research Geologist, 552 Los Nidos Dr, Santa Fe, NM, 87501, jimgeology@centurylink.net

A short normal paleomagnetic polarity interval has been documented within the Ojo Alamo Sandstone at six localities in the southern San Juan Basin of New Mexico. Where the top and base of this normal polarity interval have been determined it is 11–12 meters thick. This polarity interval was initially thought to be magnetochron C29n, but

relatively new <sup>40</sup>Ar/<sup>39</sup>Ar ages (Fassett, 2013) and published palynologic data (Fassett, 2009) prove that this interval must be within the upper (Paleocene) part of chron C29r and is labeled C29r.1n. This paleomagnetic normal chron is a previously unrecognized normal chron within C29r. The Cretaceous-Paleocene boundary is known to be within C29r and palynologic data clearly show that chron C29r.1n is above the K-Pg boundary and is thus in Paleocene strata. Williamson et al. (2008) indicated that this short normal magnetochron is chron C30n however published palynologic data clearly indicate that Maastrichtian-age strata are absent in the San Juan Basin and thus C30n, that is within the Maastrichtian, cannot be present in the basin. Dinosaur fossils within C29r.1n, and above in the Paleocene Ojo Alamo Sandstone, are therefore indisputably Paleocene in age.

#### SOIL CHRONOSEQUENCE STUDY OF LONG VALLEY, NORTHERN NEW MEXICO: INSIGHTS INTO THE DEVELOPMENT OF SOILS ON CATENAS IN A POST-GLACIAL VALLEY

Anthony David Feldman<sup>1</sup> and James Bruce Harrison<sup>2</sup>

<sup>1</sup>New Mexico Institute of Mining and Technology, 713 Bursum Place, Socorro, NM, 87801, anthonydfeldman@gmail.com

<sup>2</sup>New Mexico Institute of Mining and Technology, 801 Leroy Place, Socorro, NM, 87801

The history of glacial advance and retreat cycles in mountain watersheds is recorded in a variety of landforms including moraines, lake sediments, and outwash deposits. The Sangre De Cristo mountain range in northern New Mexico contains some of the southernmost glacial activity in North America; yet there have been few studies to determine how these advances correlate with the mountain glaciations of the Rocky Mountains. In this study, we combine field geomorphic reconnaissance, terrain analysis, and soil development indices to determine the relative size and extent of glacial advances in Long Valley, a formerly glaciated valley in the Sangre de Cristo Mountains. The relative ages of Pleistocene and Holocene glacial deposits were investigated through a soil chronosequence established across several moraines in Long Valley extending east from Big Costilla Peak to the Costilla Vega playa. A soil profile development index (SPDI) utilizing several soil development parameters was used to identify differences in soil development between the different moraines. Utilizing the calculated SPDI values as well as field and DEM observations of moraine morphology, four glacial cycles are observed within the Long Valley moraine sequence. These cycles were correlated with the glacial/paleoclimate history of the southern Rocky Mountains. One Bull Lake advance, two Pinedale advances, a prealtithermal Latest Pleistocene /Early Holocene glaciation, and two small

post-altithermal Neoglacial advances were identified. Several studies have suggested that soils developed on moraine summits are often eroded and cannot be utilized to separate glacial advances of significantly different ages. Soils developed along moraine catenas were described in this study. Summit soils exhibited the greatest correlation with age compared to toeslope and backslope soil profiles. While the SDI based on soil morphological parameters clearly separated different aged deposits, several pedogenic chemical alterations were also investigated. Soil clay content increased uniformly with age across all catenary positions as well as increasing downslope. Hydroxylamine extractable poorly ordered iron decreased with age while Dithionite extractable secondary iron oxyhydroxides increased with age. The ratio of poorly ordered to secondary iron oxyhydroxides decreased with time. Organic carbon content could distinguish between moraines within the cirque and valley sequences but not between individual moraines.

#### THE TIMING OF NEOGENE EXTENSION IN THE SOUTHERN RIO GRANDE RIFT AND SOUTHEASTERN BASIN AND RANGE PROVINCE USING APATITE (U/TH)-HE THERMOCHRONOMETRY

Michelle M. Gavel<sup>1</sup>, Jeffrey M. Amato<sup>1</sup>, and Jason W. Ricketts<sup>2</sup>

<sup>1</sup>Dept. Geological Sciences, New Mexico State University, gavel@nmsu.edu

<sup>2</sup>Dept. of Geological Sciences, University of Texas at El Paso

The Rio Grande rift and Basin and Range are two of the most widely studied extensional provinces in the world, yet thermochronologic data allowing for the temporal constraint of their evolution remains sparse in southern New Mexico where the two provinces physiographically blend. Apatite (U-Th)/He thermochronologic (AHe) methods were applied to 24 apatite grains from six samples from footwalls of fault-block uplifts across southern New Mexico (the Burro Mountains, Cooke's Range, Caballo Mountains, and the San Andres Mountains) in order to investigate possible differences in timing of extension between the Basin and Range and Rio Grande rift. AHe ages range from 6.2±0.4 Ma to 31.8±1.1 Ma across all sample locations. Five out of six samples have standard deviation of <20% for all crystals from each sample. Effective uranium concentration (eU)-age correlations are observed in samples from the San Andres and Burro Mountains but are not detected in Cookes or Caballo samples. Thermal history models were generated for each sample in the program HeFTy that combine existing apatite fission-track and U-Pb ages where possible, as well as new AHe ages. This will allow for the evaluation of cooling trends and timing of active faulting across the southern rift and easternmost Basin and Range. Future work

will include generating additional AHe data and zircon (U-Th/He) data to better refine time-temperature models for additional locations across southern New Mexico.

## THE GEOLOGY AND HYDROLOGY OF ENVIRONMENTAL HAZARDS FROM AEOLIAN DUST AND SAND IN THE CHIHUAHUAN DESERT

Thomas E. Gill<sup>1</sup>, Miguel D. Acosta<sup>2</sup>, Matthew C. Baddock<sup>3</sup>, Jeffrey A. Lee<sup>4</sup>, Iyasu Eibedingil<sup>5</sup>, and Junran Li<sup>6</sup>

<sup>1</sup>University of Texas- El Paso, Department of Geological Sciences, 591 W University Avenue, El Paso, TX, 79968, tegill@utep.edu

<sup>2</sup>Universidad Autonoma de Ciudad Juarez, Instituto de Ingeniería y Tecnología, Ciudad Juarez, Chihuahua, Mexico

<sup>3</sup>Loughborough University, Department of Geography, Loughborough, Leicestershire, LE11 3TU, U.K.

<sup>4</sup>Texas Tech University, Department of Geosciences, Lubbock, TX, 79409

<sup>5</sup>University of Texas- El Paso, Environmental Science and Engineering Program, El Paso, TX, 79968

<sup>6</sup>University of Tulsa, Department of Geosciences, Tulsa, OK, 74104

The Chihuahuan Desert, covering much of southern New Mexico, is one of most active areas of aeolian processes in the Western Hemisphere. Blowing sand and dust represents one of the principal environmental hazards in the Chihuahuan Desert and areas downwind. The dynamics of Chihuahuan Desert dust and sand storms are modulated by weather (wind), earth surface dynamics (land cover and sediment characteristics), hydrology (drought and lake-filling floods), and human activities (land use). Sand and dust events from the Chihuahuan Desert have impacts on ecosystems, including those far downwind of the desert: and also have adverse effects on human health (respiratory disease) and safety (highway crashes). More than a decade of research by the authors, detecting hundreds of dust point sources in NASA MODIS and NOAA GOES satellite images coupled with fieldwork at many of those sites, has advanced understanding of drivers and triggers of aeolian processes in the Chihuahuan Desert and beyond.

Aeolian dust and sand does not arise randomly or everywhere within the landscape, but rather is associated with specific landforms (“preferential source areas”). Playas and lake basins cover ~4% of the Chihuahuan Desert surface but emit ~50% of dust plumes visible from satellite. Within basins, contacts between sand sheets/dunes and playas/ephemeral lakes—merging coarse grains for saltation and fines for suspension—are dominant sites of dust emission. Alluvial lowlands, although less active and intense sources than playas, produce more total sediment due to their larger spatial coverage in the Chihuahuan Desert. Sand sheets and dunes produce varied levels of

aeolian action based on vegetative stabilization and physical properties. Anthropogenic land disturbance, especially for agriculture (particularly abandoned or fallow croplands just across the border in Chihuahua) initiates additional “hotspots” of dust/sandstorms. Hydrology acts as an on/off switch of dust emission through filling and moistening playa basins, and controlling land cover through soil moisture; dust/sandstorm sources are concentrated in areas of severe to extreme drought. Within New Mexico, aeolian focus areas include the Paleolake Palomas basin connecting with the Mimbres River sinks, and the Lordsburg Playa (site of dozens of fatal dust-related highway crashes). Dust from the White Sands impacts topsoil chemistry in the Sacramento Mountains >100km downwind and is regularly transported downwind to other states: conversely, dust and sand from outside New Mexico (Casas Grandes River Basin in Mexico; Willcox Playa in Arizona) blows into the state causing impacts. Dust and sand storms have a documented association with coccidioidomycosis (valley fever), a sometimes-fatal infection of soilborne fungus; and are associated with increased incidences of cardiovascular and respiratory diseases in Las Cruces.

The Chihuahuan Desert has become a global test bed for understanding the geological and hydrological characteristics and environmental impacts of aeolian processes, continuing to reveal the wind’s secrets.

## REVISITED MAJOR-SOLUTE OBSERVATIONS AND PRELIMINARY TRACE ELEMENT ANALYSES OF GEOTHERMAL SALINIZATION OF THE JEMEZ WATERSHED, NM

Jon Golla, Laura Crossey, and Abdul-Mehdi Ali

University of New Mexico, Northrop Hall, 221 Yale Blvd NE, University of New Mexico, Albuquerque, NM, 87131, jkgolla@unm.edu

The Jemez Watershed (JW) is in north-central New Mexico within the Jemez Mountains, which overlies the intersection between the Rio Grande Rift and the Jemez Lineament. A prominent feature of the JW is the Valles Caldera, which houses a world-class, high-temperature, liquid-dominated geothermal system ( $\leq 300^\circ\text{C}$ ). Such highly mineralized geothermal systems usually have a significant environmental footprint. Geologic evidence suggests that the JW is influenced by the Valles Caldera geothermal system (VC). Multiple outflow thermal expressions, namely Jemez Springs Hot Springs and Soda Dam Springs, of the VC surround the main tributary (Jemez River or JR) of the JW. Furthermore, just southeast of the VC Ring Fracture Zone, headwaters of Sulphur Creek mixing with intra-caldera, acid-sulfate springs contribute to the JW further downstream. We aim to characterize hydrochemical mass movement between JW and VC waters with

refined major-ion chemistry and new trace element analyses.

Recent Fall 2017 sampling during low-flow (~23–26 cfs) conditions reflects impairments of VC geofluids on JW water quality. There is bulk salinization (net ~500 ppm increase in total dissolved solids) of JR waters from just above Soda Dam Springs to San Ysidro Bridge. Upstream JW acidification (from pH 6.2 to 1.61) and trace metal salinization ([Al]: 0.03–21ppm & [Fe]: 0–10ppm) occur in the Sulphur Creek subbasin, and similar downstream influences are observed in Redondo Creek (from pH 7 to 4.7; [Al]: 0.01–1.5ppm), a JW tributary. We display these geochemical influences spatially and through multivariate statistics (principal component analysis). A tentative binary Cl/Br mixing model reveals bulk-salinized waters contain 19–30% geothermal spring/seepage contributions; this mixing model is not applicable to acidified waters, as Cl and Br lose conservative behavior under a pH of 2.

From the same sample suite, concentrations of twenty-four trace metals and rare earth element (REEs) are detected through inductively coupled plasma mass spectrometry. Tentatively, these results show that ~71% of analyzed metals (Sb, Cr, Pb, Se, Cd, V, etc.) appear the most concentrated in the acidified and  $\text{SO}_4$ -rich waters. Comparatively, the outflow thermal springs and bulk-salinized JR waters contain the greatest concentrations of As, U, Li, Rb, and Cs. Interestingly, among these two classes, Ni and Ti appear in equal amounts. Analyzed REEs data reveal patterns congruent with those observed by previous investigators. The acidic waters show the highest REEs content (at least one order of magnitude more concentrated) and exhibit positive Eu anomalies. The outflow thermal and bulk-salinized fluids are characterized by the documented negative Eu anomalies, but REEs patterns for these waters appear the most incomplete (Nd is nonexistent in some) and fluctuating, which may indicate below-detection values.

These observations set up the upcoming stages of this study, which will employ radiogenic isotopic systems for more sensitive mixing models and reaction path modeling for determining sinks and sources. Further development of trace element and coupled major-trace element interpretations and necessary repeat analyses are also in view. This research aims to ultimately further understanding of continental geothermics, in hopes of serving as an analog to environmental assessments of other hydrothermal systems.

## AIRBORNE HEALTH HAZARDS ON NATIVE AMERICAN TRIBAL LANDS: THE URANIUM MINING LEGACY

Tylee M. Griego<sup>1</sup>, Matt Campen<sup>2</sup>, Johnmye Lewis<sup>3</sup>, and Adrian J. Brearley<sup>1</sup>

<sup>1</sup>University of New Mexico, Dept. of Earth and Planetary Sciences, MSC03-2040, 1 University of New Mexico, Albuquerque, NM, 87131, Tgrieg05@unm.edu

<sup>2</sup>University of New Mexico—Health Sciences Center, Dept. of Pharmaceutical Sciences, 1 University of New Mexico, Albuquerque, NM, 87131

<sup>3</sup>University of New Mexico, Community Environmental Health Program, MSC09-5360, 1 University of New Mexico, Albuquerque, NM, 87131

From 1952–1982, uranium ores were mined extensively at numerous mine sites in the Southwest USA, a significant number on them on Native American Tribal Lands. During their periods of operation, these mines caused significant health hazards both to miners and the communities living in close proximity to the mine sites. Although these mines are now shut down, the environmental legacy of mining continues to be of major concern to the local communities. Although some of these abandoned uranium mines (AUM) sites have been reclaimed under the US EPA Superfund program, many have not. The potential exposures to uranium through water, air, and food sources, such as livestock, even from reclaimed mines are still poorly understood. In particular, the potential past and present risks of exposure to toxic metals by inhalation of airborne particles derived from contaminated soils and mine wastes from AUM is essentially unknown. New research is underway to assess the concerns of Native American communities living close to the recently designated Superfund sites at Blue Gap/Tachee in Arizona and at Laguna Pueblo in New Mexico. The research is supported by the newly-established University of New Mexico's Metal Exposure Toxicity Assessment on Tribal Lands in the Southwest (METALS) Superfund Research Project funded by the National Institute of Environmental Health Sciences.

The overall goal of the research is to determine if wind-blown, re-suspended particulate matter (PM) from these two AUM sites is a potential pathway for human exposure to toxic metals, such as uranium, vanadium, arsenic, and copper. In particular, the <2.5 micron PM size fraction is especially hazardous to human health because it is respirable and retained deep in the lungs when inhaled. We are investigating this problem using both laboratory experiments and in situ sampling of airborne particulates from the mine sites. Soil and mine waste samples from the mine sites undergo laboratory resuspension following initial sieving into coarse-size fractions and SEM characterization. Resuspension is carried out using a cascade impactor collector to separate the dust into different fine-grained size fractions. These different

fractions are analyzed in detail using SEM and TEM techniques and ICP-MS to define the chemical, physical, and mineralogical characteristics of the metal mixtures. This work provides a characterization of the key characteristics of the local source materials which may undergo aeolian transport. We especially want to understand if toxic metals are present within these source materials as nanoparticles that would be highly reactive in lung fluids if inhaled and could result in a low level, constant exposure to these metals.

These data will then be integrated with similar analyses of airborne particulates collected from the mine sites to develop a more complete understanding of potential toxic metal exposures for communities downwind of the mine sites. The results of the study will better quantify and understand the exposure risks associated with airborne particulates. The data are critical to developing more effective exposure mitigation strategies for at-risk communities, such as an early warning system initiated by specific wind direction and/or velocity conditions.

## HYDROGEOLOGIC-FRAMEWORK, WATER-SUPPLY WELL PUMPING, AND ACEQUIA-IRRIGATION CONTROLS ON SUBSURFACE-WATER FLOW AND CONTAMINANT TRANSPORT IN SANTA FE GROUP AND ALLUVIAL-TERRACE DEPOSITS BENEATH HISTORIC SANTA FE, NEW MEXICO

John W. Hawley<sup>1</sup> and Baird H. Swanson<sup>2</sup>

<sup>1</sup>Retired, 1000 Vassar Drive NE, Albuquerque, NM 87106-2631, hgeomatters@gmail.com

<sup>2</sup>Swanson Geoscience LLC, 6508 Natalie NE, Albuquerque, NM, 87110

Between 1609 and 1880 the historic center of the present City of Santa Fe (COSF) was a small Colonial-Provincial-Territorial Capital sustained by acequia-irrigation agriculture, livestock and timber production, and a military-post/trade-route location. The vital roles played by Santa Fe (SF) River and its interlinked acequia system are of special environmental interest. Significant anthropogenic groundwater contamination, however, dates to the SF Railroad's arrival in February 1880 and the expansion of automotive tourism soon thereafter. More serious environmental problems (EPs) are related to accelerated urbanization that occurred soon after 1942 when the AT&SF Railyards became the primary staging area for Manhattan Project-LANL construction. The 1942 to 1952 period also coincided with public water-supply (PWS) well and SF-River dam construction, and essential cessation of acequia irrigation. Besides the former Railyards District, adjacent parts of COSF include at least 20 other EP sites that are known or potential sources of groundwater contamination in Santa Fe Gp (SFG) aquifer system and overlying SF River-terrace deposits. The former PNM Santa Fe Generating Station (SFGS) Site is one of them. Contaminants detected in PWS

wells and monitor wells (MWs) include gasoline/diesel-fuel and chlorinated-solvent derivatives. Source areas include bulk-fuel storage facilities, gas stations, dry cleaners, and a drywell disposal site. From the perspective of geohydrologic, and hydrochemical mechanisms of subsurface-water flow and contaminant transport, the hydrogeologic framework of the SFG-Tesuque Fm aquifer and overlying vadose-zone material beneath central COSF has two primary components: 1. Lithologic and structural—with hydraulic and chemical properties determined by standard geoscience-based methods (e.g. geology-geomorphology, geophysics, and geochemistry); and 2. Anthropogenic—where acequias and/or large-production wells form the primary controls on the location and timing of vadose-zone/saturated-zone potentiometric transitions in subsurface-water flow regimes.

This presentation focuses on a 2 mi<sup>2</sup> area of central COSF where a logged-borehole data base allows preparation of 1:3,000-scale hydrogeologic maps and fence-diagram grids based on records from 1) four exploratory and PWS wells with depths ranging from 1,200 to 2,660-ft, and 2) more than 150 MW boreholes at major EP sites, some of which are in the 300 to 500-ft depth range. Primary hydrogeologic-framework components are illustrated at multiple scales: 1. A conceptual perspective of a mid-Miocene piedmont landscape includes a reconstruction of the Tesuque Fm-Lithosome S (Tts) fluvial fan and its ancestral Santa Fe-Range sediment-source area (Google Earth® image). 2. The internal fractal fabric of fan-distributary channel and inter-channel facies is shown on an idealized fan-piedmont diagram. 3. Study area framework depiction includes a 1:1, 1:6000-scale block diagram that shows its basic Tts west-tilted structural and fluvial-fan lithofacies framework to a 3,500-ft amsl base elevation. 4. Hydrostratigraphic and structural relations at the most-detailed level are illustrated by 1:3,000-scale maps and a 1,000-ft fence-diagram grid of 26 cross-sections on a 2-ft contour base; with surficial-geologic and “post-Tesuque erosion surface” structure-contour maps included. 6. A 7,000-ft long, 3,000-ft deep cross section, with potentiometric-surface drawdown time-lines, schematically illustrates the hydraulic/hydrologic impacts of about 62 years of SF-PWS-well pumping on an ever-diminishing saturated thickness of westward-dipping Tts deposits.

## ASSESSMENT OF EPISODIC HYDROTHERMAL ACTIVITY IN THE RINCON GEOTHERMAL SYSTEM

Melinda Horne<sup>1</sup>, Mark Person<sup>1</sup>, Shari Kelley<sup>2</sup>, Matthew Folsom<sup>1</sup>, Jeff Pepin<sup>1</sup>, and James Witcher<sup>3</sup>

<sup>1</sup>New Mexico Tech Hydrology Program, melindahorne@icloud.com

<sup>2</sup>New Mexico Bureau of Geology and Mineral Resources

<sup>3</sup>Witcher and Associates

The Rincon geothermal system is located in the East Rincon Hills 56 km north of Las Cruces, at a topographic high dividing the Rio Grande and Jornada del Muerto basins. Rincon is a blind geothermal system that has no surface expression, and its exact size and extent are unknown. Temperatures are as high as 96°C at 310 m depth on the hanging wall of an east-dipping normal fault known as the East Rincon Hills Fault (ERHF). Five thin (<1 m thick) opal beds have been mapped adjacent to the ERHF. An overturned temperature profile (from well-bore SLH-1) and the distribution of opal deposits indicate that the geothermal system has been active episodically for at least 2 Ma. We have completed two transient electromagnetic (TEM) transects that extend across the foot- and hanging-wall of the ERHF. An additional magnetotelluric (MT) survey is planned for the Fall of 2018. Formation resistivity maps based on 1D TEM inversions collected from our two transects have identified a laterally extensive conductive feature near the water table that may be associated with a geothermal outflow plume of hot, brackish water. We hypothesize that fault permeability increases following relatively low magnitude (<M 5) seismic events and then gradually declines due to silica mineralization. Future work will focus on integrating MT surveys into our study.

## A NEW *STEGOMASTODON* SKULL (PROBOSCIDEA: GOMPHOTHERIIDAE) FROM THE CAMP RICE FORMATION, DOÑA ANA COUNTY, NEW MEXICO.

Peter Houde<sup>1</sup> and Danielle Peltier<sup>2</sup>

<sup>1</sup>Department of Biology, New Mexico State University, Box 30001 MSC 3AF, Las Cruces, NM, 88001, phoude@nmsu.edu

<sup>2</sup>Department of Geological Sciences, New Mexico State University

*Stegomastodon* is among three mastodon-like elephant cousins of the family Gomphotheriidae native to the Plio-Pleistocene of New Mexico. We report what is, to the best of our knowledge, the first associated cranium and mandible of *Stegomastodon* (NMSU 15723) from New Mexico. It was excavated from the Camp Rice Formation in Las Cruces, Doña Ana County, NM. The Camp Rice in this general area is said to have a temporal range of 3.6–0.8 Ma (early Blancan to early Irvingtonian or Gauss to Matuyama

chrons). *Stegomastodon* is believed to have become extinct at 1.2 Ma. The nearby *Stegomastodon*-bearing Tortugas site was biostratigraphically dated to 1.6–1.2 Ma, but the two sites have not yet been stratigraphically correlated. NMSU 15723 was excavated from unconsolidated mostly well-sorted multi-story cross-bedded fluvial channel sands. Large rip-up clasts of presumably allochthonous brown and gray clays/paleosols as well as a few intercalated beds of clays/paleosols and of gravels suggest proximity to flood plains and alluvium.

NMSU 15723 includes a complete mandible and a cranium with all four third molars (M3/m3) and the left tusk (I1), but lacking the right tusk. We refer it to *Stegomastodon primitivus* because it is brevirostrine, the tusk (I1) is up-curved, and upper M3 is tetralophid and lower m3 is pentalophid, or tetralophid if the two distal rows of worn conules correspond to the talonid or ‘heel’.

*Stegomastodon* skulls are extremely rare, so every new specimen has the potential to significantly broaden knowledge of these little-known polymorphic behemoths. NMSU 15723 is most notable for three reasons. 1) A previously undocumented weak enamel band is present on the medial side of the tusk. A lateral enamel band is variously present in the South American *Notiomastodon*, with which *Stegomastodon* has historically been confused, as well as in some other more primitive proboscideans. A spiral enamel band is also characteristic of the two other New Mexican genera of Plio-Pleistocene gomphotheres, *Cuvieronius* and *Rhynchotherium*. 2) NMSU 15723 combines *S. primitivus*-like molar and *S. mirificus*-like molar and mandibular morphologies. Specifically, its molars are tetra/pentalophid as in *S. primitivus*, but they exhibit ptychodonty (i.e., plication or crenulation of enamel) and the mandibular ramus is recumbent as in *S. mirificus*. 3) NMSU 15723 exhibits extreme antemortem tooth wear. This could be evidence of great age or that the animal consumed a more abrasive diet than that for which it was well adapted or both. The latter interpretation is consistent with the hypothesis that *S. mirificus* is a chronospecies of *S. primitivus* that was somewhat better adapted for grazing in that tooth wear could be a strong evolutionary selective pressure. Gomphotheres were ultimately entirely replaced by obligate grazers, mammoths, as New Mexico became increasingly arid.

## SR AND PB FELDSPAR GEOCHEMISTRY OF MIDDLE-LATE EOCENE VOLCANIC ROCKS OF THE PALM PARK FORMATION AND OREJON ANDESITE, SOUTH-CENTRAL NEW MEXICO

Makayla R. Jacobs, Frank C. Ramos, and Brian A. Hampton

New Mexico State University, 1255 N. Horseshoe St., Gardiner Hall, Las Cruces, NM, 88003, makk117@nmsu.edu

During middle-late Eocene time, southern New Mexico was marked by a resurgence of intermediate volcanism that took place just after Laramide deformation and prior to the late Eocene (~36 Ma) ignimbrite flareup and initiation of the Rio Grande rift. Volcanism and volcanoclastic sedimentation during this time are recorded in south-central New Mexico by rocks of the Palm Park Formation, Orejon Andesite, and equivalent units (i.e., Cleofas Andesite). Although recent efforts have been made to constrain the age and duration of middle-late Eocene volcanism in southern New Mexico, very little is known about the geochemistry and magmatic sources of these rocks. We present Sr and Pb isotope ratios of single plagioclase crystals from eight sample localities in the Doña Ana, Organ, Robledo, and Sierra de Las Uvas Mountains in south-central New Mexico. Plagioclase crystals were extracted from volcanic flows and ash-fall tuffs from the Palm Park Formation and Orejon Andesite. Results are summarized from stratigraphic oldest to youngest.

Some of the oldest parts of the Palm Park Formation crop out in the Robledo Mountains (Apache Canyon; 45.0±0.7 Ma) and are characterized by unradiogenic age-corrected <sup>87</sup>Sr/<sup>86</sup>Sr signatures (0.70498–0.70519) and Pb isotopes (e.g., <sup>206</sup>Pb/<sup>204</sup>Pb = 17.20–17.22). Compared to Apache Canyon, the slightly younger Orejon Andesite in the Organ Mountains (Fillmore Canyon; 43.8±0.4 and 42.8±0.5 Ma) have variable Sr and Pb isotopes. The first Orejon Andesite lava flow is more radiogenic than the later. <sup>87</sup>Sr/<sup>86</sup>Sr signatures (0.70617–0.70644) are more radiogenic than the second lava flow (0.70470–0.70480). Pb isotopes are similar in that the first flow is more radiogenic (e.g., <sup>206</sup>Pb/<sup>204</sup>Pb = 17.65–17.96) than the second (17.24–17.26). Samples from some of the younger parts of the Palm Park Formation in the Doña Ana Mountains (Cleofas Canyon; 41.6±0.7 and 41.3±0.7 Ma) have unradiogenic <sup>87</sup>Sr/<sup>86</sup>Sr signatures (0.70450–0.70468) and less radiogenic Pb isotopes (e.g., <sup>206</sup>Pb/<sup>204</sup>Pb = 17.23–17.53). Palm Park Formation volcanic rocks in the Robledo Mountains (Faulkner Canyon; 41.0±0.6 Ma) have unradiogenic <sup>87</sup>Sr/<sup>86</sup>Sr signatures (0.70438–0.70471) and Pb isotopes (e.g., <sup>206</sup>Pb/<sup>204</sup>Pb = 17.18–17.33). Finally, the youngest parts of the Palm Park Formation crop out in the Sierra de Las Uvas Mountains (Bell Top Mountain;

39.6±0.5 Ma) have radiogenic  $^{87}\text{Sr}/^{86}\text{Sr}$  signatures (0.70572–0.70688) and unradiogenic Pb isotopes (e.g.,  $^{206}\text{Pb}/^{204}\text{Pb} = 17.27\text{--}17.39$ ).

Overall, feldspars from some of the early-erupted lavas (~45–44 Ma) have more radiogenic Sr and Pb isotope ratios than those in late-erupted lavas (~41–39 Ma). These variations likely resulted from involvement of different, discrete magmatic sources or magmatic systems that were incorporating more crust. The two ash-fall tuffs with large variation in Sr and Pb values from the oldest (~45 Ma) and youngest (~39 Ma) parts of the Palm Park Formation were likely far-traveled and derived from a distal magmatic source (vent).

#### UPDATED STRATIGRAPHIC NOMENCLATURE OF THE PLIO-PLEISTOCENE PALOMAS FORMATION (UPPER SANTA FE GROUP), SOUTH-CENTRAL NEW MEXICO

Andy Jochems, Dan Koning, and Colin Cikoski  
New Mexico Bureau of Geology & Mineral Resources, 801 Leroy Place, Socorro, NM, 87801, andy.jochems@nmt.edu

The upper Santa Fe Group in south-central New Mexico was formally defined as the Palomas Formation over 30 years ago and is interpreted as representing alluvial fan and axial-fluvial depositional environments (Lozinsky and Hawley, 1986). The Palomas Formation was previously subdivided into 3 to 5 member-rank lithostratigraphic units based on their general provenance (derived from the hanging wall or footwall of surrounding uplifts versus ancestral Rio Grande). Through recent mapping efforts in the Engle and Palomas Basins, we have established a more detailed Palomas Formation stratigraphy that reveals up-section trends in lithology and texture. These trends have significant implications for depositional setting, tectonics, paleoclimate, and groundwater hydrology in the arid basins of the southern Rio Grande rift. Our revised Palomas Formation stratigraphy uses provenance and texture to differentiate 5 member-rank units whose respective contacts are typically gradational or interfingering. These 5 units are mappable at 1:24,000 across an area of ~3,000 km<sup>2</sup> in Sierra and Socorro Counties, and can locally be expanded to as many as 15 subunits.

The 5 primary lithostratigraphic units and their estimated ages are: lower (~5–3.6 Ma), middle (~3.6–2.2 Ma), transitional (~2.5–2.0 Ma), upper (~2.0–0.8 Ma), and axial-fluvial (~5–2 Ma, where preserved). Age ranges are from radiometric ages, magnetostratigraphy, and biostratigraphy. The lower Palomas Formation consists of cemented pebbly channel-fill gravel with subordinate massive, sandy to silty hyperconcentrated flow deposits. Fine sand and silt, including hyperconcentrated flow deposits, and <20% pebbly, clay-free channel-fills characterize the middle unit. The transitional unit features

silty sand, prominent carbonate ledges, and more channel-fill gravels than the middle unit but fewer than the upper unit. The upper unit consists of laterally extensive channel-fills and sand lenses interbedded with subordinate silty to clayey deposits. Interfingering with the lower and middle units is another member-rank unit, the axial-fluvial facies, consisting of cross-stratified sand with lesser gravel (including extra-basin lithologies) and finer floodplain deposits.

A newly recognized coarsening-fining-coarsening pattern in alluvial fan facies of the Palomas Formation indicates subdued deposition of coarse debris-flow or channel-fill gravel during the latest Pliocene to early Pleistocene (3.6 to 2.0 Ma), followed by significant fluvial deposition in transverse Rio Grande tributaries. We interpret this trend to reflect paleoclimate-modulated clastic input from the Black Range to the west. Lower sediment flux from these highlands coincided with a slightly wetter middle-late Pliocene (4–2.6 Ma). Progressive drying trends in the Pleistocene corresponded with piedmont progradation, perhaps due to more intense summer monsoons coupled with sparser hillslope vegetation. Other potential research avenues from our updated stratigraphy include testing models of axial-transverse sedimentation in extensional basins and incorporation into hydrostratigraphic units containing or confining aquifer systems in the Engle and Palomas Basins.

#### ADDITIONS TO THE ICHNOTAXA AND ICHNOASSEMBLAGES OF THE CRETACEOUS (ALBIAN) MESILLA VALLEY FORMATION AT CERRO DE CRISTO REY, SUNLAND PARK, NM

Eric J. Kappus<sup>1</sup> and Spencer G. Lucas<sup>2</sup>  
<sup>1</sup>Southwest University, 1414 Geronimo Dr., El Paso, TX, 79925, ekappus@southwestuniversity.edu  
<sup>2</sup>New Mexico Museum of Natural History and Science, 1801 Mountain Rd. NW, Albuquerque, NM, 87104

Ongoing field reconnaissance and research of the ichnology of the Lower Cretaceous (Albian) Mesilla Valley Formation (Washita Group) at Cerro de Cristo Rey, Sunland Park, NM, has led to discovery and identification of several additional ichnotaxa as well as characterization of eight ichnoassemblages from the *Cruziana* and *Skolithos* ichnofacies. These ichnotaxa and ichnoassemblages are preserved in shallow marine facies as epichnia, endichnia, and hypichnia within thinly bedded sandstones. Sandstone beds are intercalated with black/dark gray shales, and often have sharp (or fluted) erosive bases and are massively bedded, laminar, or have ripple laminae or hummocky cross-strata. These sandstones are interpreted as tempestites (storm deposits) within shales deposited on the upper/middle shelf.

New taxa identified are as follows: *Chomatichnus*, *Gordia*, *Fuersichnus*,

*Protovirgularadichotoma*, *Rhizocorallium*, *Rugalichnusmatthewii*, *Spongeliomorphaoraviense*, *Spongeliomorphasublumbricoides*, and *Treptichnus*. Ichnoassemblages are the following: 1) *Planolites-Chondrites-Ophiomorpha*, 2) *Protovirgularia-Arenicolites-Skolithos*, 3) the *Arenicolites ichnocoenose* of the *Skolithos Ichnofacies*, 4) *Palaeophycusstriatus*, 5) *Palaeophycus-Spongeliomorpha*, 6) *Thalassinoides/Planolites-Chondrites*, 7) *Cardioichnus*, and 8) *Spongeliomorpha-Palaeophycus*. Ichno-assemblages 3, 4, and 7 are hypichnial, with the rest being epichnial. The ichnoassemblage with the largest ichnodiversity is 8, with up to eight different ichnotaxa present in convex hyporelief. The ichnoassemblage with the least diversity is 4, although dense, overcrossing, hypichnial, monospecific assemblages of *Palaeophycusstriatus* are common. Ichnoassemblage 1 has similar ichnotaxa to 6, however the latter has burrow fill consisting mainly of the foraminifera *Cribratinatexana* and may represent a similar community in a shallower environment. The *Cardioichnus* assemblage is only found in one bioclastic conglomerate with ammonoid fragments and *Peiliniaquadruplicata*, and is approximately 10 m below the upper contact of the unit in the western portion of the field area. Ichnoassemblages 2 and 3 were found in the upper 10 m of the Mesilla Valley Formation, within the gradational contact with the overlying Mojado Formation. Both 2 and 3 contain *Skolithos* burrows, and ichnoassemblage 3 is part of the *Skolithos* ichnofacies, which coincides with coarser-grained delta lobe front deposits of the lower Mojado Formation.

Coarser-grained interbeds and burrow fill (often bioclastic) are associated with the western portion of the field area, and finer-grained beds without coarse-grained burrow fill are associated with the eastern portion. This is evidence that the eastern portion was more seaward during the late Albian.

Based on burrow fill and trace preservation, cross-cutting, and composite traces (ie *Chondrites* reworking epichnial *Planolites*), it appears the equilibrium community consisted of *Thalassinoides*, *Planolites*, *Chondrites*, and/or *Bergaueria*. Different beds reveal different equilibrium communities and further investigation is needed.

#### GROUNDWATER TEMPERATURE RISE DURING AQUIFER RECOVERY AT THE BUCKMAN MUNICIPAL WELL FIELD, SANTA FE, NEW MEXICO

Shari Kelley<sup>1</sup>, Matthew Folsom<sup>2</sup>, Ronni Grapenthin<sup>2</sup>, and Mark Person<sup>2</sup>  
<sup>1</sup>New Mexico Bureau of Geology & Mineral Resources, New Mexico Tech, Socorro, NM, 87801, shari.kelley@nmt.edu  
<sup>2</sup>New Mexico Institute of Mining and Technology, Department of Earth & Environmental Sciences, New Mexico Tech, Socorro, NM, 87801

During the past five years, students attending the Summer of Applied Geophysical

Experience (SAGE) field program in Santa Fe have been annually measuring temperature-depth profiles in the Buckman well field. The Buckman field has delivered municipal water to Santa Fe for more than 35 years, and has a history of substantial (> 100 m) draw-down and inelastic subsidence, followed by significant water level recovery and surface rebound after 2003. Repeat measurements of vertical thermal gradients in two monitoring piezometers, SF3 and SF4, showed little to no change between 2013 and 2014. Temperatures at the bottom of these wells rose by 0.33–0.37 °C ( $\pm 0.05^\circ\text{C}$ ) between 2014 and 2017, with the most dramatic change occurring between 2014 and 2016; artesian flow at two wells began in 2015. The increased temperatures are observed at shallow depths (<100 m) and coincide with surface uplift detected through InSAR analysis of satellite data from 2007 to 2010. Geothermal gradients in SF3 and SF4 are 73 to 80°C/km; the elevated gradients are associated with a small fault near SF4. A deeper piezometer, SF2, located 300 m to the east of SF3, has a geothermal gradient of 45°C/km and a complex warming signal that has shifted to shallower depths through time. The abrupt change in geothermal gradient between SF3 and SF2 coincides with a north-trending stratigraphic discontinuity that is resolved by the InSAR observations and water level and chemistry data. A deep piezometer located outside the zone of water level rise and surface rebound, SF6 (geothermal gradient of 35°C/km), showed no temperature change between 2013 and 2016. Simple, one-dimensional hydrothermal models of pumping, downward flow and convective cooling, followed by water level recovery and conductive heating are qualitatively consistent with the observed increases in groundwater temperature.

#### NEW INORGANIC-ORGANIC CARBON-BASED HYBRID MATERIAL FOR SELECTIVE URANIUM CAPTURE

*Chase Kicker<sup>1</sup>, Liliya Frolova, and Snezna Rogelj*

<sup>1</sup>801 Leroy Pl, # 2261, Socorro, NM, 87801, chase.kicker@student.nmt.edu

Uranium contamination in drinking water is a major health concern in some parts of the United States, including New Mexico, and many other parts of the world. To minimize health risks from uranium contamination in drinking water, an efficient uranium filtration method is highly desired. Based on our experience of organic modification of carbon surfaces, we made an organic modification of commercial graphite particles for selective uranium adsorption from natural water sources. The material is high-cost effective and very chemically stable. The modified graphite shows high selectivity toward uranium even in the presence of competing cations such as calcium and magnesium. It further demonstrates that uranium adsorption is not hindered by the presence of many other

cations or by a change in the pH of the natural water samples. To reuse the water filter, it is important to release all of the adsorbed uranium yet maintain the full functionality of the adsorbent. We have shown that a simple acidic or basic wash of our filter is sufficient to remove all of the bound uranium; this fully regenerates the filter. In fact, our material remains stable and fully functional after several washing cycles. Finally, thus collected uranium can be easily be extracted for further use in industry as an alternative to uranium mining. Current work is being done to scale up the filtration process.

#### MAPPING ROCKFALL SUSCEPTIBILITY ACROSS NEW MEXICO AT 1:750,000 SCALE

*Daniel J. Koning and Mark Mansell*  
New Mexico Bureau of Geology & Mineral Resources, 801 Leroy Place, New Mexico Tech, Socorro, NM, 87801, dan.koning@nmt.edu

We present two 1:750,000 maps that provide a first-order approximation of rockfall susceptibility for the state of New Mexico. The maps are intended for regional planning purposes and determining where detailed studies may be warranted. ‘Susceptibility’ describes the natural propensity (likelihood) of the landscape to produce rockfall given adequate driving forces. An essential input for these maps was a preexisting, statewide map of rockfalls produced by Cardinali et al. (1990) using aerial photography. This map has a bias towards larger rockfalls and captures only a fraction of the total rock falls in the state, but nonetheless it is assumed to be a statistically valid subsample of the total. The first susceptibility map shows the point densities of the mapped rockfalls of Cardinali et al. (1990), which are contoured using the kernel function. It may serve as a proxy for where large rockfall events may occur in the future.

The second rockfall susceptibility map relates mapped rock falls to nearby slope values. Using a 28 m DEM in ArcGIS, a slope map is created. We capture the maximum slope around a mapped rock fall point using a 300 m-radius window, which corresponds to the median of the error range in the mapped rockfall points. The average and maximum value of the slope within this window was obtained, but the frequency distribution curve for the average value is heavily skewed to low values, probably because most of New Mexico is relatively flat and spatial errors would result in a rockfall being on low-sloping ground. However, the maximum value within the window gave a quasi-normal distribution centered on a mean value of 29° and having a standard deviation of 12°. We chose to use these maximum values within the 300 m-radius window, with the assumption that most rock falls tend to accumulate on relatively steep talus slopes.

Using the mean and standard deviations calculated from the distribution of these maximum slopes, we categorize the

aforementioned slope map into three susceptibility classes. “Likely susceptible” zones correspond to slopes lying at or above the mean-less-one standard-deviation (17°). Locally in this zone are rockfall-generating ledges and steep slopes allowing rockfall transport. “Potentially susceptible” zones correspond to slopes in the range of 8–17°, bracketed by the mean-less-one standard-deviation and the 5th percentile of the aforementioned maximum slope frequency distribution. This zone may have small rockfall-producing ledges; it also includes a 470 m-wide buffer extending downslope (on 5–17° slopes) of Likely susceptibility areas, designed to capture rockfalls having sufficient momentum to travel notably downhill of  $\geq 17^\circ$  slopes. The 470 m value corresponds to the 90th percentile (excluding outliers) of mapped rockfall distances from the Likely susceptible zone. “Unlikely susceptible” zones include very low slopes (<8°) lying outside of the aforementioned buffer. Final processing steps involved down-sampling to 500 m grid-size consistent with a 1:750,000 final map scale.

#### PRELIMINARY BASIN MODEL AND HYDROGEOLOGIC ASSESSMENT FOR THE NORTHEASTERN SAN AGUSTIN PLAINS, NEW MEXICO

*Daniel J. Koning and Alex J. Rinehart*  
New Mexico Bureau of Geology & Mineral Resources, 801 Leroy Place, New Mexico Tech, Socorro, NM, 87801, dan.koning@nmt.edu

Understanding the basin structure and Santa Fe Group (SFG) basin fill stratigraphy in the northeastern San Agustin Plains is critical for accurate estimations of groundwater volume and drawdown effects associated with a proposed groundwater withdrawal project. We present a preliminary basin model based on well analysis coupled with synthesis of previous geologic mapping, electrical resistivity soundings, and gravity data. These indicate that a 4–8 km wide, NNE trending graben with two sub-basins is present north of a south-down fault that extends WSW from the VLA headquarters.

Analysis of cuttings and geophysical logs for two deep wells allows partial characterization of the SFG. The northern well (SA-222, 1565 ft TD) is located 11 km north of Hwy 60 on a fault-bounded structural shelf. It encountered 724 ft of SFG underlain by 841 ft of interbedded basaltic andesites, cemented volcanoclastic sediment, and ignimbrites (Vicks Peak, La Jencia, and Hells Mesa Tuff). The well’s location and sand+gravel composition is consistent with a piedmont SFG lithofacies assemblage. The southern well (SA-221, 3495 ft TD) was drilled in the middle of the southern sub-basin and did not encounter bedrock. Both wells exhibit coarsening-upward trends culminating in a 320–340 ft thick, upper interval consisting of sandy gravels interbedded with clayey sands. A lower interval (2075–3495 ft in

SA-221; 507–724 ft in SA-222) consists of a fine-grained upper subunit and a coarser lower subunit.

SFG lithofacies assemblages interpreted in SA-221 include basin floor as well as western and eastern piedmont. Basin floor deposits are characterized by low neutron and resistivity signatures and variable sand composition. The petrology of western piedmont deposits consists of intermediate volcanic detritus with up to ~50% tuffs (proportion of latter increasing up-section). Inferred eastern piedmont deposits contain angular-subangular sand composed predominately of interpreted Vicks Peak Tuff (VPT). This sand gives particularly high gamma ray readings (170–200 API), collaborated by similar values for in situ VPT in well SA-222. Although a local footwall source cannot be ruled out, we favor an eastern provenance for VPT detritus because a 250–260 ft thick, sandy gravel interval composed primarily of VPT occurs in a well 9 km to the east. As would be expected per Walther's Law, in SA-221 fine-grained basin-floor deposits lie between the VPT sand and western piedmont intervals.

Preliminary hydrogeologic assessments are made for the SFG. In SA-221, we have estimated a porosity compaction curve based on density, neutron and sonic geophysical logs. The upper SFG shows high total porosities (10 to 40%), though clay content significantly lowers the effective porosity (consistent with relatively low resistivity values in the upper gravely interval of SA-222). The lower SFG interval has lower total porosities (5% to 15%) and higher clay content that likely translates to poor groundwater yields. Two sandy intervals in SA-221, at 680–1210 ft and 1555–2075 ft, exhibit relatively high resistivity and neutron values and total porosities of 24% to 48%. In general, the total aquifer storage should be lower than previously estimated both because of the higher clay fraction and the degree of compaction.

#### PALEOENVIRONMENTAL INVESTIGATIONS OF PLIOCENE INTERTRAPPEAN PALEOSOLS, TAOS PLATEAU, NEW MEXICO, SUGGEST LONG-TERM SEMIARID PEDOGENESIS

Gage Richards Lamborn, April Bates, Victor French, and Kevin Hobbs  
University of New Mexico Valencia,  
280 La Entrada, Los Lunas, NM, 87031,  
glamborn@unm.edu

Lava flows on the Taos Plateau preserved paleosols that existed beneath the flows when they were erupted at approximately 4 Ma. These paleosols provide a record of the climate conditions under which they formed. We are investigating two paleosols from within the Servilleta Basalts in northern New Mexico, USA, in an effort to determine the paleoenvironmental conditions present during pedogenesis. Using bulk geochemical

composition of paleosol B horizon materials, we performed a geochemical climate analysis (GCA) in order to estimate mean annual precipitation (MAP) during pedogenesis. Our GCA results suggest MAP of up to 1030 mm/yr. However, the presence of a stage III pedogenic carbonate horizon, which typically forms under MAP conditions of 400–600 mm/yr, seems to contradict GCA results. In addition, during thin-section optical microscopy we observe well-developed argillans and possible weakly developed ferrans on many of the grains within paleosol B horizons, further suggesting MAP conditions typically found in arid or semi-arid environments. Within the paleosols we observe quartz and potassium feldspar, neither of which are present in the encapsulating Servilleta Basalts. We interpret these compositions as having resulted from aeolian deposition onto the soil during pedogenesis. The collected samples are from two paleosols that are separated by a two-m-thick tholeiitic basalt flow and are similar in both chemical and mineral composition. These similarities suggest that relatively constant paleoenvironmental conditions persisted during the formation of both paleosols. The presence of a stage III pedogenic carbonate horizon in the lower paleosol suggests a pedogenesis duration of ~100,000 years.

#### THE CRETACEOUS-PALEOCENE BAENID TURTLE *NEURANKYLUS*: EVIDENCE OF SEXUAL DIMORPHISM

Asher J. Lichtig<sup>1</sup> and Spencer G. Lucas<sup>2</sup>  
<sup>1</sup>New Mexico Museum of Natural History,  
1801 Mountain Rd. NW, Albuquerque, NM,  
87104, ajlichtig@gmail.com  
<sup>2</sup>New Mexico Museum of Natural History  
and Science

Fossil turtles are often studied as though they were static objects rather than the remains of living, growing individuals. This is particularly true of archaic groups with no living descendants. Sexual dimorphism has largely been either lumped in with more random variations or, in some cases, the two genders were recognized as distinct species. Baenid turtles are a family of cryptodire turtles from Cretaceous–Eocene strata of western North America, and include Paleocene–Eocene *Neurankylus*, particularly well known from the San Juan Basin of New Mexico and the Grand Staircase-Escalante National Monument of Utah. Several large specimens of *Neurankylus baueri* excavated in the Kaiparowits Formation of Utah, were described as two distinct taxa, *N. hutchisoni* and *N. utahensis*. This was in part based on the assumption that the smaller *Neurankylus* shells known from the San Juan Basin are ontogenetically mature. We suggest that rather than being mature and not fusing their shells at maturity, as in other baenids, the San Juan Basin specimens were still immature and thus capable of further growth. These larger specimens in Utah show the same pair of one elongate and one round shell morphotype seen

in the San Juan Basin specimens. It is more parsimonious to consider them one species with two morphotypes than two individual lineages that happen to always occur together in the Kaiparowits, Fruitland, Kirtland and Nacimiento formations, independently. The most frequent form of dimorphism present in extant turtles with two morphotypes is sexual dimorphism, most commonly with the male being smaller. With this will often come differences in shell shape, such as that seen in *Graptemys*, in which females are more elongate as well as larger. Another common dimorphism seen in some modern river turtles is that midline spines present in both genders as juveniles will be more reduced in one gender. For example, many adult female *Graptemys* almost completely lack these midline spines but they remain prominent in males. A great degree of variation in the development of the midline spines is seen in *Neurankylus* and may have a similar cause. Thus, we consider *N. hutchisoni* and *N. utahensis* to be based on two mature sexual dimorphs of *N. baueri*.

#### THE TRIONYCHID TURTLE *AXESTEMYS MONTINSANA* FROM THE PALEOCENE NACIMIENTO FORMATION, SAN JUAN BASIN, NEW MEXICO

Asher J. Lichtig<sup>1</sup> and Spencer G. Lucas<sup>2</sup>  
<sup>1</sup>New Mexico Museum of Natural History,  
1801 Mountain Rd. NW, Albuquerque,  
NM, 87124, ajlichtig@gmail.com  
<sup>2</sup>New Mexico Museum of Natural History  
and Science, 1801 Mountain Rd. NW

*Axestemys montinsana* is a trionychid turtle that was originally named and described from the Scarritt Quarry of the early Tiffanian interval of the Melville Formation in the Crazy Mountains Basin of Montana. We report the discovery of a skull attributable to this taxon from the Torrejonian interval of the Nacimiento Formation in Kutz Canyon, San Juan Basin, New Mexico. This identification of the first San Juan Basin record of *Axestemys* is based on comparison to the holotype skull, which compares closely with the New Mexican specimen. Thus, it is identified as an *Axestemys* based on its large (length) and triangular-shaped skull as well as the presence of a wide, smooth, unsculptured border of the carapacial callosity in an associated carapace fragment. The San Juan Basin and holotype specimens differ from other *Axestemys* in the extent of the parietals, with the frontal and postorbital broadly separating the parietals from the orbits. Furthermore, the anterior elongation of the cavum tympani in the New Mexican specimen is similar to the holotype of *A. montinsana*. This first New Mexican record of *Axestemys montinsana* extends the known range of *A. montinsana* south from Colorado, resulting in a range covering the Rocky Mountain region from Montana to New Mexico. It also fits with models of little or no provinciality of vertebrates in the western U.S.A. during the Paleocene.

## GEOCHEMISTRY, TRANSPORT, AND REMEDIATION OF CHROMIUM IN AN OXIDIZING AQUIFER SYSTEM, PAJARITO PLATEAU, NEW MEXICO

Patrick Longmire

New Mexico Environment Department;  
Ground Water Quality Bureau, 1190 St.  
Frances Drive, Santa Fe, NM, 87502,  
patrick.longmire@state.nm.us

Potassium dichromate ( $K_2Cr_2O_7$ ) used as an anticorrosion agent and a biocide was discharged from a cooling tower from 1956 to 1972 to upper Sandia Canyon at Los Alamos National Laboratory (LANL), New Mexico. Between 31,000 to 72,000 kg of this chemical were discharged directly to surface water dominantly sourced from the cooling tower and another outfall releasing treated sewage effluent. Chromate ( $CrO_4^{2-}$ ) migrated through the 300-meter thick vadose zone reaching the regional aquifer and created an extensive groundwater plume approximately 2.74 km in length and 1.13 km in width. Groundwater in the regional aquifer at LANL is aerobic and is characterized by a mixed calcium-sodium bicarbonate composition and a circumneutral pH. Chromate is mobile under these geochemical conditions and does not adsorb significantly onto ferric (oxy)hydroxide and clay minerals, with the highest concentration of dissolved chromium exceeding 800  $\mu\text{g/L}$  or 0.80  $\text{mg/L}$  at the site. The New Mexico Water Quality Control Commission (WQCC) groundwater standard for total dissolved chromium is 0.050  $\text{mg/L}$  (50  $\mu\text{g/L}$ ). Chromium contamination occurs in the upper 33 meters of the saturated zone in the regional aquifer and is migrating to the east and southeast nearly at the same rate of groundwater flow, averaging approximately 42 meters per year. The chromium plume in the regional aquifer beneath Mortandad Canyon mixes with (1) a treated sewage effluent plume, containing boron, chloride, nitrate, sulfate, and other chemicals, released from Sandia Canyon near the cooling tower and (2) a groundwater plume consisting of treated-industrial effluent that contains 1,4-dioxane, fluoride, nitrate, perchlorate, tritium, uranium, and other chemicals and radionuclides. The centroid of the chromium plume has greater than 400  $\mu\text{g/L}$  of dissolved chromium, between 150 and 240  $\text{pCi/L}$  of tritium, from 4 to 8  $\text{mg/L}$  of nitrate plus nitrite(N), and concentrations of chloride and sulfate typically exceeding 30 and 60  $\text{mg/L}$ , respectively. Initial phases of aquifer remediation of the chromium plume are currently being evaluated by LANL and NMED, consisting of (1) pump and treat followed by reinjection and (2) injection of sodium dithionite and molasses to bio(geo)chemically reduce chromate to chromium(III). Injection of these two reductants result in precipitation of amorphous chromium hydroxide with dissolved concentrations of chromium (VI) typically less than 5  $\mu\text{g/L}$  in zones of

application. Geochemical modeling using PHREEQC was conducted to evaluate chromate reduction, reaction products, and aqueous speciation in the presence of 0.059 molar sodium dithionite and 0.057 molar sodium sulfite (pH buffer) at regional aquifer well R-42. Results of the PHREEQC simulations confirm that sodium dithionite initially promotes reductive dissolution of manganese dioxide (pyrolusite) and ferric hydroxide under reducing conditions, as sodium dithionite disproportionates ultimately to sulfate and hydrogen sulfide. Mackinawite and iron sulfide ppt, stable as transient intermediate phases, are calculated to approach equilibrium under reducing and acidic conditions prior to chromium(III) precipitation. Dissolved ferrous iron enhances precipitation of chromium(III) hydroxide under slightly oxidizing and circumneutral pH conditions with dissolved Mn(II) stable in groundwater. Manganese(II) is a redox buffer for chromium(III) hydroxide inhibiting reoxidation to chromium(VI).

## COMPOSITIONS AND ELEVATIONS OF DEPOSITS BETWEEN RECENTLY IDENTIFIED QUATERNARY FAULTS COMPLICATE STRUCTURAL INTERPRETATIONS OF THE SOUTHWESTERN ALBUQUERQUE BASIN, NEW MEXICO

David W. Love<sup>1</sup>, Eda Celep<sup>1</sup>, and Brad Sion<sup>2</sup>

<sup>1</sup>New Mexico Bureau of Geology and Mineral Resources, New Mexico Tech, 801 Leroy Place, Socorro, NM, 87801, david.love@nmt.edu

<sup>2</sup>Department of Earth and Environmental Science, New Mexico Institute of Mining and Technology, 801 Leroy Place, Socorro, NM, 87801

North-trending normal fault traces and scarps cutting deposits between the Loma Blanca and Cliff faults in the southwestern Albuquerque Basin of the Rio Grande rift complicate interpretations of basin structure, but may lead to better understanding of ages of fault offsets. Deposits in a gravity-defined graben between the larger faults include a 1,553-m-high drainage divide between the Rio Puerco (north) and Rio Salado (south). Clasts along the divide and farther north show that the Rio Salado used to enter the Rio Puerco valley down to an elevation of 1,494 m, where sediments of the two streams may interfinger. The high divide appears to be on a horst between several poorly exposed faults. The top of the down-to-the-east hanging wall of the Loma Blanca fault is locally about 1,564 m whereas the top of the eroded footwall of the Cliff fault (down-to-the-west) is 1,553 m, which is the same elevation as the top of the ancestral Rio Grande deposits to the east and the top of the Rio Puerco-Llano de Albuquerque deposits to the north. The northern part of the Loma Blanca fault offsets alluvial-fan deposits of late-middle Pleistocene age graded toward

intermediate terrace levels of the Rio Puerco. Farther east, the same alluvial deposits are offset by east- and west-facing scarps 1–4 m high. The exposed northerly trace of the Cliff fault is about 6 km long between the Rio Salado and Rio Puerco valleys and appears to have at least 75 m of offset. The Cliff fault does not offset the highest terraces along the Rio Puerco and Rio Salado valleys. Two high levels (1,540 and 1,534 m elevations) of Rio Salado terraces bevel both tilted beds of the hanging wall and horizontal beds of the footwall, with at least 15 m removed below 1,551 m elevation. West of the Cliff fault, the slightly lower terrace (estimated to be at least 600 ka) is offset by three subparallel north-south faults, forming a small horst and narrow graben. Farther west are suspected fault scarps that mark the western edge of the larger horst on the drainage divide but these probably are truncated and buried by a later, lower terrace of the Rio Salado. Although others mapped a Rio Puerco fault in the Rio Puerco valley to the north and projected it into the area, the numerous faults with small offsets suggest that a large, down-to-the east fault does not cut the surface here. As in other parts of the Albuquerque basin, younger fault scarps appear to be active toward the center of the broader graben.

## PREFERENCES OF GRANULE SIZES AND COMPOSITIONS FROM HARVESTER ANTHILLS ON DIVERSE SUBSTRATES ACROSS SEVILLETA NATIONAL WILDLIFE REFUGE, CENTRAL NEW MEXICO

David W. Love<sup>1</sup> and Adam Nash<sup>2</sup>

<sup>1</sup>New Mexico Bureau of Geology and Mineral Resources, New Mexico Tech, 801 Leroy Place, Socorro, NM, 87801, david.love@nmt.edu

<sup>2</sup>Biology Department, Iowa State University, Ames, IA, 50011

Large anthills attributed to harvester ants were examined on several types of soil substrates across Sevilleta National Wildlife Refuge. Typically *Pogonomyrmex rugosus* build broad, low, shield-like mounds with entrances off-center whereas *Novomessor cockerelli* build more compact, steeper cone-shaped mounds with entrances in a central crater. Single-rock-type substrates include weathered granite, schist, limestone, and gypsum. Mixed-granule substrates are primarily on alluvial fans and ancestral Rio Grande gravel. No harvester anthills were found on thick petrocalcic soils or on pebbly sand terrace deposits of the Rio Puerco. Densities of anthills ranged from 74 hills per hectare on grus west of the Los Pinos Mountains to less than 1 per hectare on Popotosa badlands, Permian gypsum, and Baca Formation (conglomerate). Densities per hectare did not correlate to major vegetation types. Three types of grain-size distributions are exhibited on linear-log-differential plots of coarse sand and granules

(typically between 1 and 4.5 mm with modes ~2.6 mm, perhaps related to ant mandible size) gathered at the surface by the ants. One type is a log-hyperbolic distribution with relatively steep decreases in coarse and fine amounts. A second type of distribution is lognormal with broader parabolic shapes. The third type appears to be lognormal with more coarse grains (possibly due to sample locations on anthills). Due to the lack of ant activity at the surface during the summer heat, we could not determine whether specific granule distributions can be attributed to a single species. On most substrates, the ants gathered locally available granules and did not appear to choose particular minerals or rocks over others. It is possible that on some local substrates, ants chose quartz grains more than other grains and avoided ironstone concretions and sandstone. The ants did not choose rounded grains over angular grains. Limited tests concerning seed preferences showed that *P. rugosus* chose blue grama seeds and ignored juniper and creosote seeds. *N. cockerelli* ignored all three seeds and must prefer other local seeds.

#### ICHTHOLOGY OF A PLIOCENE SANDFLAT, ALBUQUERQUE BASIN, NEW MEXICO

Spencer G. Lucas<sup>1</sup>, Nasrollah Abbassi<sup>2</sup>, Paul Knight<sup>3</sup>, Heitor Francischini<sup>4</sup>, and Paula Dias<sup>5</sup>

<sup>1</sup>New Mexico Museum of Natural History, 1801 Mountain Road N.W., Albuquerque, NM, 87104, spencer.lucas@state.nm.us

<sup>2</sup>University of Zanjan, Department of Geology, Faculty of Sciences, Zanjan, 45371-38791, Iran

<sup>3</sup>Marron and Associates, 7511 4th Street NW, Albuquerque, NM, 87107

<sup>4</sup>Universidade Federal do Rio Grande do Sul, Laboratório de Paleontologia de Vertebrados, Av. Bento Gonçalves, Porto Alegre, 7500, Brazil

<sup>5</sup>Universidade Federal do Rio Grande, Núcleo de Oceanografia Geológica, Instituto de Oceanografia, Av. Itália km 8, Rio Grande, Brazil

Although the paleontology of the Upper Cenozoic Santa Fe Group in New Mexico has been collected and studied since the 1870s, little is known of its ichnofossils. A newly discovered vertebrate tracksite in the Pliocene Santa Ana Mesa Member of the Ceja Formation at Rio Rancho, Sandoval County, is the most extensive ichnoassemblage known from the Santa Fe Group. This assemblage is in a large (at least 500 m<sup>2</sup>), bedding plane surface of a 0.1–0.2-m-thick bed of wavy bedded sandstone in which wave crests are 4–6 cm high and separated by ~40 cm; crest shapes indicate that paleoflow was to N30°E. The surface is also marked by some east-west oriented swales that were water filled during track-making. We cleared ~14 m<sup>2</sup> of this surface to reveal a low diversity invertebrate ichnoassemblage, salamander

trackways and over 170 bird footprints that represent at least 18 trackways. *Cochlichnus*, the sinusoidal, bedding-plane parallel grazing trace of a small arthropod, dominates the invertebrate ichnofossils, which also include a few larger, horizontal and tubular grazing traces assignable to *Palaeophycus* and *Scoyenia*. The salamander tracks form at least one trackway of small (15–20 mm long), tridactyl or tetradactyl footprints of a quadruped with long, scratch-like digits. These closely resemble the “*Gracilichnium*” extramorphological variant of the amphibian footprint ichnogenus *Batrachichnus*. The bird footprints are mostly tridactyl, but tetradactyl where well preserved. They show three long and pointed, anteriorly directed digits II-IV, and well preserved tracks also have a short, and spur-like digit I impression directed backwards. In better preserved footprints, a sole imprint connects the bases of the forward-directed digits. These bird footprints are assigned to the ichnogenus *Gruipeda*, most similar to *Gruipeda calcarifera* Sarjeant & Langston. These are the footprints of anisodactyl shorebirds. On the uneven trackway surface, bird footprints in the swales are more deeply sunk into the sediment than those outside of the swales. Most unusual is a salamander trackway that emerges from a swale, turns to the northeast and walks to disappear among bird footprints, possibly because one of the birds preyed upon the salamander. The sediments and ichnoassemblage at the Rio Rancho tracksite indicate a large, lower energy sandflat, either along a lake or channel margin associated with the large, fluvial, ancestral Rio Grande system. Similar habitats, though less active depositionally, are present along some reaches of the Rio Grande today.

#### LITHOSTRATIGRAPHY, PALEONTOLOGY AND DEPOSITION OF THE CAMBRO-ORDOVICIAN BLISS FORMATION, SIERRA COUNTY, NEW MEXICO

Spencer G. Lucas<sup>1</sup> and Karl Krainer<sup>2</sup>

<sup>1</sup>New Mexico Museum of Natural History, 1801 Mountain Road NW, Albuquerque, NM, 87104, spencer.lucas@state.nm.us

<sup>2</sup>Innsbruck University, Innrain 52, Innsbruck, A-6020, Austria

The Cambro-Ordovician Bliss Formation is the oldest Phanerozoic sedimentary unit in New Mexico. It crops out in the mountain ranges of Sierra County where it rests nonconformably on Proterozoic basement and is conformably overlain by the Lower Ordovician Sierrite Formation of the El Paso Group or, at its northernmost outcrops, disconformably by the Middle Pennsylvanian Red House Formation. In Sierra County, the Bliss Formation is up to 55 m thick and can be divided into two members: (1) a lower member dominated by crossbedded and bioturbated quartz-rich sandstone; and (2) an upper member with numerous beds

of ripple-laminated glauconite and some coarse carbonate beds. The lower member contains brachiopods, trilobites and a *Skolithos*-dominated ichnoassemblage. The upper member yields numerous graptolites and a *Palaeophycus*-dominated ichnoassemblage. Previously published conodont and trilobite biostratigraphy in the Caballo Mountains indicates that most or all of the lower member is late Cambrian (Sunwaptan) in age, whereas most or all of the upper member is Early Ordovician (Skullrockean) in age. The Cambrian-Ordovician boundary is stratigraphically high in the lower member. The upper member graptolite assemblage is dominated by *Rhadinopora flabelliformis* (Eichwald), which confirms its Early Ordovician age. Deposition of the lower member was in a shallow marine siliciclastic setting, whereas the upper member indicates a mixture of shallow tidal flat sedimentation intercalated with deeper, subtidal marine deposition. In the iron oolite beds of the lower member in the Caballo Mountains (Sierrite Mine), two types of ooids are present: (1) tangential concentric ooids composed of hematite and (2) structureless ooids composed of hematite, berthierine and chamosite. We interpret the iron ooids to have formed during diagenesis from carbonate ooids. Glauconite is abundant in the upper member and occurs as rounded grains, rarely also as cement. It is cryptocrystalline and most probably formed by glauconitization of fecal pellets. Both iron ooids and glauconite indicate that the Bliss Formation is the result of an extensive regional transgression (“Sauk Transgression”) coupled with low rates of sedimentation.

#### GROUNDWATER LEVEL MONITORING ALONG THE ANIMAS RIVER, NEW MEXICO, AFTER THE GOLD KING MINE 2015 MINE-WATER RELEASE

Ethan Mamer, B. Talon Newton, and Stacy Timmons

New Mexico Bureau of Geology & Mineral Resources, 801 Leroy Place, Socorro, NM, 87801, ethan.mamer@nmt.edu

The Gold King Mine spill that occurred in August 2015 drained water that was backed up in the mine adit rapidly, quickly eroding the waste rock pile that was outside of the mine. As result, roughly 490,000 kg of sediment was released with the water, turning the water an orange color. While the river has since returned to its normal color, there is still concern that the metals left on the streambed may affect the shallow alluvial aquifers and impact the communities in the surrounding area.

To determine if water from the river was infiltrating into the alluvial aquifers of New Mexico during or after the spill, a water-level monitoring network was developed. The monitoring network consisted of roughly 60 existing wells and was used to construct

groundwater elevation contour maps to determine the direction of groundwater flow in the Animas Valley between Farmington and the NM/CO boarder. The monitoring network of wells was measured four times per year, over two years, during hydraulically significant periods to understand the seasonal fluctuations of the water table and how it affects the groundwater/ surface water interactions; during baseflow conditions (late-January), the initial snowmelt/onset of irrigation season (mid-March), peak snowmelt/extended irrigation season (early-June), and at the end of irrigation season (mid-October).

A subset of wells were instrumented with pressure transducers to continuously collect water-level data. The groundwater hydrographs recorded at these wells showed distinct patterns that were used to categorize most of the measured wells based on their different hydrograph characteristics. Wells close to the river typically had a direct correlation to river stage with a distinct increase that correlates to peak snowmelt in the river followed by a rapid drop in groundwater levels through August. Most of the hydrographs begin increasing in late March at the beginning of irrigation season and continue to increase through July and do not begin to decrease until the end of irrigation in late October.

In most areas, the Animas River is gaining water from the groundwater, as groundwater from the surrounding valley flows down gradient, discharging to the river. However, in some areas, water-levels in close proximity to the river have a nearly flat hydraulic gradient between groundwater and the river, where small seasonal fluctuations in groundwater levels and river stage can turn a slightly gaining reach to a slightly losing reach. Groundwater levels in the valley are generally lowest in March, before the irrigation season begins, and highest in October, near the end of the irrigation season. High seasonal water-level fluctuations were observed near the Cedar Hill and Inca communities, where we observed an apparent reversal in gradient that changes the river in those areas from a gaining stream in the summer during irrigation season to a losing reach in the winter. The results of this study indicate river water does infiltrate into the alluvial aquifer primarily from irrigation return or infiltration through the ditch network, as demonstrated by the hydrograph response to the irrigation season.

#### PHOTOGRAMMETRY OF FLUVIAL OUTCROPS IN TOADSTOOL GEOLOGIC PARK, NEBRASKA AND ANGEL PEAK, NEW MEXICO

Wade Walter Mans and Gary Weissman  
Department of Earth & Planetary Sciences,  
University of New Mexico, Albuquerque,  
NM, 87131, wmans@unm.edu

Large-scale 3D models of fluvial outcrops can improve our ability to map and interpret

geometries of sedimentologic structures (facies) in complex fluvial systems. 3D modeling can be used to generate ultra-high-resolution digital elevation models and orthophotosaics of the fluvial outcrops and provide high spatial details of the study areas. Objectives include the further development of procedures to take photographs from both ground-based cameras and UAVs to build 3D models of outcrops. Agisoft Photoscan software is used to perform the structure-from-motion photogrammetric processing of the digital images and generate both 3D spatial and multispectral models of the outcrop. Preliminary mapping of the two study sites, Toadstool Geologic Park in Nebraska and Angel Peak Natural Area in New Mexico, demonstrates that high-resolution modeling over these complex large-scale stratigraphic structures (e.g., bounding surfaces, faults, compositional changes) allows for quicker more comprehensive understanding of the development and arrangement of the geology of the areas studied. The resolution of the models makes drawing relationships between smaller isolated features in stratigraphic structures to the surrounding region more effective, and the 3D nature of the models allows for correlation of features around complex terrain because these features can be viewed from multiple angles not accessible from the ground.

These technologies and procedures allow the gathering of detailed information from remote areas and terrain which is difficult to navigate or study in any other way. It is cost effective and time efficient, allowing for frequent study of large areas. The very high-resolution information can be used in GIS applications as well as with the UAV gathered imagery. This study has implications for understanding the permeability structure of rock, thus it has importance for both petroleum and ground water studies.

#### HYDROLOGIC MONITORING OF SPRINGS ALONG THE NACIMIENTO FAULT

Chris McGibbon, Laura Crosse, and Karl Karlstrom  
University of New Mexico, Albuquerque,  
NM, 87108, mcgibbon@unm.edu

Continuous monitoring of springs along the Nacimiento Fault was carried out to provide new insight into changes in the groundwater regime of this complex geological area. The focus has been to highlight the connectivity of springs along faults, assess temporal and spatial variations, recognize signals present in the data and identify relationships between spring parameters.

The parameters monitored are pressure (a proxy for depth), temperature, and conductivity. Multi-parameter sensors were deployed in the study area from December 2012 until May 2015. Resolution was set at 15 and 5-minute intervals.

The springs are situated along the Nacimiento fault both north and south of the Rio Salado. Fluids are carbonic, and

have a demonstrably endogenic component evidenced by helium isotopes and key tracers such as lithium. All springs are between ~10–100 m higher elevation than the proximal Rio Salado, indicating artesian characteristics. The elevation and the co-alignment along the fault indicate a confined or semi-confined aquifer sealed by the Triassic Chinle Formation, with fluid movement along the fault. Three springs are collinear and located along the fault that cores the Tierra Amarilla anticline, the fourth is off axis of the fault. The latter is noted as being geochemically distinct from the rest, with greater temporal variation. A fifth spring, north of the Rio Salado was monitored for the final 6 months of the study period. Where springs discharge, they form pools within travertine mounds and cisterns whose depth range from 0.2 to 8 m. The sizes of the spring pools vary along their long axis from 0.1 to 5 m. Travertine occurs at all locations, and many inactive springs are represented by dry travertine mounds and vent orifices. U-series age geochronology indicates springs have been active intermittently since 270 ka, at highest elevations, to modern actively forming mounds. Degassing of CO<sub>2</sub> occurs as bubbling at most springs and pool surfaces are often at depth below ground level, in collapsed travertine mounds, up to 5m deep, confirming that water elevations were higher in the past.

Depth variations highlight seasonal as well as event driven fluctuations, however not all springs respond in the same manner, possibly due to the nature of the spring vent active versus collapsed mound. Water temperature tracks atmospheric temperature with maximum values in the summer. Analysis of conductivity was problematic due to biofouling.

Fluid connectivity between springs is highlighted most prominently by near-synchronous changes in water depth for each spring. Spectral analysis indicates water depth has spectral peaks of 1 and 0.5 days, which coincide with solid Earth tides of ~12 and ~24 hours. Water temperature has spectral peaks at 24 hours, associated with daily maximum air temperature, while specific conductivity also has peaks at 24 hours, which could be associated with maximum daily temperature.

This work has implications to help understand the role of faults as conduits for fluid movement, define the degree of confinement of the aquifer and estimate storage coefficient.

#### PROTECTING NEW MEXICO'S BURIED TREASURE: A SUMMARY OF GROUNDWATER QUALITY PROTECTION IN NEW MEXICO

Dennis M. McQuillan  
New Mexico Environment Department,  
1190 St. Francis Drive, PO Box 5469,  
Santa Fe, NM, 87502, dennis.mcquillan@state.nm.us

Groundwater is a vital resource for the residents of New Mexico. Approximately 95% of the state's 2.1 million people depend on

groundwater for all or part of their domestic water supply, including more than 300,000 people who rely on private domestic wells. Many farms, ranches and businesses also use wells for water supply. For more than a century, the Legislature and state and local governments have pioneered efforts to protect groundwater resources, and the health of citizens who drink groundwater.

Pressure decreases in the Roswell artesian basin aquifer were observed in 1904. The Territorial Legislature passed a law in 1905 requiring permits and logs for new wells in the basin, along with measurements of flow and pressure. Since 1910, water tables in the Mimbres Basin and Portales Valley have declined significantly. In response to the effects that groundwater development was having on streamflow and on the rights of other groundwater users, the State Legislature passed the Groundwater Code in 1931, granting the State Engineer authority to declare groundwater basins and appropriate water rights. Groundwater depletion, an ongoing issue in many areas of New Mexico, can reduce aquifer porosity and storage capacity, diminish well production, deteriorate water quality, and cause land subsidence.

In 1934, the infant death rate in New Mexico was 145 deaths per 1,000 live births, the highest in the nation and twice the national average, caused in part by dysentery and diarrheal illness from unsafe water supplies. The State Board of Public Health issued regulations in 1937 to prevent pollution of water resources, including wells. In 1947, the Legislature passed the Sanitary Projects Act which funded many improvements to water infrastructure that prevented groundwater pollution and waterborne illness.

In the 1950s and 60s, groundwater contamination with crude oil, nitrate, uranium mill waste, gasoline, tritium, and oil-field brine was documented in New Mexico. The Legislature amended the Oil and Gas Act in 1961 to protect fresh water. State public nuisance statutes enacted in 1963 prohibited the pollution of water, explicitly including springs and groundwater, and provided authority to require abatement. The pioneering N.M. Water Quality Act of 1967 led to the adoption of a comprehensive set of groundwater quality regulations, the first in the nation, that included a permitting program for discharges onto or below the surface of the ground, and numerical groundwater quality standards.

After the U.S. Environmental Protection Agency was created in 1970, numerous state and federal laws were passed that provided for groundwater quality protection. In New Mexico these additional laws included: Environmental Improvement Act (1971), Radiation Protection Act (1971), Pesticide Control Act (1973), Subdivision Act (1973), Utility Operators Certification Act (1973), Hazardous Waste Act (1977), Surface Mining Act (1979), Mine Dewatering Act (1980), Groundwater Protection Act (1990), Solid Waste Act (1990), Department of Environment Act (1990), Mining Act

(1993), Natural Resources Trustee Act (1993), Voluntary Remediation Act (1997), Groundwater Storage and Recovery Act (1999), and Geothermal Resources Development Act (2016).

#### EVALUATING THE POTENTIAL OF MAGNETIC SURVEYING TO PREDICT PARTICLE SIZE DISTRIBUTION OF SOILS

Victoria Moreno<sup>1</sup> and Diane I. Doser<sup>2</sup>

<sup>1</sup>The University of Texas at El Paso, 500 W University Ave, El Paso, TX, 79968, vmoreno11@miners.utep.edu

<sup>2</sup>The University of Texas at El Paso, 500 W University Ave, El Paso, TX, 79968

Particle size distribution of soils play a crucial role in controlling the flow of water through the critical zone, making it an important quality to consider for environmental restoration. Recent studies have found that geophysical analyses of soils can give insight into their particle size distribution. It would be useful to have a quick, non-invasive method of identifying soil types; this study aims to use magnetics surveying for that reason.

The location of this study is a recreational area called Valley Creek Park in the Upper Valley of El Paso, Texas. Recent efforts have been made to restore this area by planting riparian species such as Rio Grande Cottonwoods, which tend to have higher survival rates in coarse-grained, non-saline soils. Geophysical surveys have the potential to be implemented before introducing riparian plant species to determine if an environment will facilitate their survival. Magnetics surveys can be used to estimate the particle size distribution of soils by relating a soil's grain size to its magnetic qualities; smaller grain sizes tend to have lower magnetite content and therefore a lower magnetic signature, and vice versa. This study utilizes a magnetometer survey to estimate grain size variations in soils along a transect. These magnetics readings will be compared to data from laser diffraction particle size analyses of soils from the same area to test correlation between the two data sets.

Preliminary analysis of magnetics data show anomalies that appear to be too large to attribute to grain size variations alone. The results from the laser diffraction particle size analysis show varying particle size distributions not only at different locations within the study site, but variations with depth as well. This is likely due to earlier deposition in historic channels of the Rio Grande that no longer exist due to channelization of the river in the 1930s. Comparison of the magnetics and laser diffraction particle size analysis data is not possible until the large anomalies in magnetics are ruled out. A Ground-Penetrating Radar (GPR) survey will be conducted along this same transect to see if these anomalies can be attributed to a metallic object below the surface of the study site. If that is the case, then the data can be

considered without the anomalies, and the magnetics and laser diffraction particle size analysis data can be tested for a correlation.

#### LATE PLIOCENE (BLANCAN) VERTEBRATES FROM THE CAMP RICE FORMATION IN THE VICINITY OF HATCH, DOÑA ANA AND SIERRA COUNTIES, SOUTHERN NEW MEXICO

Gary S. Morgan<sup>1</sup>, Paul L. Sealey<sup>1</sup>, Andrew P. Jochems<sup>2</sup>, and Philip A. Gensler<sup>3</sup>

<sup>1</sup>NM Museum of Natural History, 1801 Mountain Road, NW, Albuquerque, NM, 87104, gary.morgan1@state.nm.us

<sup>2</sup>New Mexico Bureau of Geology and Mineral Resources, 801 Leroy Place, Socorro, NM, 87801

<sup>3</sup>U.S. Bureau of Land Management, 301 Dinosaur Trail, Santa Fe, NM, 87502

Two Pliocene vertebrate faunas referred to the Blancan North American land mammal age, the Hatch Local Fauna (LF) and Arroyo Cuervo LF, are described from the Camp Rice Formation in the Hatch-Rincon basin west of Hatch in Doña Ana and Sierra counties, southern New Mexico. These two faunas occur in a stratigraphic section of the Camp Rice Formation about 70 m in thickness, primarily consisting of the axial-fluvial facies. The Hatch Siphon section of the Camp Rice Formation occurs in close proximity to the Pliocene vertebrate sites, and includes a dated pumice and magnetic polarity stratigraphy. The fossiliferous portion of this section encompasses much of the Gauss chron, ranging in age from slightly older than 3.33 Ma in the lowermost Gauss chron to the Gauss/Matuyama boundary at 2.58 Ma. The Hatch Siphon pumice, with a <sup>40</sup>Ar/<sup>39</sup>Ar date of 3.12 Ma, is located 28 m above the base of the section, within the Kaena subchron. The top of the Kaena at 3.04 Ma, about 30 m above the base of the section, marks the approximate boundary between the Arroyo Cuervo and Hatch faunas.

The early Blancan Arroyo Cuervo LF consists of 11 species of vertebrates: 2 land tortoises, *Gopherus* and *Hesperotestudo*; mud turtle *Kinosternon*; freshwater emydid turtle; and 7 mammals: horses *Equus simplicidens* and *Equus* small species; peccary *Platygonus*; 2 camels, *Camelops* and *Hemiauchenia blancoensis*; deer *Navahoceros lascrucensis*; and gomphotheri proboscidean *Rhynchotherium falconeri*. The mammals from Arroyo Cuervo limit the age of this fauna to between 3.6 Ma (first appearance of *Equus simplicidens*, *Platygonus*, *Camelops*, *Hemiauchenia blancoensis*, and *Rhynchotherium falconeri*) and 2.6 Ma (last appearance of *E. simplicidens* in New Mexico). The absence of South American immigrant mammals that participated in the Great American Biotic Interchange indicates the Arroyo Cuervo LF is older than 2.7 Ma. Mammalian biochronology and magnetostratigraphy constrain the age of the Arroyo Cuervo LF to ~3.0–3.4 Ma (late early Blancan).

The late Blancan Hatch LF consists of 18 species of vertebrates: 2 tortoises, *Gopherus* and *Hesperotestudo*; mud turtle *Kinosternon*; snake *Rhinocheilus lecontei*; unidentified bird; and 13 species of mammals: glyptodont *Glyptotherium texanum*; 2 species of rabbits, *Sylvilagus* sp. and indeterminate small leporid; pocket gopher *Geomys paenebursarius*; badger *Taxidea*; indeterminate small cat; 3 horses, *Nannippus peninsulatus*, *Equus cummingsii*, and *E. simplicidens*; 2 camels, *Camelops* and *Hemiauchenia blancoensis*; pronghorn *Capromeryx arizonensis*; and indeterminate proboscidean. The mammals from Hatch limit the age of this fauna to between 3.0 Ma (first appearance of *Sylvilagus* and *Geomys paenebursarius*) and 2.6 Ma (last appearance of *Equus cummingsii*, *E. simplicidens*, and *Nannippus peninsulatus* in New Mexico). The presence of *Glyptotherium texanum* provides an important biostratigraphic indicator, with the first appearance of glyptodonts and other South American Interchange mammals in temperate North America at about 2.7 Ma. Mammalian biochronology and magnetostratigraphy constrain the age of the Hatch LF to ~2.6–3.0 Ma (early late Blancan).

#### GEOCHEMISTRY OF THE ANIMAS RIVER ALLUVIAL AQUIFER AFTER THE GOLD KING MINE SPILL, SAN JUAN COUNTY, NEW MEXICO

B. Talon Newton, Ethan Mamer, and Stacy Timmons

NM Bureau of Geology and Mineral Resources, 801 Leroy Place, Socorro, NM, 87801, talon.newton@nmt.edu

On August 5, 2015 the accidental breach of the Gold King Mine (GKM), located in Colorado, resulted in the movement of millions of gallons of bright orange water through the Animas River in northwestern New Mexico. This water, which was loaded with dissolved metals and contaminated sediments, posed a potential risk to groundwater quality in the Animas Valley. The Animas River from the Colorado-New Mexico border flows through Quaternary alluvial deposits, which are largely made up of sediment eroded from Paleogene rocks into which the Animas River has incised. While most water for domestic use and irrigation in the area is largely sourced from the Animas River, there are many private domestic and irrigation wells in the valley completed in the alluvial aquifer with depths of about 30 to 60 feet.

We collected water samples from up to 26 wells within and near the Animas Valley between the NM-CO border and Farmington, NM several times between January 2016 and June 2017. The objectives of this study were to characterize the hydrogeologic system, investigate groundwater/surface water interactions, and assess the possible impacts of the GKM spill to shallow groundwater.

General water chemistry, stable isotope and environmental tracer data, and modeling of

two-endmember mixing indicate that shallow groundwater is primarily comprised of young river water and older regional groundwater from the underlying Nacimiento Formation. The river water end-member is characterized by total dissolved solids (TDS) concentrations less than 500 mg/L, a calcium bicarbonate water type, and tritium values above 5 tritium units. The regional groundwater end-member is characterized by much higher TDS concentrations close to 10,000 mg/L, a sodium sulfate water type, undetectable tritium content, and an apparent carbon-14 age of approximately 20,000 years before present. The upwelling of regional groundwater due to the gradual thinning of the Nacimiento Formation to the south, significantly affects water quality by increasing the TDS content to above 1,000 mg/L in some areas south of Aztec.

The main process that may potentially introduce contaminants from upstream mines into the shallow groundwater is the seepage of irrigation water (diverted river water) through the bottoms of ditches and agricultural fields to recharge the aquifer. Potential groundwater contaminants associated with the GKM spill, which include iron, aluminum, manganese, lead, copper, arsenic, zinc, cadmium, and mercury, were found to be below U.S. Environmental Protection Agency (USEPA) maximum contaminant levels (MCLs). Several wells in the shallow aquifer produced water that exceeds USEPA secondary MCLs for dissolved iron and manganese. It is difficult to determine the source of these trace metals, which were observed to be present in the shallow groundwater before the GKM spill. While the GKM spill exhibited high iron and manganese concentrations, these metals are also known to be ubiquitous in fluvial sediments, such as those that make up the alluvial aquifer. Therefore, results from this study do not suggest that the groundwater quality has necessarily been impacted by the GKM spill. However, continued monitoring of groundwater quality is recommended.

#### DRIEST PERIOD OF THE HOLOCENE IN THE SOUTHWESTERN UNITED STATES FROM CORALLOIDAL STALAGMITE GROWTH

Holly Olivarez, Victor Polyak, and Yemane Asmerom

Department of Earth & Planetary Sciences, University of New Mexico, Albuquerque, NM, 87131, holivarez@unm.edu

Evidence from multiple climate proxies worldwide reflect an arid climate in the Northern Hemisphere during parts of the Early and Middle Holocene (~9500 to 4200 yr B.P.). Stalagmite studies from the Guadalupe Mountains, New Mexico have concluded that effective moisture was greater in the southwestern United States during the Younger Dryas and into the Early Holocene,

as shown by a hiatus of stalagmite growth in the Guadalupe Mountains for a period from ~9500 to 7500 yr B.P., and during the Late Holocene; thus implying the Middle Holocene was drier. Only one high-resolution stalagmite study has been published for this region that exhibited growth through the entire Holocene, and that study, based on  $\delta^{13}\text{C}$  and  $\delta^{18}\text{O}$  isotope time-series, does not provide clear indications of aridity.

Cave coralloids (also referred to as cave popcorn) are formed by evaporation of water films from condensation on cave walls, or formed by evaporation of water films on stalagmites and stalactites generated by splashing water; therefore, such growth can be considered a proxy for aridity. Cave coralloid growth on mid-sections of stalagmites from Helens Cave, Carlsbad Caverns National Park in the Guadalupe Mountains are not simply surficial deposits, but are characteristic of stalagmite growth itself, and therefore represent a period that can be interpreted as increased aridity. The period of growth represented by the coralloidal stalagmite growth from two Helens Cave samples, stalagmites Helens-1 and Helens-2, are bracketed by two uranium-series dates of ~8792±127 yr B.P. to ~7215±252 yr B.P., which is consistent with a hiatus of stalagmite growth previously reported. Our interpretation of this proxy is that climate conditions were more arid and likely warmer than any other time in the Holocene in this region of the southwestern United States. Cave coralloids are not often used in climate studies, and we illustrate here their possible value.

#### PARAMETRIZING TOTAL AVAILABLE WATER (TAW) FOR PREDICTION OF ROOT ZONE SOIL MOISTURE USING THE EVAPORATION, TRANSPIRATION AND RECHARGE MODEL (ETRM)

Gabriel E.L. Parrish, Jan M.H. Hendrickx, Juliet Ayertey, Brian Borchers, and Daniel Cadol

New Mexico Institute of Mining and Technology, NM, gbrlparrish@gmail.com

Total available water (TAW) is one of the most difficult-to-ascertain parameters necessary for predicting water storage in the root zone. As such, a method for parametrizing TAW is necessary given the paucity of in-situ measurements that are available. TAW is determined in a novel way as a model fitting parameter. A soil water balance model, the Evaporation, Transpiration and Recharge Model, is used to simulate root zone soil moisture for an area of interest. The TAW parameter of the model is varied until agreement is found between the model simulated and remotely-sensed root zone soil moisture observations on a pixel by pixel basis. In this study, we present initial modeling efforts and a remotely sensed validation data set that will be used to optimize TAW for the area of interest: the Jornada Long Term Ecological Research station (Jornada LTER) in south

central New Mexico. Within the Jornada LTER, the model predictions and remote sensing datasets of root zone soil moisture are compared to neutron probe data from an approximately 2.7 kilometer-long transect of 89 neutron soil moisture probes within the Jornada LTER.

#### **EOLIAN SEDIMENTATION IN THE BOLSON SAND SHEETS OF THE NORTHERN CHIHUAHUAN DESERT: SLOW AND CONTINUOUS OR PUNCTUATED?**

*David M. Rachal<sup>1</sup> and H. Curtis Monger<sup>2</sup>*

<sup>1</sup>Tierra Vieja Consulting, 640 College Pl, Las Cruces, NM, 88005, geoarchnewmexico@gmail.com

<sup>2</sup>USDA-NRCS, National Soil Survey Center, 100 Centennial Mall North Federal Building, Lincoln, NE, 68508

Eolian sand sheets of the Chihuahua Desert commonly exhibit buried paleosols. These buried soils have been viewed as evidence for a punctuated response to climate change characterized by erosion-sedimentation; followed by landscape stability and soil formation during the Late Quaternary. However, a recent chronology of sand sheets, using optically stimulated luminescence (OSL), has challenged this view for sand sheet formation. This has invoked debate about eolian sedimentation and whether it was slow and continuous or punctuated since the Last Ice Age to the middle Holocene Altithermal. In order to improve our understanding of eolian sedimentation, we tested both hypotheses using radiocarbon and OSL dating techniques to evaluate a ~2.5-meter section of eolian paleosols in southern New Mexico. These dates and soil stratigraphy indicate that eolian sedimentation occurred until ~42 ka when a sedimentation hiatus occurred. This permitted the formation of a “Btk” horizon during the last Ice Age. Eolian sedimentation resumed sometime before ~12 ka during the onset of warmer conditions of the Bølling-Allerød. The second break in sedimentation occurred when the water table rebounded during the Younger Dryas Chronozone. This event hydrologically altered the eolian sand and permitted the formation of a mottled “Bg” paleowetland horizon. Water table conditions fluctuated for ~3.7 ka and dropped immediately during the early Holocene no later than ~8.3 ka. This surface was exposed for ~3 ka. Eolian sedimentation resumed sometime around ~5.3 ka during the onset of Antevs’ mid-Holocene Altithermal. The third break in sedimentation occurred by ~4.5 ka with the start of slightly wetter conditions during late Holocene. This permitted the formation of a “Bk” horizon. Our results do not support the “Slow and Continuous Hypothesis”, but instead finds evidence that eolian sedimentation was punctuated and was followed by three periods of landscape stability and soil formation since the last Glacial Maximum to the middle Holocene Altithermal.

#### **LIFETIME PROJECTIONS FOR THE HIGH PLAINS AQUIFER IN EAST-CENTRAL NEW MEXICO**

*Geoffrey Rawling<sup>1</sup> and Alex Rinehart<sup>2</sup>*

<sup>1</sup>New Mexico Bureau of Geology and Mineral Resources, New Mexico Institute of Mining and Technology, 2808 Central Avenue, SE, Albuquerque, NM, 87106, geoffrey.rawling@nmt.edu

<sup>2</sup>New Mexico Bureau of Geology and Mineral Resources, New Mexico Institute of Mining & Technology, 801 Leroy Place, Socorro, NM, 87801

Several thousand water level measurements spanning over 50 years, from over a thousand wells, were used to create aquifer lifetime projections for the High Plains Aquifer in east-central New Mexico. Projections are based on past water-level decline rates calculated over ten- and twenty-year intervals, for two scenarios. One scenario is the time until total dewatering of the aquifer, and the other is the time until a 30-foot-saturated-thickness threshold is reached, the minimum necessary to sustain high-capacity irrigation wells. Agricultural water use has determined water-level decline rates in the past—assuming future decline rates match those of the past ten to twenty years, the scenarios may be viewed as the usable aquifer lifetime for domestic and low-intensity municipal and industrial uses, and the usable lifetime for large-scale irrigated agriculture.

Projected lifetimes and progressively enlarging areas of zero saturation are shown on maps. Areas of declining water-levels and decreasing aquifer life are more reliable projections than areas where these quantities have increased. There is high confidence in the results in the region surrounding Clovis and Portales. Discrepancies between lifetime projections derived from the past and current conditions are largely due to differences between actual decline rates and those projected into the future from any given time period in the past. The results match very well across the state line with lifetime projections for the Texas Panhandle region. The effects of groundwater pumping and water-level declines in east-central New Mexico are similar to those observed in the High Plains aquifer across northwest Texas and western Kansas. Much of the region already has insufficient saturated-thickness for large-capacity irrigation wells. Even when considering the lifetime of the entire thickness of the aquifer, projected lifetimes across much of the study area are a few tens of years or less.

#### **GIS ANALYSIS AND (U-TH)/HE THERMOCHRONOLOGIC INVESTIGATION OF PROTEROZOIC ROCKS IN SOUTHERN NEW MEXICO**

*Nathan Z. Reade<sup>1</sup>, Julian M. Biddle<sup>1</sup>, Jason W. Ricketts<sup>1</sup>, and Jeffrey M. Amato<sup>2</sup>*

<sup>1</sup>Department of Geological Sciences, University of Texas at El Paso, 500 W University Ave, El Paso, TX, 79968, nzread@miners.utep.edu

<sup>2</sup>Department of Geological Sciences, New Mexico State University, P.O. Box 30001, Las Cruces, NM, 88003

Multiple thermochronologic methods (apatite fission-track and (U-Th)/He) have been used to place important time constraints on periods of Cenozoic extension in the Rio Grande rift and Basin and Range Province. However, Proterozoic-aged rocks in this region have experienced a much longer thermal history that is not typically recorded by these data. To investigate long-term (>1 Ga) thermal histories, we combine GIS analysis of past deformational events with zircon (U-Th)/He (ZHe) thermochronology to document periods of pre-Cenozoic burial and exhumation. Recent advancements in the understanding of differential radiation damage and helium retention in zircon suggest that long-term thermal histories experienced since their formation in the Proterozoic, may be extracted from the rocks. We analyzed samples along a transect across the Rio Grande rift—Basin and Range transition zone in west Texas, southern New Mexico and south-eastern Arizona. This region serves as natural laboratory to investigate the Proterozoic-Cenozoic thermal histories of rocks exposed in fault block uplifted mountain ranges. Prior to recent exhumation in the Cenozoic, Rio Grande rift and Basin and Range extension, the Rio Grande rift – Basin and Range transition zone has been affected by multiple deformation events, including the Ancestral Rocky Mountains, Jurassic rifting and the Laramide Orogeny. GIS was used to combine published deformational maps of New Mexico to construct a deformational sequence map of southern New Mexico, illustrating areas that experienced uplift and/or burial during the Ancestral Rocky Mountains, Laramide Orogeny and Rio Grande rift. For each sample location, forward models and predictive age-eU plots were constructed using HeFTy software that include periods of exhumation and/or burial due to each tectonic event. Inverse modeling of ZHe data will be done using HeFTy software to compare to forward models and predicted age-eU plots, to test whether ZHe data record long and complex cooling histories. Preliminary data from some of these ranges yield ZHe ages that range from 19–649 Ma and show a negative correlation with eU, suggesting that ZHe data obtained from this region are an important record of pre-Cenozoic tectonic exhumation. Results from this study will constrain long-term timing, magnitude and rates of cooling experienced

in these fault blocks across the Rio Grande rift—Basin and Range transition zone, and may yield important insight into the timing and duration of deformation related to the Ancestral Rocky Mountains, Jurassic rifting, Laramide Orogeny, and Cenozoic extension.

## REGIONAL WATER CHEMISTRY COMPARISON, LA CIENEGA, SANTA FE COUNTY, NEW MEXICO

Madeline Richards<sup>1</sup>, Stacy Timmons<sup>1</sup>, Cathryn Pokorny<sup>1</sup>, and Dennis McQuillan<sup>2</sup>

<sup>1</sup>New Mexico Bureau of Geology and Mineral Resources, 801 Leroy Pl, Socorro, NM, 87801, USA, madeline.richards@student.nmt.edu

<sup>2</sup>NM Environment Department

The springs of La Cienega provide an important source of water for the people and wetlands in the southern portion of Santa Fe County. The groundwater that discharges at La Cienega comes from aquifers within the Santa Fe Group. The Santa Fe Group is a thick alluvial deposit, comprised of deeper 1,000-foot-thick Tesuque Formation overlain by up to 300 feet of coarser Ancha Formation. The Tesuque Formation is a late Oligocene to late Miocene unit composed of sand, with subordinate gravel, silt, and clay. The Ancha Formation is a late Pliocene to early Pleistocene unit composed of arkosic sand, silty-clayey sand, and gravel found in paleochannels that unconformably overlies the tilted Tesuque Formation basin fill.

A study by Johnson et al. (2016) looked at water chemistry, among other things, from several wells and springs in the La Cienega area, and noted the principle water bearing strata. Chemical analysis showed two major groups: Ca-HCO<sub>3</sub> dominate waters in shallow wells near streams that correlated to the Ancha Formation, and Na-HCO<sub>3</sub> or Na-Ca-HCO<sub>3</sub> waters in deeper Tesuque wells. Shallow wells and springs not in close proximity to streams generally had a mixed chemical signature.

In 2017, as part of a citizen science and water quality awareness effort with the New Mexico Environment Department, 25 private well owners collected grab samples of their well water. These samples were analyzed by the New Mexico Bureau of Geology and Mineral Resources. It was possible to infer the water-bearing formations of these 25 wells by comparing chemical signatures to those reported by Johnson et al. (2016) that had known source formations. A few wells clearly had a source of either Ancha or Tesuque, but most had a chemical signature indicative of mixing of the two sources, which is typical of this region. After comparing chemistry to infer source units, well logs for a few of the sites were found through the New Mexico Office of the State Engineer, and water-bearing strata was confirmed.

Additionally, these data show that maximum contaminant levels from the U.S. EPA quality standards for arsenic were exceeded

in four of the 25 wells sampled. These data were only available because the citizens of La Cienega had questions about the source and quality of their water. This shows that in regions where previous hydrogeochemistry data have been collected, such as La Cienega, citizen water sampling campaigns can provide useful scientific contributions. With help from the local community, it is possible compare current results with previous data to show potential changes to water quality.

## COLLAPSIBLE SOIL SUBSIDENCE SUSCEPTIBILITIES ACROSS NEW MEXICO AT 1:750,000 SCALE

Alex J. Rinehart, Colin T. Cikoski, David Love, Mark Mansell, and Daniel J. Koning

<sup>1</sup>New Mexico Bureau of Geology and Mineral Resources, New Mexico Tech, 801 Leroy Pl, Socorro, NM, 87801, alex.j.rinehart@gmail.com

We present the method used and the resulting 1:750,000 scale map of collapsible soil susceptibility for New Mexico, the first time such a map has been generated in the western United States. Collapsible, or hydrocompactive soils are sedimentary deposits that under combined wetting and loading will subside significantly (up to 30% strains). Composed of water-sensitive-clay-rich sediments, these deposits present a common but difficult to map hazard across the desert Southwest, including New Mexico. However, because compaction of collapsible soils usually happens after structures have been built on them, their incidents are not well reported nor are they readily apparent from surface morphology. Maps of hydrocompaction susceptibility generally are done at scales greater than 1:24,000, allowing for detailed geotechnical sampling to take place combined with geologic mapping. This was not tenable at the scale of New Mexico. To overcome the lack of observable morphology, the paucity of reported incidents and the lack of statewide geotechnical data, we compiled a map of known but geotechnically-unconfirmed locales and then developed a multi-proxy-based spatially weighted average (i.e., an overlay method) of susceptibilities. Proxies used in this study are surficial deposit maps of depositional style, age, geomorphic setting, sediment provenance, and deposit texture; NRCS gSSURGO maps of both soil texture of the bottom 1/3 of the pedon, and the soil taxonomic classification to the great group level; a Köppen-Geiger climate zone map; NLCD land-use maps; and reported static water levels from the NMOSE Water Rights Reporting System. Not all proxies are available throughout the state, meaning that the number of proxies available at a location affected the reliability of the estimated susceptibility. Each proxy was iteratively assigned a weight, or quality factor, and a range of susceptibilities between zero (not susceptible) and four (extremely susceptible) depending on the proxy value. We assessed the effectiveness of each proxy by comparing the frequency of

occurrence in and within 500-m of mapped hydrocompactive locales; at this point, we iterated on both the proxy quality and proxy susceptibility. Then, 500-m resolution rasters of quality-weighted susceptibility (total susceptibilities), average quality and the number of proxies used were generated. Breaks in raw total susceptibilities were assessed by examination of the histograms in and near (within 500-m) mapped hydrocompactive soils: <0.5 was not susceptible, 0.5–1.5 was low susceptibility, 1.5 to 2.5 was moderate susceptibility, 2.5 to 3 was highly susceptibility, and >3 was extremely susceptible. The new 500-m resolution, 1:750,000 scale maps of total hydrocompaction susceptibility, average quality of estimated susceptibility, and number of proxies used should be used together as a planning aid to assess the susceptibility of a region to hydrocompactive soils. They are not, however, substitutes for detailed, location specific geotechnical or geohazards analyses.

## FAULT KINEMATICS OF THE SOUTHERN RIO GRANDE RIFT: A PALEOSTRESS ANALYSIS

Georgina Rodriguez Gonzalez, and Jason W. Ricketts

University of Texas at El Paso, 500 W. University Ave, El Paso, TX, 79968, grodriguezgonzalez@miners.utep.edu

Understanding brittle deformation patterns and their sequence of events in southern New Mexico is vital for the discovery and extraction of natural resources. The purpose of this project is to understand the scarcely studied nature and kinematics of faults located within the southern Rio Grande Rift. The region of interest preserves multiple fault populations, most notably NS-trending faults and NW-SE-trending faults. The main hypothesis to test is that, while both fault sets have contributed to extension in the southern Rio Grande rift, the NW-SE-trending faults also preserve evidence for multiple deformation events dating back possibly to the Precambrian era. In order to correlate the existing faults and their kinematics to previously studied tectonic events, a paleostress analysis was performed to determine the orientations of the maximum ( $\sigma_1$ ) and minimum ( $\sigma_3$ ) principal stresses of fault populations.

Initial results are presented from the Cooke's Range, southern New Mexico. NS-trending faults preserve slickenlines with steep rakes. These faults are interpreted to be normal faults based on younger rocks on top of older rocks and inspection of shear sense criteria along the fault plane (Fossen, 2010). In contrast, minor faults along NW-SE-trending faults have a range of orientations, and slickenlines vary from strike-slip to dip slip. Although future careful investigation of these faults will help to determine the sense of slip, preliminary findings suggest that some of these faults may record reverse-sense slip.

In addition to Rio Grande rift extension, NW-SE-trending faults in southern New Mexico have also been attributed to contraction during the Laramide orogeny (Chapin C. and Cather S., 1981), extension along the border of the Mesozoic Chihuahua Trough (Haenggi W.T., 2002), and may even be related to strike-slip movement during the Precambrian (Muehlberger W., 1965). Future research will focus on relating fault populations to these previously recognized periods of deformation in southern New Mexico. To do this, additional localities in the southern Rio Grande rift will be investigated where NS-trending faults and NW-SE-trending faults are both preserved. We will specifically look for the relative ages of these two fault populations to determine in NS-trending faults consistently cross-cut NW-SE-trending faults. Our preliminary findings based on fault analysis in the Cookes Range suggest that, while EW extension in the northern and central segments of the rift produced new NS-trending faults, in southern New Mexico this stress field may have resulted in the reactivation of much older faults and fractures in the crust, producing the large bend in the rift as it continues into Texas and northern Mexico.

**BACULITES BACULUS FROM THE UPPERMOST PIERRE SHALE NEAR RATON DEMONSTRATES THAT THE FINAL REGRESSION OF THE LATE CRETACEOUS SEAWAY FROM NORTHEASTERN NEW MEXICO OCCURRED DURING EARLY MAASTRICHTIAN TIME**

Paul L. Sealey and Spencer G. Lucas

New Mexico Museum of Natural History, 1801 Mountain Road, NW, Albuquerque, NM, 87104, ammonoidea@comcast.net

The ammonite *Baculites baculus* Meek and Hayden, 1861 was recently recovered from the uppermost part of the Pierre Shale (about 15 m below the base of the Trinidad Sandstone) west of Raton in northeastern New Mexico. This ammonite was found in sandy strata of the distal lower shoreface of the Trinidad shoreline. The *B. baculus* Zone is earliest Maastrichtian in age. The youngest ammonite zone previously reported from northeastern New Mexico was the upper Campanian *Baculites reesidei* Zone (Cobban, 1976). This zone was inferred by the occurrence of *Inoceramus oblongus* Meek, 24–35 m below the top of the Pierre Shale. The *B. baculus* Zone is three ammonite zones higher than the *B. reesidei* Zone, and *B. baculus* in the uppermost Pierre Shale demonstrates that the Pierre seaway regressed from northeastern New Mexico later than previously thought. Across northern New Mexico, the western shoreline of the Western Interior Seaway regressed north and east during late Campanian to early Maastrichtian time. The uppermost lower Maastrichtian *Baculites clinolobatus* Zone occurs in the uppermost

part of the Pierre Shale near Trinidad, Colorado (Berry, 2018). The first/last occurrences (FO/LO) of the *B. clinolobatus* Zone are 69.67/69.28 Ma and the FO/LO of the *B. baculus* Zone are 72.18/70.62 Ma (Scott, 2014). By these estimates of the LO of *B. baculus* and the FO of *B. clinolobatus*, regression of the Pierre seaway from Raton to Trinidad took slightly less than one million years.

The NMMNH specimen of *Baculites baculus* from locality 12043 is a moderately-preserved, large, incomplete, adult shell in two pieces, slightly flattened on one lateral side. The larger piece, mostly body chamber, has a length of 215 mm and a maximum diameter of 65.3 mm. The cross section is stout and almost quadrate. The flanks bear low, broad, arcuate undulations. The degree of taper is low. The poorly-preserved suture has simple, broad, rectilinear elements. These are characteristics of *B. baculus*. It is most similar to its smaller, presumed ancestor *B. undatus* Stephenson, which occurs much lower in the section with a range of 45–61 m below the top of the Pierre Shale west of Raton (Cobban, 1976). *B. grandis* Hall and Meek, the descendant of *B. baculus* and the next ammonite zone higher, is larger and has an almost trigonal cross section.

Therefore, the occurrence of the *Baculites baculus* Zone in the Raton area establishes an earliest Maastrichtian age for the uppermost Pierre Shale there, places the Campanian-Maastrichtian stage boundary at the base of that zone in the uppermost Pierre and demonstrates that the Pierre seaway regressed from northeastern New Mexico during early Maastrichtian time.

**FIRST REPORT OF A JAW IN THE LATE CRETACEOUS AMMONITE GENUS SPATHITES KUMMEL AND DECKER, 1954**

Paul L. Sealey<sup>1</sup>, Michael P. Foley<sup>1</sup>, Neil H. Landman<sup>2</sup>, and Spencer G. Lucas<sup>1</sup>

<sup>1</sup>New Mexico Museum of Natural History, 1801 Mountain Road, NW, Albuquerque, NM, 87104, ammonoidea@comcast.net

<sup>2</sup>American Museum of Natural History, 79th St. and Central Park West, New York, NY, 10024

A lower jaw was recently discovered embedded in a concretion in association with the Late Cretaceous (Turonian) ammonite *Spathites puercoensis* (Herrick and Johnson, 1900) in the Carlile Member of the Mancos Shale in Sandoval County, New Mexico. The jaw was revealed when the concretion was broken open. Ammonite jaws are beaks or mandibles consisting of upper and lower elements. The jaw apparatus and the radula (rasping tongue) were the primary feeding organs of ammonites. The lower jaw of New Mexico Museum of Natural History specimen P-79962 is mostly complete and well-preserved, but is almost entirely flattened. The more complete plate (wing) is divided into three parts by calcite veins in the gray

limestone concretion. It is situated next to another element that appears to be the other plate of the lower jaw. They are both offset in the concretion from a well-preserved, but weathered, partial, adult phragmocone of the robust form of *S. puercoensis*. A small portion of shell material of the ammonite was exposed during preparation. The body chamber does not appear to be preserved but could be hidden within the concretion. The elements are likely the paired calcitic plates of the lower jaw called the aptychus (*sensu stricto*). There are small areas of black material exposed directly below the light-colored outer layer of both plates that could be the remains of the inner chitinous layer. The more complete plate is approximately 52 mm long by 30 mm wide (W/L = 0.58), but is flattened. Most of the anterior and lateral margins and parts of the posterior margin are preserved. The specimen is triangular in outline and retains some of the original curvature on the lateral margins. The anterior margin is narrow and pointed. Surface sculpture consists of fine, closely-spaced co-marginal rugae paralleling the lateral margin and curving to parallel the posterior margin. The less complete plate, in juxtaposition to the other, but facing the opposite direction, has the posterior margin broken off. Approximately 1–2 mm below the surface of this broken margin, a layer of black material is exposed that could be the remains of the inner chitinous lamella. This plate has folds or creases along and near one of the lateral margins that could be the result of postmortem, plastic deformation. The two plates are not symmetrical with each other, but this could be due to the deformation. It is likely that this jaw belongs to the associated ammonite in the concretion. It is only the second reported occurrence of a jaw in the family Acanthoceratidae and the first occurrence of a jaw from the subfamily Mammitinae Hyatt, 1900 and the genus *Spathites* Kummel and Decker, 1954. It is also the first reported occurrence of an ammonite jaw from New Mexico.

**INVENTORY AND CHARACTERIZATION OF INACTIVE/ABANDONED MINE (AML) FEATURES IN NEW MEXICO**

Marcus E. Silva<sup>2</sup>, Virginia T. McLemore<sup>1</sup>, and Navid Mojtabai<sup>2</sup>

<sup>1</sup>New Mexico Bureau of Geology & Mineral Resources, 801 Leroy Place, Socorro, NM, 87801

<sup>2</sup>New Mexico Tech, Mineral Engineering, 801 Leroy Place, Socorro, NM, 87801

Abandoned mine lands (AML) are lands that were mined and left un-reclaimed where no individual or company has reclamation responsibility and there is no closure plan in effect. These may consist of excavations, either caved-in or sealed, that have been deserted and where further mining is not intended in the future. The New Mexico

Bureau of Geology and Mineral Resources (NMBGMR) and the Mineral Engineering Department at New Mexico Tech in cooperation with the New Mexico AML program is conducting research to develop a better procedure to inventory and characterize legacy, inactive, or abandoned mine features in New Mexico. Fieldwork involves completion of mine inventory forms which detail location, lithology, feature condition, vegetation, and potential environmental and physical hazards. Laboratory work on these samples includes geochemistry from a professional lab as well as in-house petrography, x-ray diffraction, electron microprobe, paste pH, and particle size analysis. Some sites have the potential to contaminate surface water, groundwater and air quality many of which also feature open shafts and adits and pose serious physical risks to nearby communities. The results of this study will prioritize the mine features in selected mining districts in New Mexico for safeguarding and remediation.

#### BIOGEOGRAPHY AND BIOSTRATIGRAPHY OF NORTH AMERICAN EUTHERIAN MAMMALS DURING THE PUERCAN FAUNAL STAGE (PALEOCENE, EARLIEST DANIAN)

Jason Silviria

University of New Mexico, UNM SRC 25,  
2700 Campus Blvd. NE,  
Albuquerque, NM, 87106,  
sympanscience@gmail.com

The Puercan Land Mammal Age (Paleocene, earliest Danian; ~66–65 Ma) is the earliest North American faunal stage of the Cenozoic era, immediately after the end-Cretaceous (K-Pg) mass extinction event. It is typified by the adaptive radiation of eutherian mammals, including placentals, following the annihilation of the non-avian dinosaurs, which opened up numerous ecological niches. Unfortunately, the spatiotemporal scale of Puercan eutherian diversification remains elusive. Several authors have increased differentiation between “northern” and “southern” faunas in western North American, as was the case in vertebrate faunas below the K-Pg boundary; additionally, endemism is widely believed to have higher in the later Pu2 and Pu3 intervals compared to the earlier Pu1 interval. However, this is complicated by a number of Pu1 sites in a possible “transition zone” between northern and southern faunal provinces with many unusual endemics.

To resolve these issues, I gathered abundance data on all currently valid Puercan eutherian genera and species, based on a critical review of the published literature and of museum catalogs. Biogeographic and biostratigraphic trends within basins and intervals were tested using DCA, PCA, and NMDS analyses in R, as well as with *agnes* hierarchical dendrograms. Scatterplots of DCA and NMDS results – based on Bray-Curtis,

Jaccard, and Kulczynski distance metrics – generally resolved Puercan eutherian localities along a north-south gradient, with “northern” sites from the Bighorn, Calgary, and Williston basins representing one end-member, “southern” sites from the Denver, Paradox and San Juan basins representing another, and sites from the Crazy Mountain, Great Divide, and Hanna basins representing the “transition zone” in between. These same scatterplots also demonstrate moderate distinction of the Pu1 interval from the combined Pu2/Pu3 intervals.

In *agnes* dendrograms based on Kulczynski distances, most sites were sorted into three well-supported clusters: a group of Pu1 “northern” sites, a group of Pu3 “northern” sites, and a group of Pu2/Pu3 “southern” sites. However, several Pu1/Pu2 northern and transition-zone sites (i.e. Alexander, Hiatt, Polecat Bench, MBHT Rav-W1) formed a fourth cluster more closely resembling the Pu2/Pu3 “southern” fauna. This supports the notion of increased faunal differentiation over the Puercan, as well as an early northward expansion of the Pu2/Pu3 southern faunal province at the expense of the Pu1 northern “disaster fauna”. Future studies will focus on the effect of site lithology and sampling techniques in these evaluations of Puercan eutherian biogeography and biostratigraphy.

#### EFFECTS OF REGIONAL CLIMATE DIFFERENCES ON RATES OF SOIL DEVELOPMENT: INSIGHTS FROM WELL-DATED CHRONOSEQUENCES IN THE RIO GRANDE RIFT

Brad Sion, Bruce Harrison, Fred Phillips, and Gary Axen

New Mexico Tech, 801 Leroy Place, Socorro, NM, 87801, bradley.sion@student.nmt.edu

Rates of soil development provide important information about geomorphic and landscape evolutionary processes. Soil development in arid and semiarid regions of the southwestern United States is predominantly controlled by influx of eolian dust, yet our ability to quantify the rates of dust and carbonate incorporation into these calcic soils is limited by available age control. We described 10 soil profiles in the Socorro area of central New Mexico and analyzed their silt, clay, and carbonate contents. These soils have well-established direct- or indirect-age control that is used to compute rates of dust and carbonate accumulation for durations of ~0.5–800 ka. We also compute the profile development index (PDI) for these soils and compare our chronofunction to PDIs from northern and southern New Mexico. Principal components analysis identifies four dominant soil properties that explain variations in soil age; total texture, color lightening, dry consistence, and CaCO<sub>3</sub> stage morphology, supporting models of soil development by incorporation of eolian dust. We find that the net silt-and-clay contents in B horizons of progressively

older soils increases at rates similar to the profile-mass carbonate contents. Our power-law regressions for these properties yield slopes of 0.34 and 0.30, respectively. We find a similar slope of 0.32 for our power-law regression through the PDI data. A well-dated chronofunction from the Los Alamos area in northern New Mexico indicates that soil development occurs more rapidly in higher latitude regions of New Mexico than in the Socorro area and farther south. We interpret this trend in light of a regional climate gradient manifested by greater mean annual precipitation and cooler mean annual temperatures at higher latitudes and/or slower rates of eolian dust accumulation into the soil profile. This would promote greater mobility of available silt and clay, and also drive faster rates of in-situ weathering, as indicated by the presence of argillans in late-Pleistocene soils of northern New Mexico.

#### GEOMORPHIC EVIDENCE FOR EPISODIC INFLATION ABOVE THE SOCORRO MAGMA BODY: TIMESCALES AND MECHANISMS RELATED TO SURFACE UPLIFT

Brad Sion, Gary Axen, Fred Phillips, and Jolante van Wijk

New Mexico Tech, 801 Leroy Place, Socorro, NM, 87801, bradley.sion@student.nmt.edu

Timescales of processes related to mid-crustal magma intrusion are poorly understood. The Socorro magma body (SMB) in the central Rio Grande rift is one of the largest known active mid-crustal intrusions and offers a unique opportunity to study the timing of processes associated with its emplacement. Surface uplift and seismicity above the SMB demonstrate ongoing magmatic unrest. Nearby Holocene volcanism illustrates the potential for a longer-lived magmatic system that was active during Holocene or pre-Holocene times. Quaternary river terraces preserved at the surface and above the SMB provide paleo-geodetic markers to interrogate the longevity of magmatism. We use high-resolution terrace elevations in the Rio Salado, a Rio Grande tributary that crosses surface-uplift contours, and new <sup>36</sup>Cl surface-exposure and <sup>14</sup>C ages to document a prehistoric surface-uplift event above the SMB. We observe longitudinal terrace patterns consistent with an arching event that began after 26 ka and ceased before 3 ka that cannot be explained by tectonic or fluvial mechanisms. This late Pleistocene-early Holocene surface uplift is related to a magma-emplacement event that predates modern magmatism and is co-located with geodetic uplift. We interpret the two temporally distinct surface-uplift events as recording episodic intrusion below the Socorro area since late-Pleistocene time. We propose that rejuvenation of magmatic activity occurs via a stationary plumbing system inferred from seismic data. This study shows that the magmatic

source-feeder system is stable and active over timescales of  $10^4$  yrs and demonstrates the utility of terraces as strain markers of low-amplitude, large-wavelength deformation caused by mid-crustal magmatic activity.

## HYDROGEOLOGIC CHARACTERIZATION AND REMEDIATION AT THREE GROUNDWATER AREAS OF CONCERN, SANDIA NATIONAL LABORATORIES, NEW MEXICO

Michael F. Skelly, John R. Copland, and Jun Li

Sandia National Laboratories, Albuquerque, NM, mfskell@sandia.gov

Groundwater monitoring is conducted at three Environmental Restoration (ER) Operations groundwater Areas of Concern, including Technical Area-V Groundwater (TAVG), Tijeras Arroyo Groundwater (TAG), and Burn Site Groundwater (BSG) for the U.S. Department of Energy, National Nuclear Security Administration at Sandia National Laboratories, New Mexico.

The TAVG is located on the East Mesa of the Albuquerque Basin in the central portion of Kirtland Air Force Base. Groundwater occurs at a depth of approximately 500 feet within unconsolidated, alluvial fan sediments of the Santa Fe Group. Historic discharges of waste waters have impacted the uppermost Regional Aquifer with nitrate and trichloroethene (TCE). The impacted sediments have low hydraulic conductivities averaging 4 to 5 feet/day. The maximum nitrate and TCE concentrations are 15 mg/L and 19 ug/L, respectively. A treatability study of in-situ bioremediation is currently being conducted. An injection well is used to distribute the bacteria *dehalococcoides* and various nutrients to the aquifer.

The TAG is located on the East Mesa of the Albuquerque Basin along the northern rim of Tijeras Arroyo. Groundwater occurs in two water-bearing zones within unconsolidated, alluvial fan sediments of the Santa Fe Group: the Perched Groundwater System (PGWS) and the Regional Aquifer. The PGWS is present at a depth of 290 feet and consists of a thin zone of saturation ranging from 7 to 17 feet thick. The PGWS was primarily created by manmade activities including sewage lagoons, landscape watering, and waste-water outfalls. Most recharge inputs have been eliminated and the PGWS is dewatering. Nitrate is the contaminant of concern with concentrations occasionally exceeding 30 mg/L (as nitrogen) in the PGWS. The Regional Aquifer occurs at an average depth of 410 feet and is vertically separated from the PGWS by approximately 200 feet of unsaturated sediments over much of the TAG area. The maximum nitrate concentration in the Regional Aquifer is 4 mg/L. Remedial alternatives for the nitrate-impacted groundwater in the PGWS are currently being evaluated.

The BSG is located along the eastern margin of the Albuquerque Basin, and the

terrain is characterized by large topographic relief exceeding 900 ft in deeply incised into Paleozoic strata and Precambrian basement. Groundwater occurs in granitic gneiss and metamorphic units (phyllite, schist, and quartzite). Groundwater is semiconfined and migrates in a generally westward direction through a diverse set of fractures and along near-vertical faults; the thin veneer of alluvium at the site is sporadically saturated. Releases to the environment include outdoor detonations of high explosives from 1967 to 1985, wastewater disposal from 1978 to 1988, and burn tests from 1969 to present. Nitrate is the contaminant of concern with concentrations exceeding 40 mg/L (as nitrogen). Remedial alternatives for the nitrate-impacted groundwater are currently being evaluated.

## FAULT CORE MICROSTRUCTURES AND THEIR RELATIONSHIP TO THE RATE OF SLIP, WEST SALTON DETACHMENT FAULT, SOUTHERN CALIFORNIA

Katrina Lucia Soundy, Gary Axen, Kierren Maher, and Jolante Van Wijck  
New Mexico Institute of Mining and Technology, Socorro, NM 87801, katrina.soundy@gmail.com

The primary rift structure in the western Salton trough is the low-angle West Salton Detachment Fault (WSDF). The WSDF is a low-angle normal fault that bounds the western Salton Trough (upper plate) from the Peninsular Ranges (footwall) in Southern California. The detachment was active from ~5–8 to ~1 Ma. Slip along the detachment ended when the dextral San Jacinto, San Felipe, and Elsinor systems cut across it ~1.1–1.2 Ma and dominated local deformation. (U-Th)/He dating of apatite and zircon of the hanging wall and footwall of the WSDF indicate at least 2.3–4 to 8 km of exhumation and >8–10 km of eastward horizontal extension starting 5 Ma.

Footwall and hanging wall fault rocks have intermediate plutonic protoliths. Footwall fault rocks were formed mainly in the upper seismogenic zone and were minimally reworked while transiting to the aseismic zone. Hanging wall fault rocks formed at <2–3 km paleodepth, lack a well-developed ultracataclastic layer, and show clay alteration.

Along most of the WSDF, the top of the footwall displays a 2-part fault core. Immediately adjacent to the principal fault plane is a thin 10–40 cm layer of black-brown ultracataclastic. The ultracataclastic is above 1–3 meters of cataclastic. Both of these layers have several random microscopic fabrics. Pseudotachylyte veins injected into both the hanging wall and footwall are observed in multiple locations throughout the center of WSDF. Significant hydrothermal alteration is seen in the southern section of the WSDF, where the ultracataclastic is thinner, the cataclastic is macroscopically foliated, and there is no pseudotachylyte.

Two study sites were selected to observe any contrast in fault microstructures: Agua Caliente and Powder Dump. Powder Dump displays the typical two-part fault core seen through most of the WSDF and has pseudotachylyte injection veins. This indicates that Powder Dump slipped seismically at some times. In contrast, Agua Caliente displays abundant hot spring activity from the detachment. The fault core rocks at Agua Caliente are different: pseudotachylyte is absent, ultracataclastic is thinner (a few cm), and cataclastic are macroscopically foliated and lineated with normal-sense S-C fabrics. The observed foliation in otherwise brittle, low-temperature Agua Caliente fault rock suggests that significant slip accumulated by creep.

Our study aims to compare the fault-rock textures (grain size distribution, grain shapes, micro- and macroscopic fabrics) and mineralogy from Agua Caliente (paleocreeping) and Powder Dump (paleoseismic). Some lab work (Keulen, et al. 2007) suggests that grain shapes are more convex when formed at high slip rates, but this has not been shown in natural examples (to our knowledge). We hypothesize that we should be able to replicate the observation of the correlation from samples in the field between the increasing rate of slip and the increasing convexity of fault grains.

## A FIELD-SCALE EXAMINATION OF FAULT CONTROLS ON SUBSURFACE FLOW

Tyler Sproule<sup>1</sup>, Johnny Ray Hinojosa<sup>1</sup>, Glenn Spinelli<sup>1</sup>, Peter Mozley<sup>1</sup>, John Wilson<sup>1</sup>, and Michael Fort<sup>2</sup>

<sup>1</sup>New Mexico Institute of Mining and Technology, 801 Leroy Place, Socorro, NM, 87801, tyler.sproule@student.nmt.edu

<sup>2</sup>HydroResolutions LLC

Geologic faults can substantially alter fluid flow fields in the subsurface. Depending on structural properties, a fault may act as either an impediment or conduit to groundwater flow; a clay-smear or cemented fault slip surface hinders the movement of water, while an unconsolidated damage zone introduces efficient new pathways for flow. In geologic settings with numerous, extensive faults (e.g. rift zones), accounting for fault-fluid interactions quickly becomes essential in evaluating groundwater resources at a regional scale. However, conventional analytical methods and commercial aquifer modeling software often assume that a fault occupies a perfectly vertical plane of minute thickness. In reality, fault structures can have complex geometries with variable thickness in space. As a result, clear relationships are not established between fault geometry or composition and impacts to subsurface flow. Implications of this phenomena are not limited to hydrogeology applications: petroleum extraction, carbon sequestration, and geothermal energy each stand to benefit from a better understanding of this topic.

We postulate that the Loma Blanca Fault, located in central New Mexico, is an ideal candidate for gaining further insights into fault-fluid flow interactions. Our study will utilize an interdisciplinary geological, geophysical, and hydrologic approach. The Loma Blanca is a north-south oriented normal fault with sections of extensive outcrop. The fault is variably cemented with carbonate, dipping approximately 70°E. Field analyses of the cemented outcrop reveals permeabilities low enough to substantially decrease fluid flow. A preliminary model of the local geology was created using samples from exploratory wells, directional cores, and near-surface geophysical data. The interim geologic model suggests that the fault extends into the subsurface with varying degrees of cementation. Multiple wells will be installed along each side of the Loma Blanca, allowing us to conduct groundwater pumping tests and gauge the aquifer response. If the fault is indeed cemented in the subsurface, we expect contrasting groundwater drawdown behavior on opposing sides of the fault following sufficient pumping. Additional field data will be obtained through innovative pneumatic oscillatory aquifer tests. Our future objectives are to analyze aquifer test data in conjunction with multiple modeling approaches to diagnose fault attributes and further explore the topic of fault-fluid flow interactions. Funding for this project is provided by the National Science Foundation.

#### EVALUATING SEDIMENT TRANSPORT IN FLOOD-DRIVEN EPHEMERAL TRIBUTARIES

*Kyle Anderson Stark and Daniel Cadol*  
Earth and Environmental Science  
Department, New Mexico Institute of  
Mining and Technology, 801 Leroy Place,  
Socorro, NM, 87801,  
kyle.stark@student.nmt.edu

One common source of uncertainty in sediment transport modeling of large semi-arid perennial rivers is sediment influx delivered by ephemeral, flood-driven tributaries. Large variations in sediment delivery are associated with these regimes due to the highly variable nature of flows within them. Flooding within these tributaries typically last on the order of hours, making it difficult to be present during an event. To better understand these regimes, automated systems are needed to continuously sample bedload and suspended load. In preparation for the pending installation of an automated site on the Arroyo de los Piños in New Mexico, manual sediment and flow samples have been collected over the summer monsoon season of 2017.

Eight flow events were recorded along the Piños from July to October. Of these eight events, data (including stage, velocity, and sediment samples) were collected from six. These events ranged in duration from 30 minutes to 4 hours and in maximum water depth of 10 cm to 75 cm. Bedload and suspended

sediment samples data reveal a channel that is dominated by sand and gravel; more than 50% of the sediment in suspension is of sand size or larger. Flow data and flood wave arrival times indicate a complex system; flow is generated primarily in areas of exposed bedrock in the center and higher elevations of the watershed. These data will be used to inform future site operations, which will combine direct sediment measurement from Reid-type slot samplers and non-invasive acoustic and seismic measuring methods. Indirect methods for measuring of bedload have never been extensively evaluated in ephemeral channels in the southwest United States. Ultimately, this experiment will provide more accurate ephemeral channel sediment loads for stream restoration studies, sediment management actions, and reservoir sedimentation reports.

#### FIRST DISCOVERY OF A TETRAPOD BODY FOSSIL IN THE LOWER PERMIAN YESO GROUP, CENTRAL NEW MEXICO

*Emily D. Thorpe<sup>1</sup>, Spencer G. Lucas<sup>2</sup>,  
David S. Berman<sup>3</sup>, Larry F. Rinehart<sup>2</sup>,  
Vincent Santucci<sup>4</sup>, and Amy C. Henrici<sup>3</sup>*

<sup>1</sup> PO Box 147, Morrisonville, WI, 53571,  
emily.thorpe@outlook.com

<sup>2</sup>New Mexico Museum of Natural History  
and Science, 1801 Mountain Road N. W.,  
Albuquerque, NM, 87104

<sup>3</sup>Carnegie Museum of Natural History, 4400  
Forbes Ave, Pittsburgh, PA, 15213

<sup>4</sup>National Parks Service, 1849 C Street, NW,  
Washington, DC, 20240

The lower Permian Yeso Group records arid coastal plain, shallow marine, and evaporitic deposition across much of central New Mexico. Generally considered to have few fossils, recent study of Yeso Group strata has discovered a diverse fossil record of marine micro-organisms (mostly algae and foraminiferans), terrestrial plants, and tetrapod footprints. We report here the first discovery of a tetrapod body fossil in the Yeso Group—a partial skeleton of a basal synapsid, varanopidae eupelycosaur. The fossil is the natural casts of bones in two pieces, part and counterpart, that were preserved in a sandstone bed of the lower part of the Arroyo de Alamillo Formation in the southern Manzano Mountains. The fossil-bearing sandstone is fine-grained, quartz rich, and pale reddish brown to grayish red unweathered, weathers to blackish red, and is in part encrusted by white caliche. The casts preserve part of the pelvis(?), 18 caudal vertebral centra, both femora and tibia-fibulae, and most of the pedes, largely in close articulation, of a single individual. The skeleton is of a relatively small (femur length = 62 mm, total length of the preserved cast from the pelvis to tip of the incomplete tail = 325 mm) and gracile eupelycosaur most similar to *Varanops*. Various early Permian eupelycosurs are known from the older strata of the Bursum Formation, Abo Formation, and

Cutler Group in New Mexico, so this discovery extends the eupelycosaur fossil record into younger, early Permian strata. It also indicates that a substantial terrestrial food chain must have been present on the arid coastal plain during deposition of the Arroyo de Alamillo Formation, as the varanopid is a relatively large, early Permian predator that likely fed on smaller vertebrates and arthropods. Furthermore, this discovery indicates the potential of additional discoveries of tetrapod body fossils in Yeso Group strata.

#### EFFECTS OF OLIVINE ON ACID ROCK DRAINAGE

*Margaret Tinsley, Ingar Walder,  
Rodrigo Embile, and Franciszka Stopa*  
New Mexico Institute of Mining and  
Technology, 801 Leroy Place, Socorro, NM,  
87801, margaret.tinsley@student.nmt.edu

Olivine has some neutralizing capacity, and has been promoted as part of remediation plans for some mine sites, especially those where olivine is a major part of the deposit. This talk examines the utility of olivine for improving drainage water quality at the former Bruvann nickel mine. A combination of lab and field studies are reviewed to determine the effects of olivine on water pH and nickel content. Columns of waste rock from the site treated with a continuous flow of pH 1.5 acid maintained a pH of 2.0 or higher, indicating some neutralization is taking place. However, kinetic columns rinsed with water produced a range of drainage pH values, including several acidic ones. These columns also consistently released nickel in their drainage. Water samples taken in the field did have approximately neutral pH, but still contained nickel. Overall, this research indicates that the presence of olivine within mine waste solves, at most, only part of the problem.

#### CAN WE USE DATA FROM KINETIC TESTING TO PREDICT FUTURE WATER QUALITY SEEPING FROM MINE WASTE?

*Ingar F. Walder<sup>1</sup>, Rodrigo Embile<sup>2</sup>,  
Margaret Tinsley<sup>2</sup>, Franciszka Stopa<sup>1</sup>, and  
Ferenc Moricz<sup>3</sup>*

<sup>1</sup>Mineral Engineering Dept., New Mexico  
Tech, 801 Leroy Place, MSEC 340, Socorro,  
NM, 87801, ingar.walder@nmt.edu

<sup>2</sup>Earth and Environmental Sciences, New  
Mexico Tech, 801 Leroy Place, MSEC 340,  
Socorro, NM, 87801

<sup>3</sup>University of Miskolc, Hungary

Long-term kinetic testing is commonly performed on rock samples when evaluating acid generation, acid neutralization, and leaching rates from mine waste material. These tests are primarily performed in the laboratory under controlled conditions on small amounts of material compared to what they are intended to represent. The tests have

been used to confirm or evaluate the result from static testing, Acid-Base Accounting, i.e. if sulfide containing waste material will go acidic or not. Field tests on larger samples set to the specific conditions of the sites are however, becoming more common as well.

This talk is reviewing and discussing kinetic tests performed on mine waste from a nickel deposit, ilmenite deposits, massive sulfide deposits, porphyry copper deposit, and the usefulness of running these tests. It is necessary to understand the parameter that are different in the laboratory compared with the natural setting to be able to scale up the result and predict what will happen in a waste rock stockpile. These may be the humidity, flow regime through the waste material, temperature, oxygen availability, rainfall/water addition. Are these differences generating different mineralogical regime between the lab tests and the natural setting? How we can improve the test methods and get more out of the expensive long-term tests that most mining operations handling sulfidic waste have to perform?

#### THE BEGINNING OF THE AGE OF MAMMALS IN NEW MEXICO: NEW INSIGHTS ON THE RISE OF PLACENTALIA BASED ON A PRELIMINARY COMPREHENSIVE PHYLOGENY

Thomas E. Williamson<sup>1</sup>, Stephen L. Brusatte<sup>2</sup>, Jan E. Janečka<sup>3</sup>, Sarah L. Shelleys<sup>4</sup>, Michelle Spaulding<sup>5</sup>, and John R. Wible<sup>4</sup>

<sup>1</sup>New Mexico Museum of Natural History and Science, 1801 Mountain Road, NW, Albuquerque, NM, 87121, thomas.williamson@state.nm.us

<sup>2</sup>University of Edinburgh, School of GeoSciences, Edinburgh, Scotland, U.K.

<sup>3</sup>Duquesne University, Department of Biological Sciences, Pittsburgh, PA

<sup>4</sup>Carnegie Museum of Natural History, Pittsburgh, PA

<sup>5</sup>Purdue University, Northwest, Department of Biology, Westville, IN

The Cenozoic radiation of mammals was a profound moment in vertebrate evolution, however, many aspects of this radiation remain poorly understood, largely because phylogenetic and macroevolutionary studies have ignored mammals from the Paleocene. In order to address this deficit, we are building a comprehensive higher-level phylogeny using anatomical and genetic data of a large number of mammalian taxa (both extinct and extant). This phylogeny will include an unprecedented number of Paleocene taxa, including many enigmatic forms that have formerly been relegated to “wastebasket” groups.

This project will incorporate a wealth of fossil specimens that have been collected from the Paleocene Nacimiento Formation of the San Juan Basin, northwestern New Mexico. The Nacimiento Formation contains the longest and most complete record of mammalian

succession through the early Paleocene. Moreover, many extraordinary specimens have been amassed from these deposits, especially over the last 2–3 decades, through focused collecting efforts by the New Mexico Museum of Natural History and Science. These fossils are being studied using a variety of new techniques, including high-resolution CT scanning, that are revealing new details of the anatomy and functional morphology, that are bringing new insights into the biology and evolution of these archaic animals.

Preliminary results of our comprehensive phylogeny of Paleocene mammals build upon previous large datasets, including most Paleocene lineages—(262 taxa [58 extant and 204 extinct]) scored for over 2,000 morphological characters. Molecular data from the extant taxa, over 35,000 base pairs from 26 nuclear genes will ultimately also be included. These results are based on use of maximum parsimony, but later analyses will also use maximum likelihood and Bayesian methodology. Our preliminary results find that most Paleocene taxa are found to be stem members of major extant clades (e.g., Primates, Afrotheria, Laurasiatheria, Carnivoramorpha, Euungulata). When coupled with high-resolution geochronological record being developed from the Nacimiento Formation record, our analyses show that many major mammalian clades originated very early in the Paleogene.

#### CHEMO-MECHANICAL ALTERATIONS DURING GEOLOGIC CARBON SEQUESTRATION IN SANDSTONE: EXPERIMENTAL OBSERVATIONS

Zhidi Wu<sup>1</sup>, Andrew J. Lubmann<sup>1</sup>, Alex J. Rinehart<sup>2</sup>, Peter S. Mozley<sup>1</sup>, Thomas A. Dewers<sup>3</sup>, Jason E. Heath<sup>3</sup>, and Bhaskar S. Majumdar<sup>4</sup>

<sup>1</sup>New Mexico Tech, Earth and Environmental Science, New Mexico Tech Socorro, NM, 87801, zhidi.wu@student.nmt.edu

<sup>2</sup>New Mexico Tech, Bureau of Geology & Mineral Resources

<sup>3</sup>Sandia National Laboratory, Dept. of Geomechanics

<sup>4</sup>New Mexico Tech, Dept. of Materials Engineering

CO<sub>2</sub> injectivity and storage capacity in sandstone may be impacted by fluid-rock interaction and resultant compaction during carbon sequestration. Although chemical, mineralogical and petrophysical changes are well characterized during fluid-rock interaction in CO<sub>2</sub>-rich systems, the coupling of CO<sub>2</sub>-driven alteration of sandstone with mechanical property changes is less known. Six flow-through experiments were conducted on Pennsylvanian Morrow B Sandstone cores from the Farnsworth Unit in West Texas, USA. CO<sub>2</sub>-rich brine flowed through core samples of poikilotopic calcite- and disseminated ankerite-siderite-cemented sandstone at flow rates that ranged from

0.01 to 0.1 ml/min at 71°C and 29.0 MPa pore fluid pressure. Fluid sample analysis performed by ICP-OES from experiments on both carbonate-cemented sandstones indicate that carbonate cement dissolution is likely the dominant chemical process. The permeability of the ankerite-siderite-cemented sandstone changed little from the reaction with carbonic acid, whereas the permeability of the calcite-cemented sandstone significantly increased by more than one order of magnitude (from 3.3×10<sup>-18</sup> to 7.8×10<sup>-17</sup> m<sup>2</sup>). P- and S-wave velocities measured from pre- and post-experiment ultrasonic tests were used to estimate the changes in dynamic Young's and shear moduli. Furthermore, cylinder-splitting tests were conducted to measure the tensile strength of the altered post-experimental samples and compared to the control samples that only interacted with pure brine. All samples underwent slight decreases in Young's and shear moduli, and the cylinder-splitting tests suggest that mechanical degradation may be concentrated on the upstream end of the calcite-cemented sample. Our findings help in predicting chemo-mechanical changes at carbon sequestration sites where the reservoir lithology is carbonate-cemented sandstone.

Funding for this project is provided by the U.S. Department of Energy's (DOE) National Energy Technology Laboratory (NETL) through the Southwest Regional Partnership on Carbon Sequestration (SWP) under Award No. DE-FC26-05NT42591. Sandia National Laboratories is a multi-mission laboratory managed and operated by National Technology and Engineering Solutions of Sandia LLC, a wholly owned subsidiary of Honeywell International Inc. for the U.S. Department of Energy's National Nuclear Security Administration under contract DE-NA0003525.

#### STATEWIDE GROUNDWATER RECHARGE MODELING AND ITS CALIBRATION

Fei Xu<sup>1</sup>, Daniel Cadol<sup>1</sup>, Fred Phillips<sup>1</sup>, and Talon Newton<sup>2</sup>

<sup>1</sup>New Mexico Tech, Earth and Environmental Science Department, 801 Leroy Pl, Socorro, NM, 87801

<sup>2</sup>New Mexico Bureau of Geology & Mineral Resources, 801 Leroy Pl, Socorro, NM, 87801

Groundwater recharge in New Mexico not only largely defines a limit for water availability in this semiarid state, but also is the least understood aspect of the state's water budget. With the goal of estimating groundwater recharge statewide, we are developing the Evapotranspiration and Recharge Model (ETRM), which uses existing remote sensing spatial datasets to model the daily soil-water balance over the state at a resolution of 250 x 250 m. The model, as currently configured, estimates only diffuse recharge over the landscape, not focused recharge from channels or playas.

We require runoff data to calibrate and test ETRM's simulations. As runoff data from ephemeral channels are sparse in NM, we have turned to the US Agricultural Research Service Walnut Gulch Experimental Watershed (WGEW) in southern Arizona, which is one of the most densely gauged and monitored semiarid rangeland watersheds for hydrology research. Runoff is calculated as Hortonian overland flow in ETRM, and it is one of the major sinks in the soil-water balance. This runoff, though not tracked through space in the model, is the source water for focused recharge, which can be estimated by transmission loss in ephemeral channels. By using the precipitation and runoff data from WGEW, we can relate rainfall intensity and antecedent soil moisture to the amount of measured runoff and subsequent channel infiltration. We will ultimately employ stochastic analytical theory to generate improved runoff estimates for ETRM based on simulated soil-water balances from ETRM and on generalized precipitation datasets.

#### DEVELOPMENT OF A WATER BUDGET FOR WETLAND UNITS ON THE BOSQUE DEL APACHE NATIONAL WILDLIFE REFUGE, NEW MEXICO

Jeffry C. Yon<sup>1</sup>, Jennifer Lindline<sup>1</sup>, Paul Tashjian<sup>2</sup>, Joseph Zebrowski<sup>1</sup>, and Michael Petronis<sup>1</sup>

<sup>1</sup>New Mexico Highlands University, Natural Resources Management Department, Las Vegas, NM, 87701, jyon@live.nmhu.edu  
<sup>2</sup>U.S. Fish and Wildlife Service

The Bosque del Apache National Wildlife Refuge in south-central New Mexico is the site of seasonal wetlands that support habitat for year-round and migratory wildlife. Water is managed at the Refuge to support agricultural plots, riparian zones, and the needs of endangered species. The Refuge currently uses a monthly time step model that integrates a variety of estimated and empirical data to develop the hydrologic budget for irrigation water. However, there have been no direct measurements of how much water is infiltrating from managed wetlands into the shallow ground water. It is important to improve the accuracy of water budget estimates by developing

infiltration rates based on empirically derived data. In order to accomplish this goal, we studied 4 hydrologically distinct wetlands (different sizes, soil textures, and water management) comprised of agriculture land, forested grass land, and flood plain mixed with conifer forest and riparian vegetation. Regularly collected data included weekly flow measurements at 4 inflow and 4 outflow structures, daily staff plate readings, and weekly ground water levels at 20 monitoring sites. These data are being integrated into a wetland ArcGIS tool to quantify the Refuge wetland water budget. The wetland units show average increases in water table elevation of 1.61–2.67 survey feet after surface water introduction over the study period. Infiltration rates are being calculated for the 4 studied wetland units and scaled out to represent all Refuge wetlands to create a more accurate water budget.

#### INSIGHTS INTO POSTCALDERA MAGMATISM AND RELATED HAZARDS USING VOLCANIC AND PLUTONIC RECORDS

Matthew J. Zimmerer<sup>1</sup> and Frank Ramos<sup>2</sup>

<sup>1</sup>New Mexico Bureau of Geology and Mineral Resources, New Mexico Tech, Socorro, NM, 87801, matthew.zimmerer@nmt.edu

<sup>2</sup>New Mexico State University, Las Cruces, NM

Ongoing geochronology research of volcanic fields from northern NM and southern CO provide insight into the timescales of post-caldera processes and associated hazards. A small, but growing dataset of ultra-high-precision Ar/Ar ages of ring-fracture domes at Valles caldera, combined with published ages, suggests a change in the eruption style and duration of individual domes throughout the current postcaldera stage. Published ages for two of the earliest postcaldera domes, Cerro del Medio and Cerro Santa Rosa, indicate total dome growth episodes of 130±29 ka and 128±19 ka, respectively. New geochronology of the younger domes indicates short-lived eruptive cycles where the ages of individual flows for each dome are indistinguishable, or define dome growth and repose periods of less than 10 ka. A comprehensive dating campaign, in conjunction with new isotope

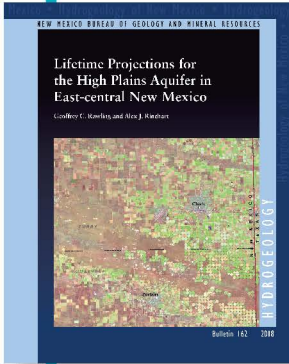
geochemical methods that involve analyzing fused single crystals from the Ar/Ar analyses, is planned for the next several years to test our hypotheses of dome eruption evolution, assess related hazards at Valles caldera, and determine best practices for interpreting ultra-high-precision sanidine ages. In contrast to dating volcanic rocks in Quaternary systems, which provides snapshots of rapid or short-lived events, geochronology of intrusive rocks at eroded mid-Tertiary systems offers insight into prolonged postcaldera magmatic processes. Numerous studies have shown that the duration of postcaldera pluton emplacement commonly exceeds that of postcaldera volcanism and can continue for as much as 5 Ma after caldera formation. Nearly completed research on the Dulce-Platoro dike swarm, which originates from the ca. 28.6–30.1 Ma Platoro caldera of the Southern Rocky Mountain volcanic field and extends nearly 125 km south into northern NM, shows that dike swarm emplacement may be a previously under appreciated post-caldera process. Approximately 40 new Ar/Ar ages indicate that the Dulce-Platoro dike swarm was emplaced in a 15 Ma period both before and after caldera collapse, although most dikes were emplaced between 24 and 27 Ma during prolonged consolidation and crystallization of the subcaldera magmatic system. Similarly, a new age of 23.71±0.60 Ma for the Tinaja Dike, exposed along I-25 south of Raton, suggests that it may be related to postcaldera magmatism associated with the 25.4 Ma Questa caldera, located approximately 80 km to the west. Dating of nearby Tertiary intrusions that crop out on the High Plains will test this preliminary interpretation. At both mid-Tertiary caldera systems erosion has removed any direct evidence that would indicate whether the injected dikes reached the surface and erupted. Regardless, widespread and shallow dike emplacement could have certainly caused damaging seismicity as well as scattered, small-volume eruptions. These examples, as well as those from other caldera systems around the globe, suggest that proximal and distal magmatic-tectonic hazards should be considered for volcanic fields currently experiencing postcaldera unrest.

---

Find a PDF of the program at: [nmgs.nmt.edu/meeting/](http://nmgs.nmt.edu/meeting/)

# NEW MEXICO BUREAU OF GEOLOGY & MINERAL RESOURCES

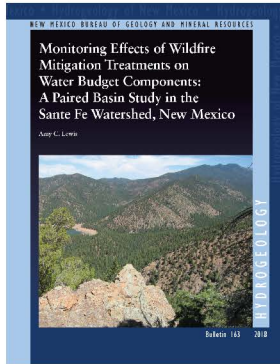
## Publications 2018



**Bulletin 162**  
Lifetime Projection  
for the High Plains  
Aquifer in East-central  
New Mexico

By Geoffrey C. Rawling  
and Alex J. Rinehart

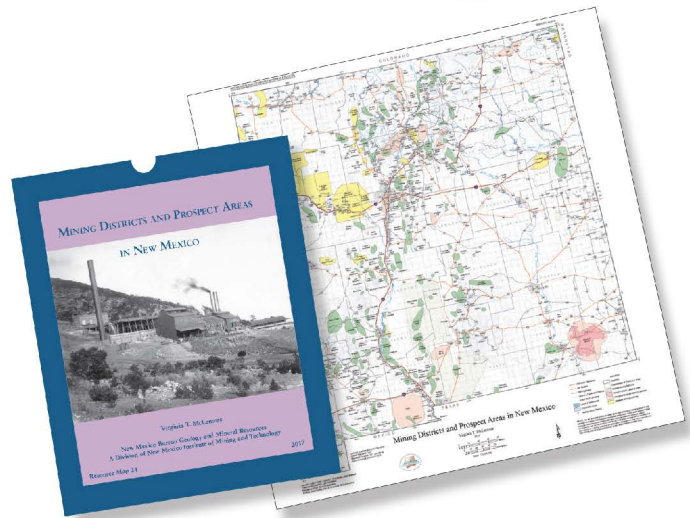
Free download



**Bulletin 163**  
Monitoring Effects of Wildfire  
Mitigation Treatments on  
Water Budget Components:  
A Paired Basin Study in the  
Santa Fe Watershed, New Mexico

By Amy C. Lewis

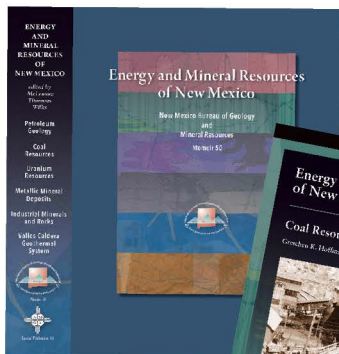
Free download



**Resource Map 24**  
Mining Districts and  
Prospect Areas in  
New Mexico

By Virginia T. McLemore  
Edited by Shari Kelley.  
Map, Booklet, and Appendix 1;  
\$18.95.

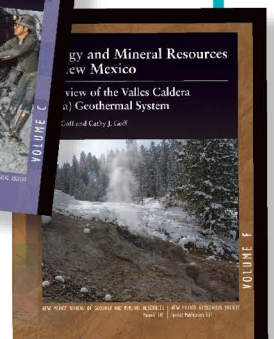
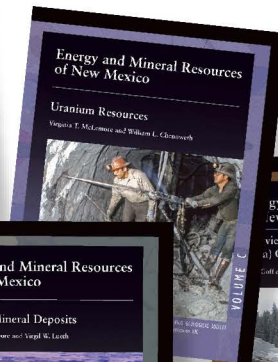
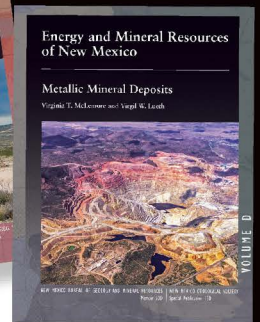
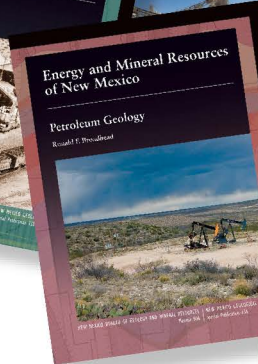
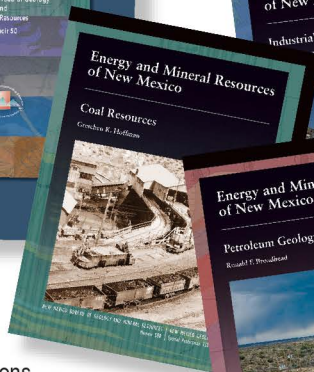
Order online  
or shop at our  
bookstore!



**Memoir 50**  
Energy and Mineral Resources  
of New Mexico

Edited by Virginia T. McLemore, Stacy Timmons,  
and Maureen Wilks.

NMBGMR Memoir 50/NMGS Special Publication 13.  
Six-volume boxed set \$125.00.  
Individually \$25.00.



For more information about the bureau and our publications:

Visit our website at <http://geoinfo.nmt.edu>

Call (575) 835-5490, e-mail us at [NMBG-Publications@nmt.edu](mailto:NMBG-Publications@nmt.edu)  
or visit our Bookstore at the corner of Bullock and Leroy  
on the campus of New Mexico Tech  
801 Leroy Place, Socorro, New Mexico, 87801

